BIPEDAL HUMANOID ROBOT CONTROL BY FUZZY ADJUSTMENT OF THE REFERENCE WALKING PLANE

by
UTKU SEVEN

Submitted to the Graduate School of Engineering and Natural Sciences in partial fulfillment of the requirements for the degree of Doctor of Philosophy

Sabanci University
July 2012

BIPEDAL HUMANOID ROBOT CONTROL BY FUZZY ADJUSTMENT OF THE REFERENCE WALKING PLANE

APPROVED BY:

Assoc. Prof. Dr. Kemalettin ERBATUR ..... 
(Thesis Supervisor)

Prof. Dr. Hakan TEMELTAŞ ..... 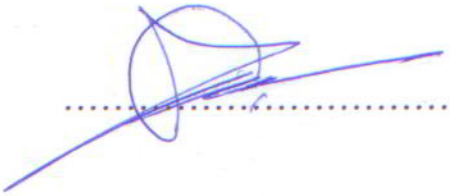

Prof. Dr. Mustafa ÜNEL ..... 

Assoc. Prof. Dr. Erkay SAVAŞ ..... 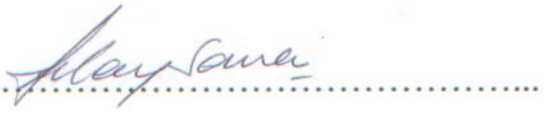

Assist. Prof. Dr. Güllü KIZILTAŞ ŞENDUR..... 

DATE OF APPROVAL: 06 / 08 / 2012

BIPEDAL HUMANOID ROBOT CONTROL BY FUZZY ADJUSTMENT OF THE REFERENCE WALKING PLANE

Utku SEVEN

Mechatronics Engineering, Ph.D. Thesis, 2012

Thesis Supervisor: Assoc. Prof. Dr. Kemalettin ERBATUR

Keywords: Humanoid robots, bipedal blind walking, inclined plane, fuzzy systems, orientation control

ABSTRACT

The two-legged humanoid structure has advantages for an assistive robot in the human living and working environment. A bipedal humanoid robot can avoid typical obstacles at homes and offices, reach consoles and appliances designed for human use and can be carried in human transport vehicles. Also, it is speculated that the absorption of robots in the human shape into the human society can be easier than that of other artificial forms.

However, the control of bipedal walk is a challenge. Walking performance on solely even floor is not satisfactory. The complications of obtaining a balanced walk are dramatically more pronounced on uneven surfaces like inclined planes, which are quite commonly encountered in human surroundings. The difficulties lie in a variety of tasks ranging from sensor and data fusion to the design of adaptation systems which respond to changing surface conditions.

This thesis presents a study on bipedal walk on inclined planes with changing slopes. A Zero Moment Point (ZMP) based gait synthesis technique is employed. The pitch angle

reference for the foot sole plane −as expressed in a coordinate frame attached at the robot body− is adjusted online by a fuzzy logic system to adapt to different walking surface slopes. Average ankle pitch torques and the average value of the body pitch angle, computed over a history of a predetermined number of sampling instants, are used as the inputs to this system.

The proposed control method is tested via walking experiments with the 29 degrees-of-freedom (DOF) human-sized full-body humanoid robot SURALP (Sabanci University Robotics Research Laboratory Platform). Experiments are performed on even floor and inclined planes with different slopes. The results indicate that the approach presented is successful in enabling the robot to stably enter, ascend and leave inclined planes with 15 percent (8.5 degrees) grade.

The thesis starts with a terminology section on bipedal walking and introduces a number of successful humanoid robot projects. A survey of control techniques for the walk on uneven surfaces is presented. The design and construction of the experimental robotic platform SURALP is discussed with the mechanical, electronic, walking reference generation and control aspects. The fuzzy reference adjustment system proposed for the walk on inclined planes is detailed and experimental results are presented.

BULANIK MANTIKLI REFERANS YÜRÜYÜŞ DÜZLEMİ AYARLAMASI İLE İKİ BACAKLI İNSANSI ROBOT KONTROLÜ

Utku SEVEN

Mekatronik Mühendisliği Programı, Doktora Tezi, 2012

Tez Danışmanı: Doç. Dr. Kemalettin ERBATUR

Anahtar Kelimeler: İnsansı robotlar, iki bacaklı kör yürüyüş, eğimli yüzeyler, bulanık mantıklı sistemler, yönelim kontrolü

ÖZET

İki bacaklı insansı yapı yaşadığımız ve çalıştığımız ortamlarda insanlara destek olacak yardımcı bir robot için avantajlar sunmaktadır. İnsansı robotların ev ve ofis ortamlarında çevreleri ile etkileşimli olarak çeşitli görevleri yerine getirmeleri, insanlar için tasarlanmış aygıt ve aletleri kullanmaları, insanlar için tasarlanmış araçlarla nakledilmeleri mümkündür. Ayrıca insana benzer şekle sahip robotların diğer şekillerdeki robotlara göre toplumla daha kolay uyum sağlayabilecekleri ve sosyal bir varlık olarak kabul edilebilecekleri düşünülmektedir.

Bununla birlikte iki bacaklı robot yürüyüş kontrolü zorlu bir görevdir. Sadece düz zeminler üzerindeki yürüyüş başarımı yeterli değildir. İnsanların sıkça karşılaştıkları eğimli yüzeyler gibi düz olmayan zeminler üzerinde dengeli bir yürüyüşü sağlamanın güçlükleri çok daha fazladır. Bahsedilen güçlükler, veri ve algılayıcı füzyonundan eğimli yüzeylere adaptasyon sağlayacak sistemlerin tasarlanması ve geliştirilmesine kadar geniş bir yelpazeye yayılmaktadır.

Bu doktora tezi değişken eğimlere sahip yüzeylerde yürüme üzerine bir çalışmayı sunmaktadır. Yürüme için Sıfır Moment Noktası (SMN) tabanlı bir referans yörünge sentez tekniği kullanılmıştır. İnsansı robot gövde koordinat çerçevesinde ifade edilmiş ayak tabanı yunuslama açısı referansı, farklı eğimlerdeki yüzeylere uyum sağlaması amacıyla, bulanık mantıklı bir kontrolör sistemi tarafından çevrimiçi olarak ayarlanmaktadır. Önceden belirlenmiş örnekleme sayıları ve süreleri ile hesaplanan ortalama bilek yunuslama momentleri ve ortalama vücut yunuslama açısı bu sistemin girdileri olarak kullanılmıştır.

Önerilen kontrol yöntemi 29 serbestlik dereceli, insan ebatlarındaki, tüm-vücutlu insansı robot SURALP (**S**abancı **Ü**niversitesi **R**obot **A**raştırmaları **L**aboratuvar **P**latformu) üzerinde gerçekleştirilen deneysel çalışmalarla denenmiştir. Yürüme deneyleri düz zeminde ve farklı eğim açılarına sahip yüzeyler üzerinde yapılmıştır. Elde edilen sonuçlar önerilen metodun %15 eğimli ($8,5^{o}$) bir yüzeye giriş, yüzeyde tırmanış ve yüzeyden çıkış konusunda başarılı olduğunu göstermektedir.

Tez, iki bacaklı yürüyüşü konu alan bir terminoloji kısmıyla başlamakta, bazı başarılı insansı robot projelerini tanıtmaktadır. Düzgün olmayan yüzeyler üzerindeki yürüyüş kontrol teknikleri hakkında bir literatür taraması sunulmuştur. Yürüyüş deneylerinin gerçekleştirildiği insansı robot platformu SURALP mekanik tasarım ve imalat, elektronik tasarım ve entegrasyon, referans yörünge sentezi ve kontrol sistem tasarımı alt başlıkları ile anlatılmıştır. Eğimli yüzeyler üzerindeki yürüyüş için tasarlanan bulanık mantıklı çevrimiçi referans ayarlama sisteminin ayrıntıları verilmiş ve deneysel sonuçlar sunulmuştur.

To my beloved father, mother and brother

ACKNOWLEDGEMENTS

One of the greatest pleasures of completing my Ph.D. study is to look over the journey past and to remember all precious people who have helped and supported me in this long and tortuous but rewarding road.

First of all, I want to express my sincerest and deepest gratitude to my advisor Prof. Kemalettin Erbatur for his continuous and round-the-clock support, never-ending patience, motivation, immense knowledge, great enthusiasm and for giving me the opportunity to work on his project: "Design, Manufacturing and Control of A Bipedal Humanoid Robot" (TÜBİTAK 106E040). His guidance helped me in all phases of this research and writing of my thesis. I could not have imagined having a better advisor, mentor and guide who could have made this Ph.D study and research possible.

Besides my advisor, I would like to thank the rest of my thesis committee: Prof. Mustafa Ünel, Prof. Hakan Temeltaş, Prof. Erkay Savaş and Prof. Güllü Kızıltaş for their detailed review, constructive criticism, encouragement, excellent advice and helpful attitude even in my defense.

My heartfelt thanks go to my fellow brothers-in-arms: Kaan Can Fidan, Tunç Akbaş, Evrim Taşkıran, Özer Koca, Metin Yılmaz, Selim Özel and Emre Eskimez (The Myrmidons). Also I would like to thank my precious friends: Ahmetcan Erdoğan, Emrah Deniz Kunt, İlker Sevgen, Osman Koç, Teoman Naskali, Ozan Mutluer, Merve Acer and Zeynep Temel for the sleepless nights we were working together before deadlines and for all the fun we have had in the last five years.

The financial support of TÜBİTAK BİDEB (2211) Doctoral Scholarship Program for this Ph.D study is gratefully acknowledged.

Last but not the least; I would like to thank my parents Nedim Seven, Ayşe Seven and my brother Özgür Seven for supporting and guiding me spiritually throughout all periods of my life.

BIPEDAL HUMANOID ROBOT CONTROL BY FUZZY ADJUSTMENT OF THE REFERENCE WALKING PLANE

TABLE OF CONTENTS

ABSTRACT iv

ÖZET vi

ACKNOWLEDGEMENTS ix

TABLE OF CONTENTS x

LIST OF FIGURES xii

LIST OF TABLES xvii

LIST OF SYMBOLS xviii

LIST OF ABBREVIATIONS xxii

1. INTRODUCTION 1

2. TERMINOLOGY AND EXAMPLES OF HUMANOID ROBOTICS PROJECTS 4

2.1. Terminology 4

2.2. Examples of Humanoid Robot Projects 8

3. A SURVEY ON BIPEDAL WALKING ON UNEVEN SURFACES 19

3.1. Contribution of the Thesis 25

4. THE EXPERIMENTAL HUMANOID ROBOT PLATFORM SURALP 26

4.1. Mechanical Design and Manufacturing 26

4.2. Electronic Hardware 57

4.2.1. Sensor System 57

4.2.2. Control Hardware 59

4.3. Walking Reference Generation for Even Floor 61

4.4. Basic Control Actions 70

4.4.1. Joint Level Control 70

4.4.2. Foot Roll Control 70

4.4.3. Ground Impact Compensation 71
4.4.4. Early Landing Modification 73
5. FUZZY ADJUSTMENT OF THE REFERENCE WALKING PLANE FOR THE BIPEDAL WALK ON INCLINED PLANES 75
5.1. The Novel Fuzzy Parameter Adjustment System for the Adaptation to Sloped Surfaces 83
6. EXPERIMENTAL RESULTS 90
7. CONCLUSIONS 100
REFERENCES 102
LIST OF AUTHOR'S RELATED PUBLICATIONS 111
APPENDIX A 113

LIST OF FIGURES

Figure 2.1 : Sagittal, frontal and transverse planes 4
Figure 2.2 : Static walk 5
Figure 2.3 : Dynamic walk 5
Figure 2.4 : A running athlete 7
Figure 2.5 : First bipedal humanoid robot prototypes of Waseda University 9
Figure 2.6 : WABIAN-RII - Waseda University 9
Figure 2.7 : WABIAN-2 - Waseda University 10
Figure 2.8 : Tokyo University JSK Laboratory Humanoid Robots 11
Figure 2.9 : KAIST KHR-1 12
Figure 2.10 : KAIST KHR-2 12
Figure 2.11 : KAIST KHR-3 (HUBO) and Albert HUBO 12
Figure 2.12 : HONDA Humanoid Robots 13
Figure 2.13 : HONDA Humanoid Robots: P3 and ASIMO 14
Figure 2.14 : HRP 2 (left) and HRP-3 (right) 15
Figure 2.15 : HRP-4C (left) and HRP-4 (right) 16
Figure 2.16 : Humanoid robot platforms of PAL Robotics: REEM-A (left) and REEM-B (right) 17
Figure 2.17 : Sony QRIO, Fujitsu HOAP-3, MAHRU-3 Samsung, DARwIn OP of RoMeLa 17
Figure 2.18 : SARCOS Humanoid Robots: DA ATR DB2 and CB-I 18
Figure 4.1 : HONDA P1 (left), P2 (middle) and P3 (right) 27
Figure 4.2 : Honda ASIMO 27
Figure 4.3 : Kawada Industries HRP 4 28
Figure 4.4 : Waseda University WABIAN-2 28

Figure 4.5 : Pal Robotics Barcelona REEM-B 28
Figure 4.6 : CNRS ROBEA Rabbit 29
Figure 4.7 : Yokohama National University MARI-3 29
Figure 4.8 : Bipedal walking robot leg module preliminary design isometric view..... 30
Figure 4.9 : Bipedal walking robot leg module preliminary design draft with 4 views an 30
Figure 4.10 : 150W Maxon DC motor and HFUC 25 series Harmonic Drive setup model 31
Figure 4.11 : 150W Maxon DC motor and HFUC 20 series Harmonic Drive setup model 31
Figure 4.12 : 150W Maxon DC motor and HFUC 25 series Harmonic Drive setup model 31
Figure 4.13 : 150W Maxon DC motor and HFUC 20 series Harmonic Drive setup technical drawing 32
Figure 4.14 : 150W Maxon DC motor and HFUC 20 series Harmonic Drive setup model top view 32
Figure 4.15 : 90W Maxon DC motor and HFUC 20 series Harmonic Drive setup model top view 32
Figure 4.16 : Manufactured performance test setups (front sides with Harmonic Drive and motor detail) 33
Figure 4.17 : Manufactured performance test setups (back sides with belt-pulley mechanism details) 33
Figure 4.18 : Humanoid robot leg design 34
Figure 4.19 : Humanoid robot leg design interior, front and exterior views with dimensions 35
Figure 4.20 : Isometric view of waist design 35
Figure 4.21 : Hip design isometric view 36
Figure 4.22 : Hip center design isometric view 36
Figure 4.23 : Upper leg design isometric view 37
Figure 4.24 : Lower leg design isometric view 37

Figure 4.25 : Ankle center design isometric view 37
Figure 4.26 : Foot design isometric view 38
Figure 4.27 : Forces and torques applied at the upper leg from the hip center..... 39
Figure 4.28 : Forces and torques applied at the upper leg from the lower leg..... 39
Figure 4.29 : Forces and torques applied at the lower leg from the upper leg 40
Figure 4.30 : Forces and torques applied at the lower leg from the wrist center..... 40
Figure 4.31 : Humanoid robot arm design 44
Figure 4.32 : Structural analysis for the left arm molded shoulder part 44
Figure 4.33 : Manufactured legs and waist assembly, front view 45
Figure 4.34 : Manufactured legs and waist assembly, side view..... 45
Figure 4.35 : Head and neck design CAD model – isometric view..... 46
Figure 4.36 : Head and neck design CAD model – front view..... 46
Figure 4.37 : Head and neck design CAD model – side view 47
Figure 4.38 : Humanoid robot leg module SURALP-L with integrated control system, front and side views..... 48
Figure 4.39 : Humanoid robot leg module and integrated control system – dimensions 48
Figure 4.40 : SURALP design CAD model..... 49
Figure 4.41 : Pan-tilt joints of the manufactured neck mechanism 49
Figure 4.42 : Neck actuation system and head structure 50
Figure 4.43 : Neck actuation system and head structure 50
Figure 4.44 : 6 DOF arm and linear actuated hand structure..... 51
Figure 4.45 : Robot hand CAD model and closed up view 51
Figure 4.46 : Rubber foot sole 52
Figure 4.47 : Welded sheet metal upper body construction..... 52
Figure 4.48 : SURALP Main assembly CAD model..... 53
Figure 4.49 : The integrated SURALP 54
Figure 4.50 : SURALP, research laboratory and Cartesian crane system 54
Figure 4.51 : The kinematic arrangement of the robot 55
Figure 4.52 : Foot sensor platform layers 58

Figure 4.53 : Electronic hardware of SURALP 59
Figure 4.54 : Pictures taken while cabling 60
Figure 4.55 : The linear inverted pendulum model 62
Figure 4.56 : Forward moving ZMP references with pre-assigned double support phases 63
Figure 4.57 : x and y -direction CoM and ZMP references 68
Figure 4.58 : x and z -direction foot frame references in as expressed in the world frame 68
Figure 4.59 : The ankle roll axis 72
Figure 4.60 : The hip height reference 72
Figure 4.61 : The basic walking controller block diagram 74
Figure 5.1 : Bipedal robot walk on changing slopes 76
Figure 5.2 : Coordinate systems associated with walking reference generation 76
Figure 5.3 : The body pitch angle β 77
Figure 5.4 : The coordinate frame A 78
Figure 5.5 : The pitch rotation by θ 79
Figure 5.6 : The membership functions 88
Figure 5.7 : The walking controller block diagram with fuzzy adjustment 89
Figure 6.1 : The robot in the walk from even ground onto the inclined plane with 15% slope and the following flat top platform 92
Figure 6.2 : Body pitch angle, ankle pitch torques, slope transition indicator and foot pitch angle reference during the 8.5 degrees (15%) slope experiment 93
Figure 6.3 : The foot pitch angle reference in 0% (0 degrees), 5% (2.9 degrees), 10% (5.7 degrees) and 15% (8.5 degrees) grade plane walking experiments 95
Figure 6.4 : Body pitch and roll angles 96
Figure 6.5 : Pitch joint (hip pitch, knee and ankle pitch) control torques 98
Figure 6.6 : Average output power of legs during walking 99
Figure A.1 : Denavit-Hartenberg joint axis representations for one leg 115
Figure A.2 : A simple leg structure with the kinematic arrangement 115
Figure A.3 : The view normal to the shank and thigh 116

Figure A.4 : The view normal to the side of the foot..... 118

Figure A.5 : The view normal to the shank and thigh. q_{L_5} is defined in this plane to

..... 118

Figure A.6 : The view normal to the shank and thigh. Computation of q_{L_5} 119

Figure A.7 : The view normal to the foot front side 119

LIST OF TABLES

Table 4.1 : Dimensions and weight data of SURALP 55
Table 4.2 : Actuator, reduction and joint limits 56
Table 4.3 : Sensory System of SURALP 58
Table 5.1 : The Fuzzy Rule Base 87
Table 6.1 : Reference Generation Parameters 90
Table 6.2 : Rule Strengths and Membership Function Corner Locations 91
Table A.1 : Denavit-Hartenberg Parameters of the biped leg 113

LIST OF SYMBOLS

P	:	Zero Moment Point reference vector
p_x	:	x-directional component of Zero Moment Point reference vector
p_y	:	y-directional component of Zero Moment Point reference vector
p_z	:	z-directional component of Zero Moment Point reference vector
CoM	:	Center of mass reference vector
x	:	x-directional component of center of mass reference vector
y	:	y-directional component of center of mass reference vector
z	:	z-directional component of center of mass reference vector
z_c	:	Constant height of the Linear Inverted Pendulum
$\ddot{c}_x$	:	x-directional acceleration of the robot body
c_x	:	x-directional position of the robot body
c_z	:	z-directional position of the robot body
$\ddot{c}_y$	:	y-directional acceleration of the robot body
c_y	:	y-directional position of the robot body
P_x^{ref}	:	Reference ZMP for x-direction
P_y^{ref}	:	Reference ZMP for y-direction
τ	:	Double support phase
T	:	Half walking period
ω_n	:	Square root of g/ c_z
A	:	Foot center to foot center distance in frontal plane
B	:	Foot center to foot center distance in sagittal plane

$c_x^{ref}(t)$	:	COM Reference for x-direction
$c_y^{ref}(t)$	:	COM Reference for y-direction
δ	:	Magnitude of peak difference between p_x^{ref} and the non-periodic component of p_x^{ref}
N	:	Approximation iteration number for Fourier Series
b	:	Half length of the foot sole
T_d	:	Double support period
T_s	:	Single support period
h_s	:	Step height
h_p	:	Ground push magnitude
C		Half of the y-directional distance between foot frame origins
θ_{roll}	:	Ankle roll joint reference angle
$\bar{\theta}_{roll}$	:	Reference ankle roll angle after the reference modification
τ_{toll}	:	The torque about the roll axis
K_{roll}	:	Low pass filter constant
λ_{roll}	:	Low pass filter constant
l	:	Hip-to-sole distance reference
$\bar{l}$	:	Shock absorber modified hip-to-sole distance reference
F_z	:	z direction component of the ground interaction
m_l	:	Desired mass parameter
b_l	:	Desired damping parameter
k_l	:	Desired stiffness parameter
t_0	:	Time at the end of the impact compensation phase
ω_{return}	:	Parameter which determines the speed of return of $\bar{l}$ to l.
β	:	Body pitch angle

F : Plane rotation coordinate frame

h_{body} : Constant body height reference parameter.

x_{offset} : The mean of the right and left foot sole frame reference trajectory x-directional components, as expressed in the body coordinate frame

θ : A rotation angle about the negative y-axis of frame F

N_p : Number of samples used in the average computation

T_p : Body pitch angle sampling period

$\overline{\beta}$: Average value of the body pitch angle

$\tilde{\tau}$: Slope transition indicator

$\overline{\tau}_R$: Right foot pitch torque average value

$\overline{\tau}_L$: Left foot pitch torque average value

τ_R : Right ankle pitch torque

τ_L : Left ankle pitch torque

N_t : Number of samples used for the torque averaging

T_t : Ankle pitch torque sampling time.

$\Delta\theta_k$: Increment of the foot pitch angle at time index k

θ_k : Foot pitch angle at time index k .

$\Delta\theta_{Pj}$: Positive rule strength values

$\Delta\theta_{ZZ}$: Zero rule strength value

$\Delta\theta_{Nj}$: Negative rule strength values

w_{ij} : Truth value of $Rule\,ij$

μ : Membership function values

$\tau_{average}$: Average torques in the ascending interval

P_{Legs} : Power consumption of the legs while ascending the slope

ω_{R_i} : Right leg joint angular velocities

ω_{L_i} : Left leg joint angular velocities

LIST OF ABBREVIATIONS

COM	:	Center of Mass
ZMP	:	Zero Moment Point
LIPM	:	Linear Inverted Pendulum Mode
DOF	:	Degrees of Freedom
2D	:	Two Dimensional
3D	:	Three Dimensional
CAD		Computer Aided Design
HTD	:	High Tension Drive
FOS		Factor of Safety
FEM		Finite Elements Method
FSR		Force Sensing Resistor
CCD		Charge Coupled Device
F/T		Force/Torque
PID		Proportional Integral Derivative
DH		Denavit-Hartenberg

Chapter 1

1. INTRODUCTION

The bipedal structure of a humanoid robot has a number of advantages in the human environment. A bipedal robot can avoid obstacles common in the human environment via the locomotion on legs. It can reach for devices, appliances and consoles built for human ergonomics. A human structured robot can fit into vehicles designed for human transportation. There are other advantages too. A human shaped robot can be accepted naturally as a social being by its users. Human gestures can be implemented in such morphology for artificial emotion expressions.

The last four decades witnessed intensive research on biped robot walking control. A number of successful projects and results are reported in the literature (Hirai et al. 1998, Sakagami et al. 2002, Kaneko et al. 2002, Lohmeier et al. 2004, Hyon and Cheng 2006, Ogura et al 2006). However, the many degrees of freedom to be controlled under coupling effects and nonlinear, hard-to-stabilize dynamics pose difficulties. Therefore, bipedal walking reference generation and control are still among the most important challenges in the field of humanoid robotics. A recent survey on reference generation techniques can be found in Xiang, Arora and Abdel-Malek 2010.

One of the most complicated problems in this field is the robust balance of the walk, not only on even floor, but on surfaces with irregularities and slopes too. The unevenness can be categorized in three main titles:

i) Unstructured surface irregularities. The majority of the experimental results in this area still comes from scenes where the even surface is perturbed by quite structured obstacles.

ii) Inclined planes. An inclined plane presents a very common floor condition. Though such planes are mostly part of the city and outdoor environments, since the indoor floors are not perfectly even, the inclined plane can be found at our homes and offices too.

iii) Stairs

A number of control methodologies are reported for the balance of the walk on uneven surfaces. A later chapter of this thesis is devoted to a survey on control systems dealing with the bipedal walk on surfaces in the first two categories. The walk on stairs is considered as a natural extension of walking on even surfaces and not elaborated upon in the presented work.

This thesis proposes a control method for bipedal walk on inclined planes with changing slopes. A Zero Moment Point (ZMP) based technique is employed for reference gait generation. The pitch angle reference for the foot sole plane - as expressed in a coordinate frame attached at the robot body - is adjusted online by a fuzzy logic system for the locomotion on varying walking surface slopes. Plane-to-plane transitions, as well as the ascending or descending walk phases are addressed by this scheme. Ankle pitch torques and the average value of the body pitch angle, computed over a history of a predetermined number of sampling instants, are used as the inputs of the fuzzy system.

The proposed reference gait adjustment method is tested via walking experiments with the 29 degrees-of-freedom (DOF) human-sized full-body humanoid robot SURALP (Sabanci University Robotics ReseArch Laboratory Platform). Walking experiments are performed on combinations of even and inclined planes with different slopes.

The contributions of the work in the framework of this Ph.D. study are twofold:

i) The design and experimental verification of the above mentioned walking reference adaptation system

ii) Mechanical design and analysis of the experimental robotic platform

The thesis is organized as follows. Chapter 2 presents bipedal walking robot research terminology and lists a number of successful humanoid robot projects. Chapter 3 surveys control techniques addressing the challenges of the walk on uneven surfaces. The first contribution of the thesis, the design of the novel reference gait modification system, is restated in more detail and compared with the background of reported studies. The experimental humanoid robot platform SURALP is introduced in Chapter 4. Mechanical design and manufacturing is detailed. Control hardware, sensors and actuator systems are outlined. Basic walking reference generation and control methods for even surfaces are presented. Chapter 5 discusses the proposed fuzzy walking reference plane change technique.

Chapter 6 presents experimental results. A discussion of the results and future research directions follow in the last chapter.

Chapter 2

2. TERMINOLOGY AND EXAMPLES OF HUMANOID ROBOTICS PROJECTS

2.1. Terminology

Human beings are the most successful bipedal walkers. Therefore, analyzing human-body structure can give us a great foresight to understand human walk. Some terms used in bipedal humanoid walking studies and human biomechanics are explained below (Whittle 2001). Biped locomotion can be defined by projections of foot and body motion on the sagittal, frontal and transverse planes shown in Figure 2.1.

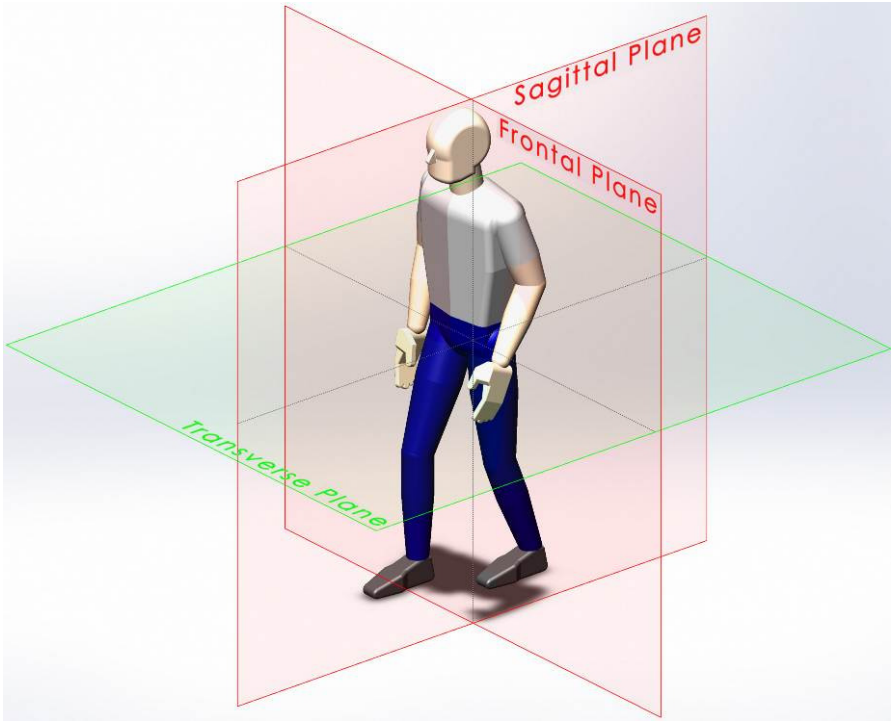

Figure 2.1 : Sagittal, frontal and transverse planes

Center of Mass (COM): Center of Mass is the point where sum of the gravitational forces of robot links are applied.

Support Polygon: The polygon composed of foot/feet regions having contact with the ground.

Step Size: The distance covered by one foot step. This term may have alternative definitions. In this study it represents the distance between the front edges of two feet in contact with the ground.

Single Support Phase: The time period when the whole body is supported by only one foot.

Double Support Phase: The time period when the whole body is supported by two feet on the ground.

Static Walk: It is the locomotion in which the COM lies in the support polygon during walk (Figure 2.2).

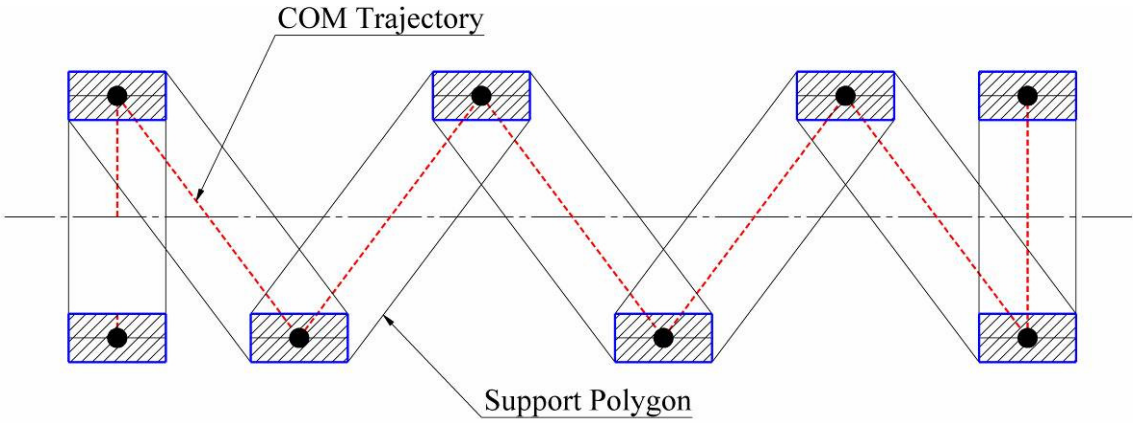

Figure 2.2 : Static walk

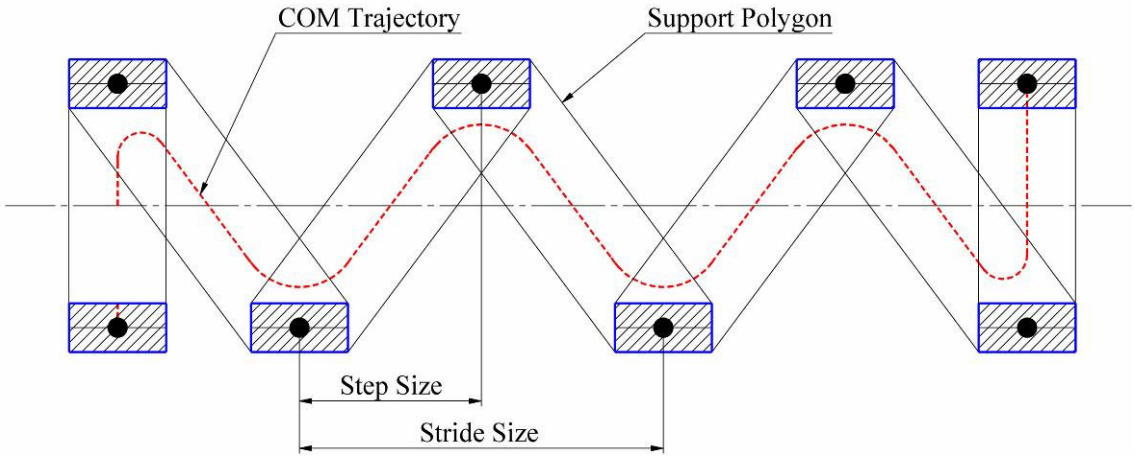

Figure 2.3 : Dynamic walk

Dynamic Walk: It is the locomotion in which the COM may exceed the boundaries of support polygon during walk (Figure 2.3).

Walk can be defined as a sequence of steps with a reference speed. For each leg, the cyclic motion consists of two phases, namely swing and stance phases. A leg is regarded to be in swing phase when floating without a ground contact, and in the stance (support) phase when having the contact with the floor.

A walking cycle, which consists of two single support and two double support phases, starts with the double support phase for the scenario that the initial velocity is zero. It is recorded that the 20% of a typical human walking cycle is spent in double support. The maximum velocity that can be achieved decreases when the percentage of this phase is increased.

The displacement of the COM with respect to the supporting foot soles can be used as a walking stability criterion. It is one of the bases for stability analysis of bipedal walk.

The so-called static and dynamic gaits are distinguished according to the position of COM during the walk. In static walk, the ground projection of the COM lies continuously in the support polygon formed by the foot sole(s) of the robot in contact with the ground (Figure 2.2). In this case the robot is statically stable at any moment. Put another way, the robot is not in the trend of tilting if stopped at any instant of walk. On the otherhand, in dynamic gaits, the ground projection of the COM can exceed the limits of the support polygon (Figure 2.3). Although this can be regarded as an indicator of instability, the walk is termed to be dynamically stable.

Zero Moment Point (ZMP): The ZMP is defined as the point on floor at which the sum of all tilting moments is equal to zero. ZMP is introduced by Vukobratovic, M. (Vukobratovic et al. 1990). As with the ground projection of the robot COM, the position of the ZMP relative to the support polygon is used as a stability criterion for legged locomotion.

Also, ZMP is an important tool for the reference generation of humanoid robots. The picture of a running athlete is given in Figure 2.4 to illustrate the ZMP concept for a humanoid robot. In this body posture, the athlete has to push his body forward in order not to fall. Acceleration in forward direction provides the balance of the body. The ZMP lies in the boundaries of the support polygon in such a scenario (under the right foot in Figure 2.4).

In this figure p_x is the x-directional component of the ZMP vector $p = [p_x, p_y, p_z]^T$ of the athlete and $c = [c_x, c_y, c_z]^T$ is his COM vector.

According to the ZMP stability criterion, the walk is regarded to be stable if the ZMP is in the support polygon. This definition is valid for both static and dynamic walks. When the ZMP is strictly inside the support polygon, there is no tilting moment on the foot edges. On the otherhand, the case when the ZMP is on one of the edges of the support polygon is a critically balanced one. This balance can be lost even with an infinitesimal change in the moments acting on the robot body, and the robot can tilt and fall.

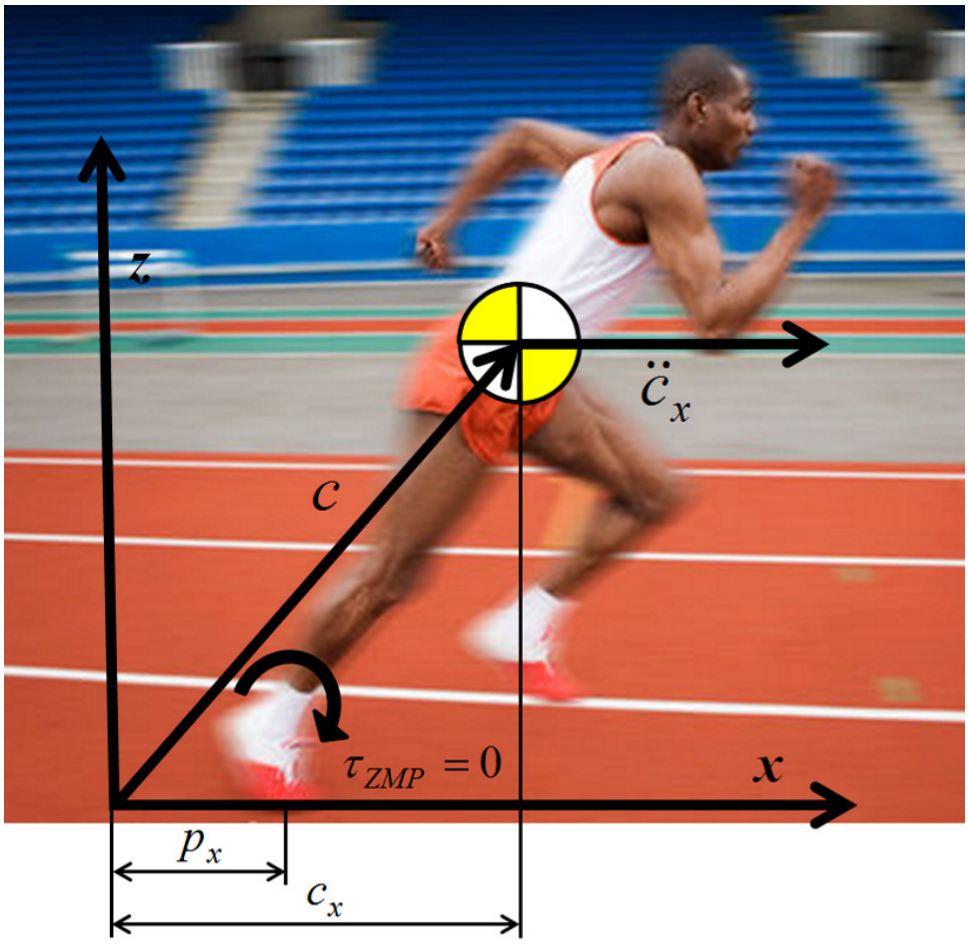

Figure 2.4 : A running athlete

2.2. Examples of Humanoid Robot Projects

Interest of researchers in humanoid robots dates back to late 1960s and a number of successful humanoid robot projects have been developed up to present. In late 1960s Prof. Ichiro Kato, one of the pioneer researchers in robotics, initiated studies on human walking and developed the bipedal walking leg module prototype WL-1 (Figure 2.5) in Waseda University in 1967 (Takanishi and Lim 2007). Using this prototype, the first analysis on bipedal human walk was committed. After improving WL-1 to newer versions WL-3 and WL-5, the first full-body humanoid robot, built in human proportions, WABOT-1 was developed. The humanoid robot is capable of walking straight, changing direction while walking, measuring distance with cameras placed in its head and interacting external environment e.g. (communicating with human in Japanese by artificial sensors). After developing nearly dynamic walking WL-9DR and planar walking WL-10DR, Takanishi et al. introduced WL-10R in 1984 which is the first dynamic walking robot. Torque sensors placed at its hips and ankles provided feedback information for compliant motion (Takanishi et al. 1985). Waseda University studies continued with a hydraulic actuated bipedal robot prototype WL-12 and planar walking robot prototypes WL-15 and WL-16. In 1996, the 35 DOF robot WABIAN (**WA**seda **BI**ped Hum**AN**oid robot), actuated by electric motors was developed which was built in human proportions and walked with a speed similar to that of humans'. Shortly after the robot-environment interaction studies carried out with WABIAN, WABIAN-RII was presented. In 1999, WABIAN-RII was capable of following human motions by parametrically defined full-body references (Takanishi et al. 2000) (Figure 2.6). Ground impact force compensation was carried out with the next introduced prototype WABIAN-RIII. In 2004, WABIAN-RIV, which can mimic human motion by visual and audio recognition systems, was built. WABIAN-RIV is a bipedal humanoid robot with 43 DOF's, a height of 1.89 m and weight at 127 kg. In 2005, the 41 DOFs humanoid robot platform, WABIAN 2 is introduced which was 1.53 m in height and 64.5 kg in weight (Figure 2.7).

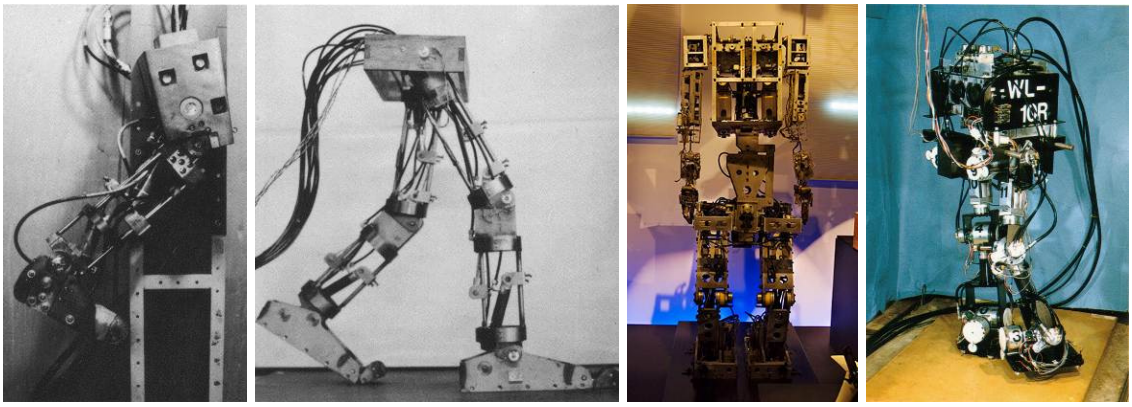

Figure 2.5 : First bipedal humanoid robot prototypes of Waseda University: WL-1, WL-3, WABOT-1 and WL-10R (from left to right)

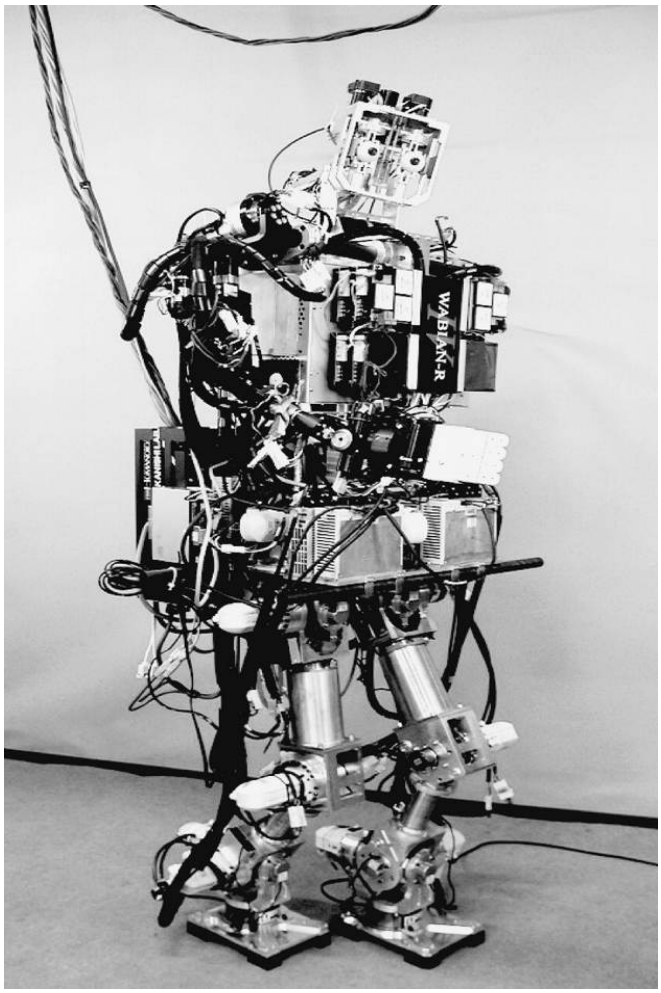

Figure 2.6 : WABIAN-RII - Waseda University

Figure 2.7 : WABIAN-2 - Waseda University

In JSK Laboratory of Tokyo University, bipedal humanoid robot prototypes H5, H6 and H7 were developed (Figure 2.8). H5, with a height of a child (1.27 m), 30 DOFs and weight of 33 kg, is built for dynamic walking and dynamically stable reference generation studies (Nishiwaki et al. 2000). This prototype is followed by H6 (30 DOFs, 1.36 m height and 51 kg weight) equipped with 3D vision and audio recognition systems. Finally, the last prototype of JSK Laboratory, H7, which is capable of fulfilling artificial tasks in human environment was presented. Similar to H6, the design of H7 was in human proportions. H7 has 30 DOFs, has a height of 1.468 m and weighs 57 kg (Nishiwaki et al. 2007). Still, experimental studies of JSK Laboratory on humanoid robots are carried out with H6 and H7 humanoid robots.

Figure 2.8 : Tokyo University JSK Laboratory Humanoid Robots: H5 (left), H6 (middle) and H7 (right)

In 2002, Korea Advanced Institute of Science and Technology (KAIST) introduced the 21 DOF humanoid robot laboratory platform, KHR-1, which was 1.20 m in length and 48 kg in weight. Stable walking experiments are realized by utilizing force/torque sensors and inertial sensors (Oh and Kim 2004). KHR-2 with 41 DOFs, an improved version by means of mechanical design, electrical system design and integration, is presented in 2004 (Kim, Park and Oh 2007-1). The next humanoid robot prototype of KAIST, KHR-3, was more successful in mimicking the human appearance when compared to previous prototypes. KHR-3 has integrated batteries as power source and is capable of hand shaking, manipulating objects and many other daily tasks with its five fingered hands (Park et al. 2006). These prototypes are shown in Figure 2.9, Figure 2.10 and Figure 2.11, respectively. KAIST also developed an android type bipedal humanoid robot named Albert HUBO which can mimic facial expressions and the bipedal robot HUBO-FX which can carry humans.

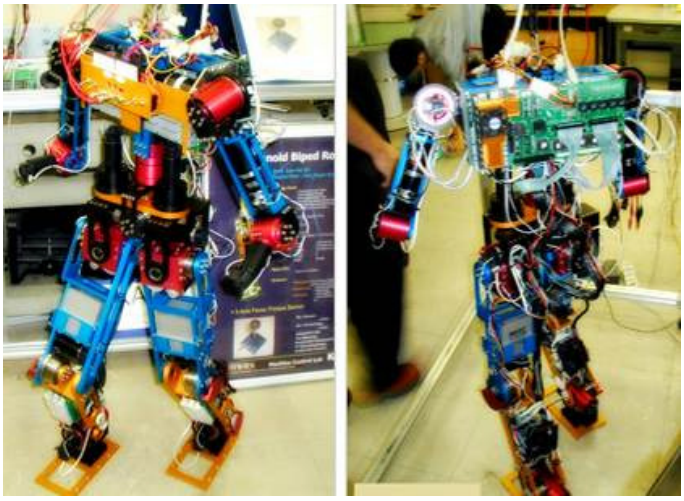

Figure 2.9 : KAIST KHR-1

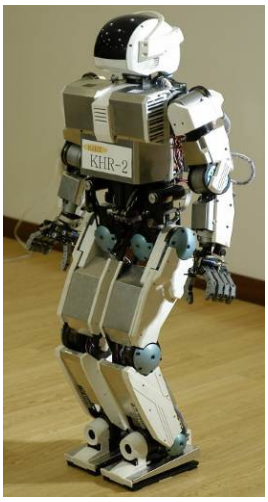

Figure 2.10 : KAIST KHR-2

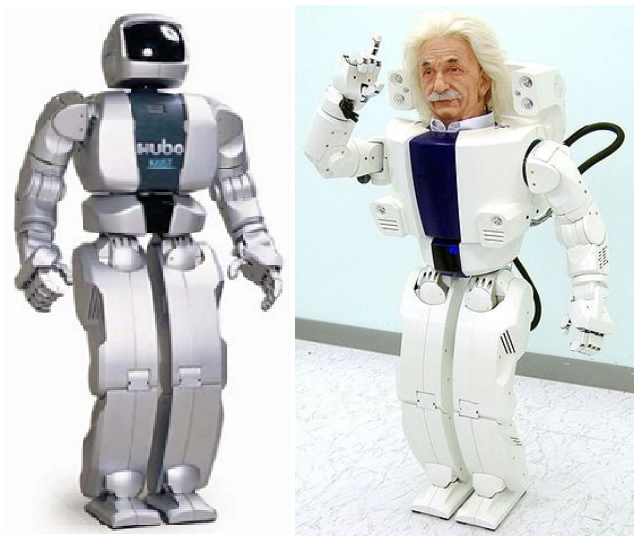

Figure 2.11 : KAIST KHR-3 (HUBO) and Albert HUBO

Another successful humanoid robot laboratory platform, JOHNNIE, was developed by Munich Technical University (Gienger, Löffler and Pfeiffer 2001). The main purpose of this project was maintaining stable and rapid walk on surfaces with irregularities. The robot was 1.80 m in height, 40 kg in weight and had 17 DOFs. The only degree of freedom of its upper body is placed at its pelvis. It reaches a satisfactory walking speed of 2.4 km/h by its light weight structure, gyroscope and accelerometer feedback. 7 DOFs have been added to the elbows, waist and toes in order to enhance the walking performance and LOLA, an improved version, has been developed. Recent studies of Munich Technical University is concentrated on the integration of a multi-focus, 6 DOFs, 4 camera vision system which can enable precise orientation estimations and accurate orientation changes while walking with visual support (Lohmeier et al. 2006).

HONDA has attracted the attention of research community and public with the bipedal humanoid robot prototypes they developed since 1986 (Figure 2.12). HONDA analyzed the basis of bipedal walk with experiments on the first prototypes E0, E1, E2 and E3. Building the E4, E5 and E6 prototypes, they improved the walking stability via walking balance enhancing control strategies (HONDA 2009). After building their first human-like bipedal walking robot P1, they developed, P2, a superior humanoid robot platform and introduced it in 1996. The robot was capable of climbing stairs, manipulating objects with its hands and walking stably with wireless communicating control architecture. Following studies are focused on improving safety. In the next prototype, P3, P2's design was followed by reducing the weight and the size of the humanoid robot. In order to obtain adaptation to human environment, with P3, the height of the robot is reduced from 1.82 m to 1.60 m and the weight of the robot is reduced from 210 kg to 130 kg by using magnesium alloy structural material.

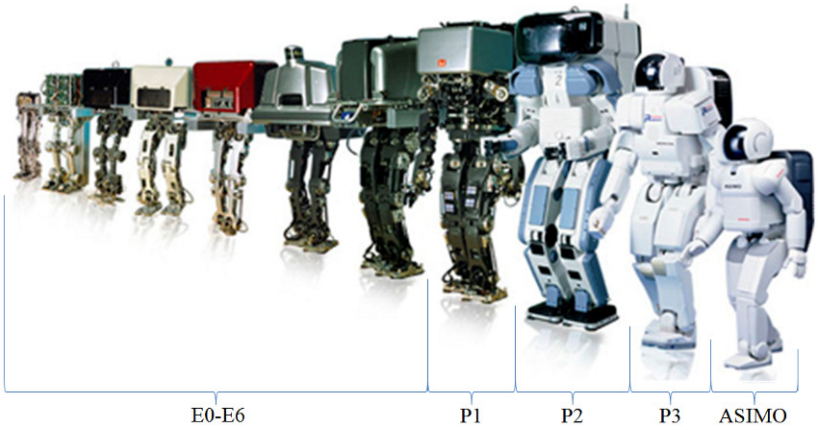

Figure 2.12 : HONDA humanoid robots; E0-6, P1-3, ASIMO

HONDA's last bipedal humanoid robot ASIMO (**A**dvanced **S**tep in **I**nnovative **MO**bility) was introduced in 2000 as a result of experience obtained from previous versions. ASIMO is more like a human being than the previous versions and its moving abilities are more human-like by means of smoothness and fluency too. It is 1.20 m in height and 43 kg in weight. ASIMO is capable of fulfilling various tasks in human environment with its compact and light weight structure, wide and functional arm movements and improved walking technology. With the new, intelligent, real-time and flexible walking strategy, i-WALK, ASIMO can change direction while walking and running and can interact with the environment simultaneously (Hirose and Ogawa 2007-1). ASIMO is used by many research groups worldwide for human-robot interaction, learning and decision making based artificial intelligence and many other research topics.

In 1998, The Ministry of Economy and Industry (METI) started the Humanoid Robot Project (HRP) in Japan to use humanoid robots as labor force in daily life and various tasks. The first prototype, HRP-1, is a version of HONDA P3 humanoid robot, improved by means of control architecture (Hirose and Ogawa 2007-2). This prototype is 1.60 m in height, 120 kg in weight and includes 30 DOFs. National Institute of Advanced Industrial Science and Technology (AIST) developed their own control architecture to control biped locomotion and adapted it to a new version prototype named HRP-1S in 2001.

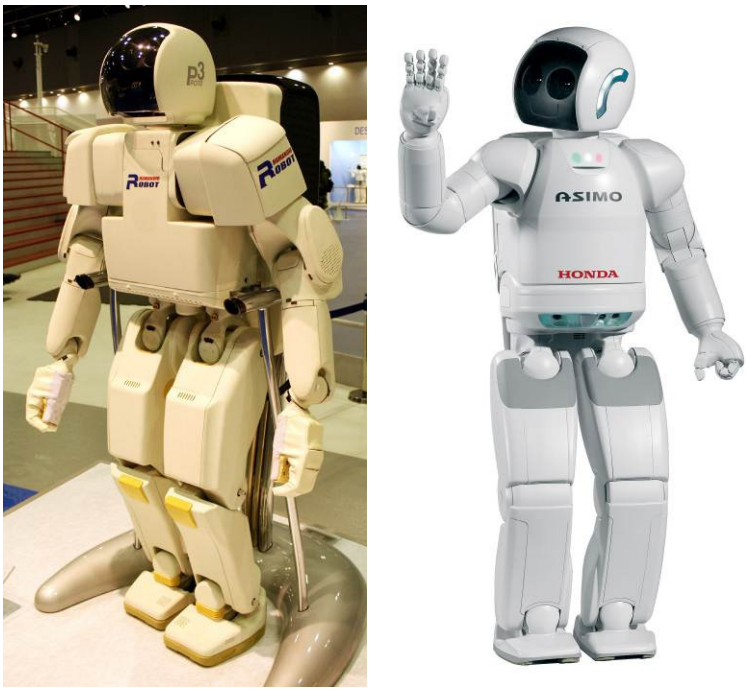

Figure 2.13 : HONDA Humanoid Robots: P3 and ASIMO

Successful experimental results were obtained with this robot in 2003 in driving industrial vehicles and maintaining elderly care. The studies on the second laboratory platform of AIST, HRP-2, is carried out on leg module HRP-2L, arm module HRP-2A and prototype HRP-2P. With the development of these modules, the new laboratory platform HRP-2 was obtained with a lightweight and compact structure (1.54 m, 58 kg). This prototype is widely used in humanoid robot research area. The next prototype of AIST, HRP-3, had a water and dust proof mechanical and electrical structure. This allows fulfilling tasks under rough conditions and open-air weather conditions. In order to extend the handling and working capabilities of previous prototypes, HRP-3 was equipped with new hand and wrist designs (Kaneko et al. 2008). HRP-2 and HRP-3 humanoid robot prototypes are shown in Figure 2.14. In 2009, AIST introduced HRP-4C that has the dimensions and appearance of a young Japanese female (Figure 2.15). The robot is 1.58 m in height and 43 kg in weight. The motion of this robot is organized by a combination of HRP walking control technology and a motion-capture system to mimic typical human motions. The last humanoid robot prototype of AIST, HRP-4, announced in 2009 (Figure 2.15), is also designed with a lightweight structure and slim body appearance. In this prototype, the main improvements are the use of optimized and cost-reduced mechanical components and the adoption of OpenRTM-aist - an open source robotic technology middleware. These humanoid robots are planned to realize tasks like providing maintenance of industrial machines, protecting houses and offices, using industrial vehicles, taking care of elderly people and cooperating with humans in working areas (Hirose and Ogawa 2007-2).

Figure 2.14 : HRP 2 (left) and HRP-3 (right)

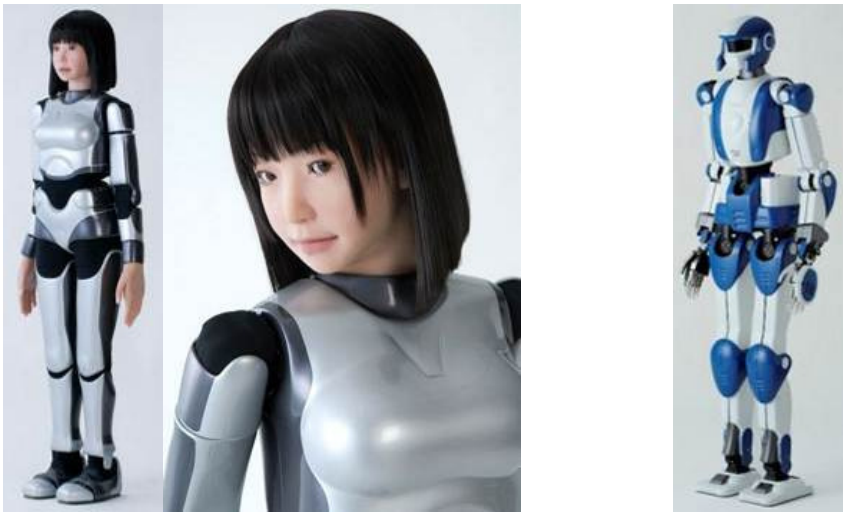

Figure 2.15 : HRP-4C (left) and HRP-4 (right)

In 2006, PAL robotics introduced their first humanoid robot platform REEM-A. The humanoid robot was 1.70 m in height and 40 kg in weight. It has 30 DOFs which enable it to mimic human behaviors. The aim of the company was to develop a service robot in human shape and proportions. The next humanoid robot platform of PAL Robotics, REEM-B, was announced in 2008. New humanoid robot platform had 41 DOFs, a weight of 60 kg and a height of 1.47 m. The continuous operating time of the humanoid robot was extended to 120 minutes from 90 minutes. Another improved skill of the robot was the 12 kg payload capacity of its hands. It was able to walk with a velocity of 1.5 km/h and interact with humans by the help of its cameras, ultrasonic sensors, force/torque transducers and laser range measurement units. REEM-A and REEM-B (PAL Robotics 2010) are shown in Figure 2.16.

CBI and ATR-DB2 of SARCOS Company are other successful humanoid robot prototypes. These prototypes of SARCOS's humanoid robot project are designed and built for the purpose of mimicking the ability required in human motions and computational brain functions. This project is developed by JST (Japan Science and Technology Agency), ICORP Computational Brain Project and ATR Computation Neuroscience Laboratories. CB prototype is a hydraulically actuated bipedal humanoid robot which weighs 92 kg and has a height of 1.575 m (Cheng et al. 2007) (Figure 2.17). Experimental studies carried out in this project are aimed at understanding the biological facts of bipedal walk and designing control algorithms based on computational brain functions. Main goals of the project are maintaining a stable bipedal walk, stabilizing balance and controlling physical interaction. Gravity compensation

techniques enable the robot to adapt and react to external forces. Full-body balance is realized via force control algorithms.

Figure 2.16 : Humanoid robot platforms of PAL Robotics: REEM-A (left) and REEM-B (right)

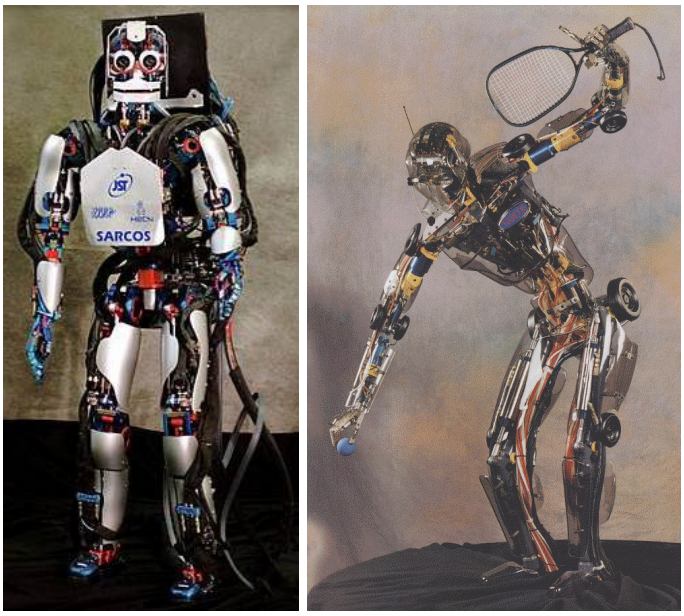

Figure 2.17 : SARCOS Humanoid Robots: DA ATR DB2 and CB-I

In addition to human-size full body humanoid robots, many successful down-sized humanoid robot platforms are developed. In 2000, Sony presented a kid-size full-body humanoid robot named SDR-3X (Sony Dream Robot) which has 24 DOFs, 0.5 m length and 5 kg weight (Ishida et al. 2001). Although the robot is mentioned as an entertainment robot, it is capable of walking stably, sitting on the ground, standing up from the ground, kicking a ball, dancing with different rhythms, recognizing sounds and colors and many other difficult tasks by its advanced control technology. The improved version of SDR-3X, SDR-4X, is improved by ground adapting locomotion control strategy, a sensor system for perceiving the external environment and a human-robot interaction capable body structure (Kuroki et al. 2003).

Sony QRIO (SDR-4XII) is announced as the first running bipedal humanoid robot (with a speed of 23 cm/sec) in 2005 (Figure 2.18).

Kid-size humanoid robot HOAP-2 which is 50 cm in height and 7 kg in weight is designed and built by Fujitsu Automation Ltd. in order to develop bipedal walking and human-robot interaction control algorithms (FUJITSU 2004). In addition to the above explained abilities, HOAP-2 is capable of fulfilling full-body motion required tasks such as autonomously standing up from the ground and performing martial arts. Some of other successful humanoid robot projects can be listed as HOAP-3 of Fujitsu, PINO of Japan Science and Technology Cooperation, MAHRU-3 of Samsung, DARwIn OP of RoMeLa (Figure 2.18), humanoid robot prototypes of Inaba et.al., KHR of Kondo Kogaku, HRP-2m of General Robotix and VisiON4G of VSTON (Yokoi 2007).

Figure 2.18 : Sony QRIO, Fujitsu HOAP-3, MAHRU-3 Samsung, DARwIn OP of RoMeLa

Chapter 3

3. A SURVEY ON BIPEDAL WALKING ON UNEVEN SURFACES

Research efforts on bipedal walking on uneven terrain can be categorized in three groups. Studies in the first group address surface irregularities, usually in the form of small height variations of a few centimeters or mild slope changes of a few degrees, distributed in an unstructured way on the walking surface. The second group concentrates on regular inclined planes, typically with slopes steeper than considered in the first group. The third category specializes on climbing or descending stairs. In the following, a survey on the first two research categories, which are closely related to the focus of this thesis, is presented.

In this survey, special attention is paid to the sensing capabilities required for the walking controllers. Also, the survey explores whether the reported control schemes depend on prior knowledge about the walking surface or not. An important term used in this context is blind walking. Blind walking refers to the locomotion without a priori knowledge about the surface topology and without range sensing capabilities (i.e. without being equipped by laser range sensors, ultrasonic sensors or cameras exploring the ground profile below or ahead). Even in the presence of topology sensors, reliable blind walking ability is an asset, since range sensor data and vision based measurements can be corrupted due to vegetation on natural ground and illumination conditions, respectively.

Results on bipedal walking on surface irregularities are reported by many researchers:

In 1994 Yamaguchi, Takanishi and Kato proposed a compliant foot structure and a controller to modify lower limb joint positions adapt to walking surface irregularities which are at most 11 mm in height (Yamaguchi, Takanishi and Kato 1994). Kajita and Tani presented a Linear Inverted Pendulum Model (LIPM) based approach for the walk of the biped robot Meltran II on known but rugged terrain (Kajita and Tani 1996-1). In Kajita and Tani (1996-2), they extended their work by mounting an ultrasonic ground surface detector to

Meltran II to sense the ground profile on-line. The use of reflex-like reaction control to alleviate tripping and slipping phenomena on rough surfaces is investigated in Boone and Hodgins (1997). Sugahara et al. applied a virtual compliance based control method for the locomotion on typical human living environment and obtained experimental results with the robot Waseda Leg 15 (Sugahara et al. 2003). In 2006, a special shoe system is integrated to the next-version Waseda University bipedal robot, Waseda Leg 16RII (Hashimoto et al. 2006). This shoe, equipped with linear solenoid actuators at its four corners, keeps a stable four point contact on irregular surfaces. A more recent robot shoe design of the same university incorporated photo sensors at the four foot corners to detect the distance between the foot and the ground surface (Kang et al 2010). The shoe, named Waseda Anthropomorphic Foot No 2, was integrated to the robot WABIAN-2R. The distance information provided by the aforementioned sensors was used in the on-line modification of the foot landing orientation and height. The method enabled the robot to walk over surface irregularities of 20 mm height and to climb a slope of 7 degrees grade. Kim, Park and Oh reported their usage of a number of controllers to modify the biped walking reference to adapt to local and global surface irregularities. The full-body humanoid KHR-2 was used in their experiments to demonstrate the performance of their proposed scheme on irregularities of a maximum 2 degrees slope (Kim, Park and Oh 2007). Hirukawa et al. employed a contact wrench based approach and applied resolved momentum control to keep the support foot or feet in contact with rough terrain and justified their results by simulations with a model of the robot HRP-2 (Hirukawa et al. 2007). In a following study (Harada et al. 2009), HRP-2 made its first steps in a rocky cliff scenario on rough terrain modeled in 3D in computer environment and known to the robot controller. Although the robot lost its balance after a few steps, this work provided a proof of concept for online applicability of an algorithm where the step and hand contact planning was carried out via a search algorithm which considers kinematic and dynamic constraints, in a full-body fashion.

Intensive research has been conducted on bipedal walk on regular inclined planes too:

Zheng and Shen worked on the walking transition from an even surface into an inclined plane with no a priori knowledge of the position and grade of the slope. They computed the inclination on-line, via data from force sensors attached at the heel and toe of the robot SD-2. In Zheng and Shen (1988) and Zheng and Shen (1990) they assumed static walk and

developed controllers, based on this computation, for the transition and inclined surface walk modes. In the transition, a compliance controller is applied for the foot orientation. The transition is divided into modes defined by the positions of the feet relative to the flat and inclined portions of the walking surface and the foot inclination is changed by processing the present mode and force sensor information. Simulation studies with the model of the SD-2 were used by Salatian and Zheng in 1992 for artificial neural network based readjustment of an even-surface walking algorithm for walking on slopes. Reinforcement based learning schemes are implemented for minimizing the readjustment time and energy consumption in Salatian and Zheng (1992-1). The learning involved is called "static" since it takes place only at prespecified moments. The "dynamic learning" version of this work is presented in Salatian and Zheng (1992-2). In this work, learning was a continuous process, which took place while the simulated robot was walking. This method improved smoothness of the walk. Simulation results on grades of 15 degrees are obtained in both 1992 studies. In 1997, Salatian, Yi and Zheng implemented the two learning schemes (static and dynamic) on their experimental platform SD-2. The bipedal robot successfully walked on slopes with grades of 7 degrees (Salatian, Yi and Zheng 1997). The transition from even to sloped surfaces, however, is not addressed in Salatian and Zheng (1992-1), Salatian and Zheng (1992-2) and Salatian, Yi and Zheng (1997). Ono, Murakami and Ohnishi (1998) reported the method of null-space to estimate the ground slope (via the use of on-off nature touch sensors at the toe and heels of the robot feet) and to control the configuration of the robot. In their experiments, a bipedal robot successfully entered a 7.2 degrees slope after walking on an even surface. Shih and Chiou exploited statically stable walking in their algorithm for climbing slopes (Shih and Chiou 1998). They assumed that the terrain characteristics are known to the robot controller and they computed biped robot walking trajectories to keep the Center of Mass ground projection within the support polygon. Their experimental robot BR-1 entered and climbed an 18 degrees slope with this approach. Pratt et al. introduced the virtual model control idea for bipedal locomotion (Pratt et al. 2001). In this control approach, the effect of imaginary mechanical elements like springs and dampers are generated by actuator outputs. Juang (2002) presents simulation results on surfaces with unknown and arbitrary slopes of up to 20 degrees grade for a bipedal robot model which is assumed to be equipped with foot contact switches. A neural network based learning scheme is developed in this study to generate reference trajectories on

varying slopes. The proposed method utilizes three different neural networks for control, dynamics emulation and slope identification purposes. Simulation studies carried out with a 15 degrees slope are used for the justification of the proposed method. In Vundavilli and Pratihar (2009) soft-computing techniques are applied to generate dynamically balanced ascending and descending gaits on slopes. Vundavilli and Pratihar proposed a neural network (NN) and a fuzzy logic (FL) controller and tuned the parameters thereof by genetic algorithms (GA), which used a ZMP (Vukobratovic et al. 1990) based dynamic balance criterion as the fitness function.

The angle of the trunk with respect to the foot soles is used in a number of studies as a control variable to adapt to and walk on slopes. This angle can be generated by a dedicated pelvis pitch angle. For robots which lack this degree of freedom, Taşkıran implemented a method to generate the trunk pitch angle by the overall action of the leg joints (Taşkıran 2009). The joint angles are computed by inverse kinematics for a desired trunk pitch angle - termed "pitch tilt angle" in Taşkıran (2009) where the method was applied with a fixed angle reference at the walking control of the robot SURALP. In Taşkıran et al (2009), fixed pitch tilt references and control methods similar to the ones in Kim, Park and Oh (2007) are applied for the blind walking of the same robot. In this study, SURALP entered and walked on a 5% graded inclined plane. In Yılmaz, Seven and Erbatur (2010), the pitch tilt angle is redefined as the "virtual pelvis pitch angle" and a fuzzy controller (which uses sampled versions of the robot body pitch angle as an input) is designed to compute this reference angle. The fuzzy control scheme is verified by simulations where a full-dynamics model of SURALP walked onto a 10% graded slope. The 10% grade blind walking result is experimentally verified by Yılmaz with SURALP (Yılmaz 2010). In Yılmaz (2010), the method in Yılmaz, Seven and Erbatur (2010) is further enhanced by the definition of a "virtual roll tilt angle" and the addition of a similar fuzzy control action about the pelvis roll axis, too. The membership functions and rule strengths of the fuzzy controllers in Yılmaz, Seven and Erbatur (2010) and Yılmaz (2010) are designed only with approximate information about the grade of the slope and no a priori knowledge of the slope entry location is assumed. Similar inverse kinematics based approaches are presented in Ali, Uğurlu and Kawamura (2010) and Ali, Amran and Kawamura (2010), too. The lastly mentioned two studies consider only the walk on the inclined plane without the passage onto it from even floor and assume that the grade is known

to the robot controller. The known slope angle is set as a fixed reference for the trunk pitch angle with respect to the foot soles. Simulation results with 11 degrees graded slopes are reported in these works.

In Yi, Zhang and Lee (2010), a compliance based method is proposed for humanoid robots to walk over an unknown, uneven terrain. The swing leg ankle is controlled compliantly in the landing phase and joint encoders at the ankle are used to probe the ground surface at every touch-down. The local ground profile is estimated via an optimization approach. Tests with the humanoid robot Nao are reported to achieve successful walk on a surface with 6 degrees grade changes.

Passive dynamic walking (McGeer 1990) down-hill on shallow slopes has long been investigated by many researchers. Changing slopes pose a difficult problem for passive walkers since parameter ranges for their stability are quite narrow. Recently, a number of studies about the negotiation of changing slopes by passive walkers are reported. Actuation in a limited number of joints or limited magnitude actuation in all joints is applied in order to achieve walking on even floor and slope changes. Tan, Fu and Chen (2010) employed a Central Pattern Generator (CPG) and reflex based control scheme for a kneed compass gait walker with intermittent actuation at its hip joint to adapt to even floor and changing down-hill slopes. Adaptation to a down-hill 5-degrees slope is shown in the simulations. The span angle between the legs is the main parameter adjusted by this control method. Step length and the walking speed are changed on-line in the feedback linearization based control method in Hu, Yan and Lin (2010). A descent down stairs is simulated with a model of a fully actuated compass gait walker. In Iida and Tedrake (2010), a control approach that utilizes an open loop hip joint reference sinusoidal oscillator and “phase locking” mechanism is presented. The locking mechanism compensates the phase delays between robot dynamics and motor oscillations. The performance of this algorithm is demonstrated by walking experiments on a ground profile with 6.5% ascent and 4.5% descent slopes with a two-degrees-of-freedom hip actuated planar point foot biped robot. The same experimental platform is employed in Manchester et al. (2011), too, where Poincare surfaces and a receding horizon control approach is employed for the exponential orbital stability of a target trajectory. Experimental verification is carried out with a stair climbing scenario.

In a recent study (Seven et al. 2011), the author of this thesis proposed a fuzzy logic bipedal blind walking control system for entering and ascending inclined planes. Based on the ZMP stability criterion and the LIPM (Kajita et al. 2003), a walking trajectory is generated as in Erbatur and Kurt (2009) and Taşkıran et al. (2010). Independent joint PID controllers are employed to track joint position references obtained via inverse kinematics from the ZMP based Cartesian Center of Mass (COM) and foot references. In Seven et al. (2011), the angle of the robot body with respect to a vertical axis is termed the "body pitch angle" and the angle of the foot soles with respect to the body is called "foot pitch angle". The latter angle also specifies a reference plane which contains the polygon of the supporting feet. The average body pitch angle computed over a history of a finite number of samples is used as the input of a fuzzy logic system which computes the foot pitch angle online, to be applied as a walking reference modification. The ankle pitch joint angle references are further modified by a supplementary compliance controller to obtain stable contact with the ground. The performance of the method for entering and climbing slopes is verified by simulations with a model of SURALP, in a 15%-grade slope blind walking scenario.

Motivated by the performance of the simple and effective algorithm in Seven et al. (2011), Seven et al. (2012) proposes a similar fuzzy logic bipedal walking control system for entering, ascending and leaving inclined planes. The focus in this work is experimental. Seven et al. (2011) and Seven et al. (2012) contrast in that in the latter the ankle pitch torques (commonly measured by ankle-mounted torque sensors in humanoid robot applications) are used as inputs for the fuzzy controller, along with the average body pitch angle. In Seven et al. (2012), in order to test the proposed fuzzy control system, experiments are carried out with SURALP - a 29 DOF full–body human–sized bipedal humanoid robot designed and built at Sabanci University, Turkey (Erbatur et al. 2009-2). As another difference from the method in Seven et al. (2011), controller building blocks for impact absorption, foot early landing modification, foot orientation roll compliance (Erbatur et al. 2009-2) are included in the general walking control scheme too.

3.1. Contribution of the Thesis

Seven et al. (2011) and Seven et al. (2012) constitute the backbone of the thesis presented in walking controller design. Since it is an experimentally verified work, the lines of Seven et al. (2012) are followed mainly.

In the light of the literature survey presented above, the contributions of this thesis are as follows:

- Introduction of a variable orientation reference for the walking plane.

- Development of an online fuzzy parameter adjustment method for varying the reference walking plane slope in order to adapt to changing walking surface slopes.

- Experimental verification of slope entry, climbing and up-hill slope to even ground transition performances of the proposed fuzzy parameter adjustment method.

The proposed system has advantages in that it does not necessitate prior information of the terrain, nor relies on range sensor information for surface topology measurement. (It is a blind walking method.) Also, it does not necessitate the large amount of training work of machine learning based methods for the exploration of the terrain and establishment of control laws.

-Another contribution of this thesis work is the mechanical design and construction of the experimental humanoid robot SURALP.

The next chapter describes the humanoid robot SURALP with discussions on mechanical design, sensor system, control hardware, basic reference generation and control algorithms.

Chapter 4

4. THE EXPERIMENTAL HUMANOID ROBOT PLATFORM SURALP

In this chapter the humanoid robot SURALP is introduced with mechanical design and electronic integration aspects. Basic reference generation and control methods for the walk on even floor are discussed, too.

4.1. Mechanical Design and Manufacturing

Firstly walking simulation studies are carried out with a 12 DOF adult size biped leg model in a 3D full-dynamics simulation environment. (This environment is a newer version of the one presented in Erbatur and Kawamura (2003). It is improved in terms of the generality of the kinematic arrangements which can be simulated). Each leg housed 6 DOFs. The link dimensions, mass and inertia parameters are inspired from similarly sized biped robots. Walking simulations yielded joint torque and velocity demands, which were used in actuation and transmission mechanism selections. Various types of actuators and control strategies are used in humanoid robot prototypes in the literature. Research on usage of pneumatic and hydraulic actuators is still in continuation. Electric motors and reduction units matured as compact torque generators under precise servo control. These types of actuators and transmission elements are chosen and implemented in SURALP, too. The mechanical systems in a number of remarkable humanoid projects also make use of electrical motors and geared reduction systems (Figures 4.1-4.7).

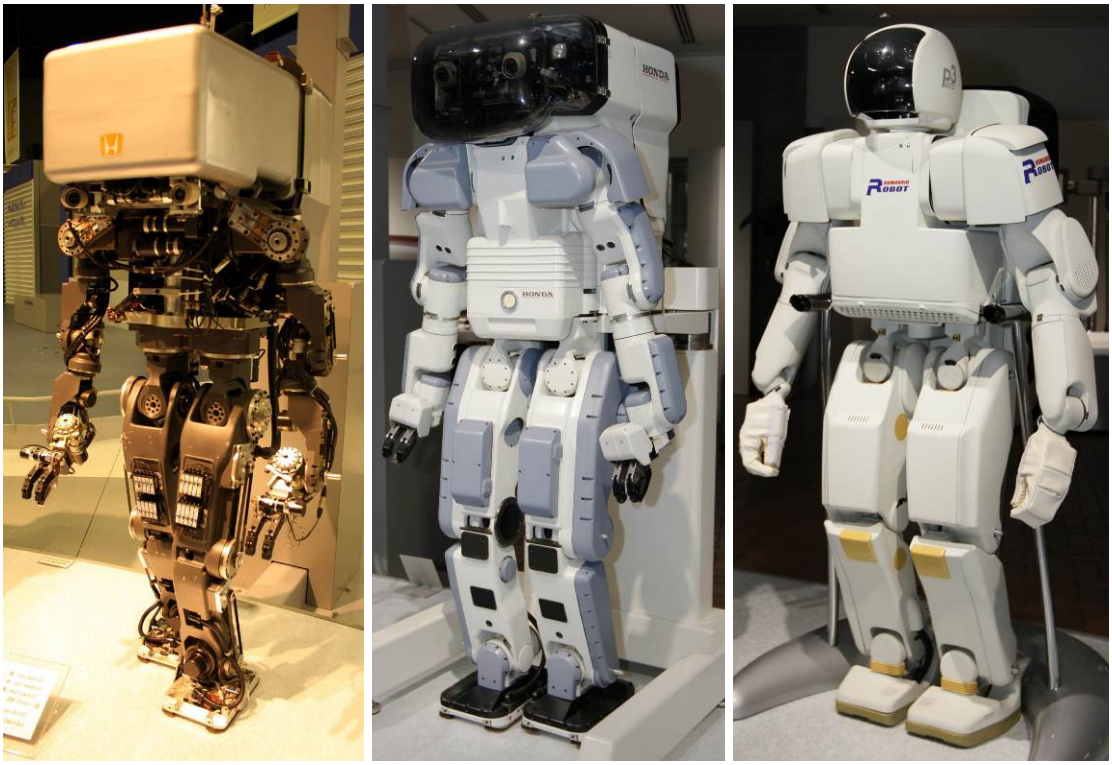

Figure 4.1 : HONDA P1 (left), P2 (middle) and P3 (right)

Figure 4.2 : Honda ASIMO

Figure 4.3 : Kawada Industries HRP 4

Figure 4.4 : Waseda University WABIAN-2

Figure 4.5 : Pal Robotics Barcelona REEM-B

Figure 4.6 : CNRS ROBEA Rabbit

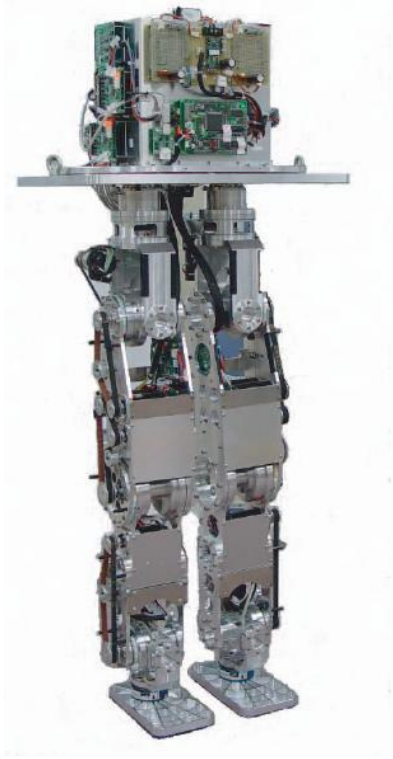

Figure 4.7 : Yokohama National University MARI-3

Maxon DC motors with the best torque/mass ratio available and compact, high gear ratio, zero backlash Harmonic Drives are considered to be the main components of actuation system. High Tension Drive (HTD) timing belt and pulley mechanisms are utilized to transmit the output torque of motors to the reduction units. HTD mechanisms are compact and allow gear ratio increases too. According to the speed and torque analysis made through the developed full-dynamic simulation environment, Harmonic Drive HFUC Series 14, 17, 20 and 25 sizes with 100, 120 and 160 reduction ratios, Maxon DC Motors with 70, 90 and 150 Watts output power, HTD-3M timing belt and pulley mechanisms are considered to be suitable and sufficient for predicted humanoid robot design. Including the chosen motors and reduction units, a 3D bipedal walking robot leg module model in human proportions with 12 DOFs is designed. This design is shown in Figures 4.8 and 4.9.

For the sake of testing the working performance and harmony of predicted DC motors and Harmonic Drives, a number of test setups are designed and manufactured. 3D Models and technical drawings of designed test setups are shown in Figures 4.10-4.15.

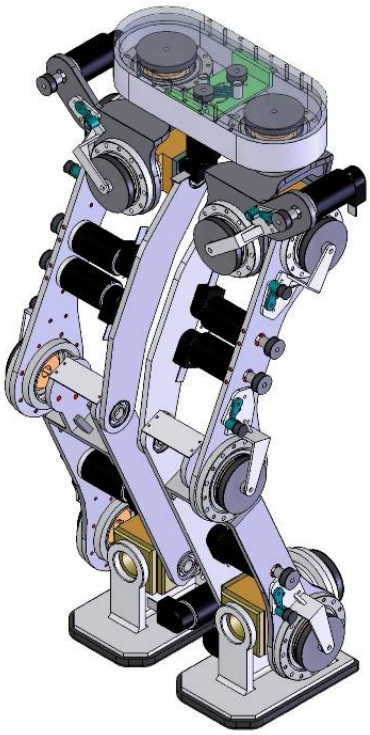

Figure 4.8 : Bipedal walking robot leg module preliminary design isometric view

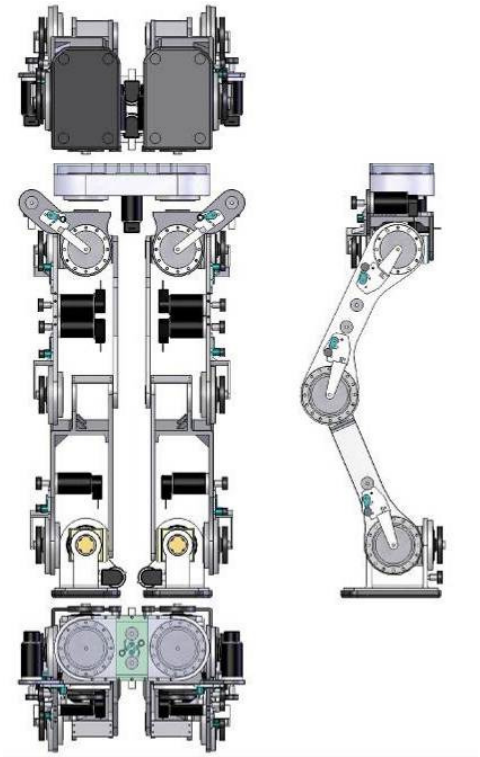

Figure 4.9 : Bipedal walking robot leg module preliminary design draft with 4 views

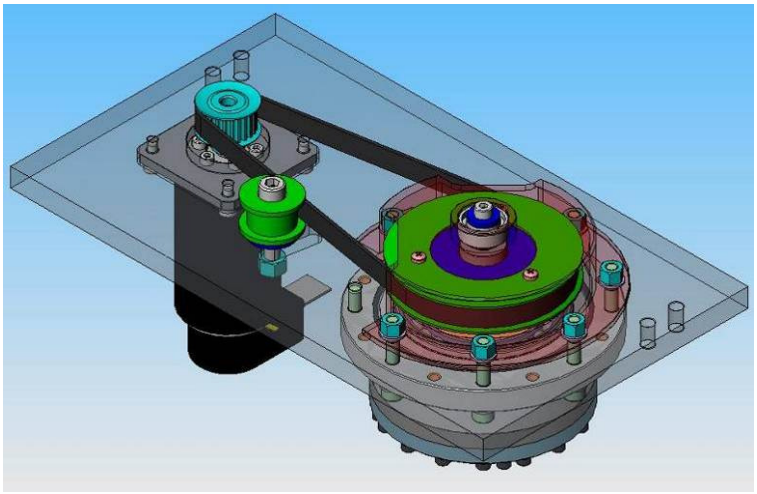

Figure 4.10 : 150 W Maxon DC motor and HFUC 25 series Harmonic Drive setup model

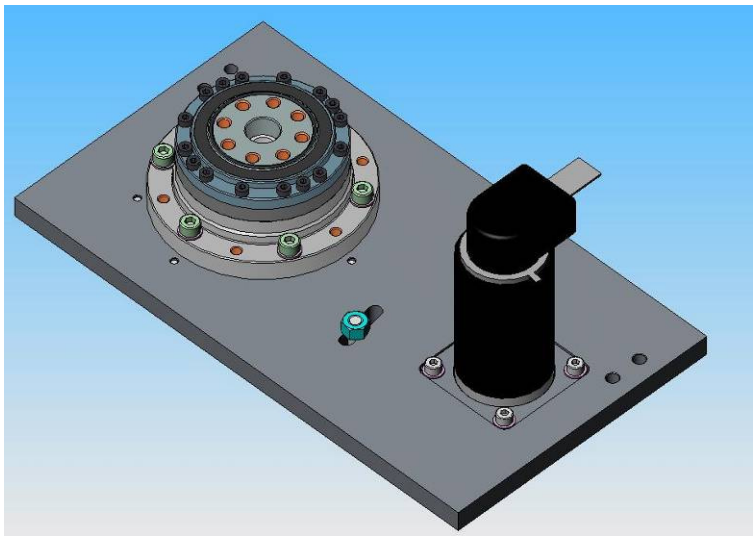

Figure 4.11 : 150 W Maxon DC motor and HFUC 20 series Harmonic Drive setup model

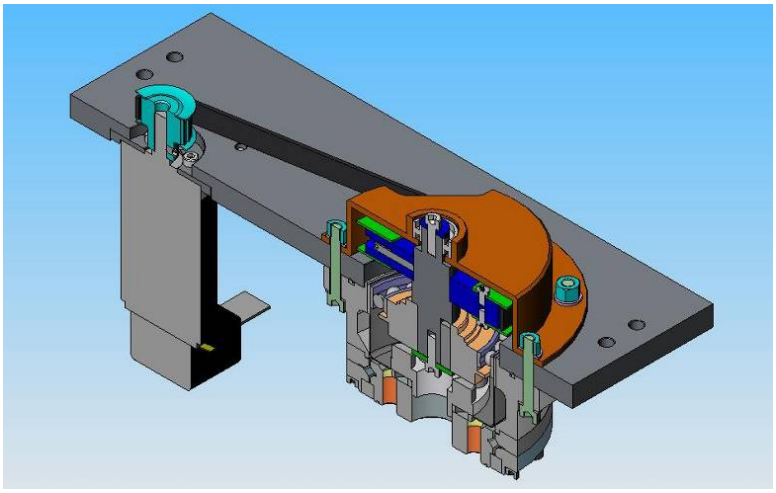

Figure 4.12 : 150 W Maxon DC motor and HFUC 25 series Harmonic Drive setup model

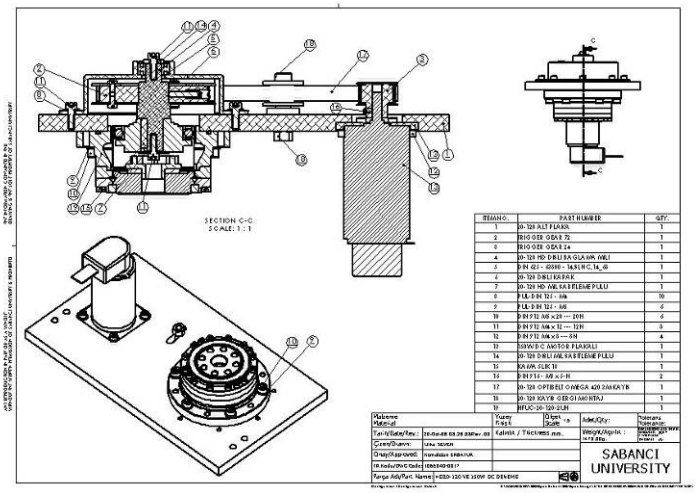

Figure 4.13 :150 W Maxon DC motor and HFUC 20 series Harmonic Drive setup technical drawing

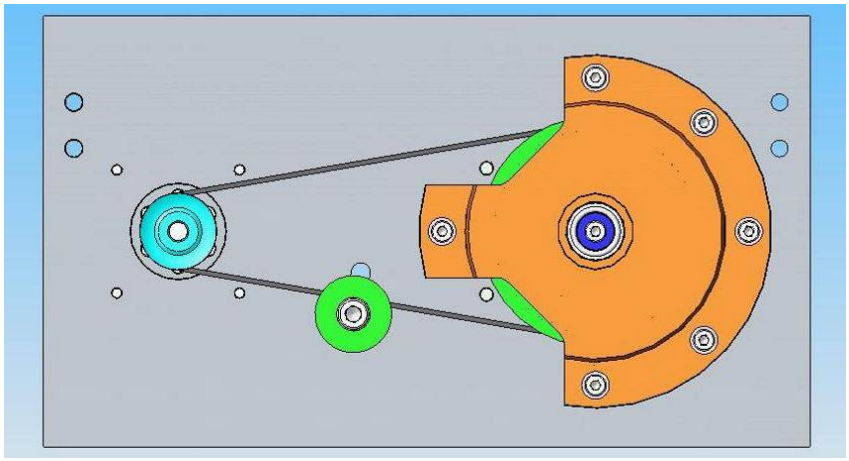

Figure 4.14 : 150 W Maxon DC motor and HFUC 20 series Harmonic Drive setup model top view

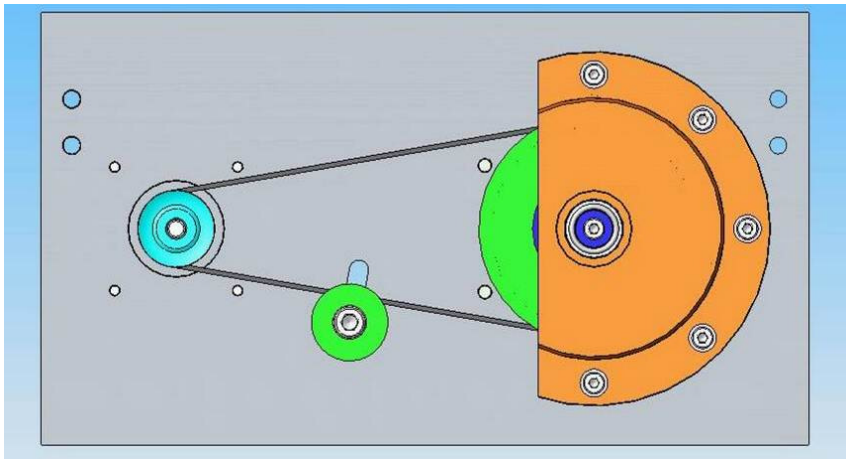

Figure 4.15 : 90 W Maxon DC motor and HFUC 20 series Harmonic Drive setup model top view

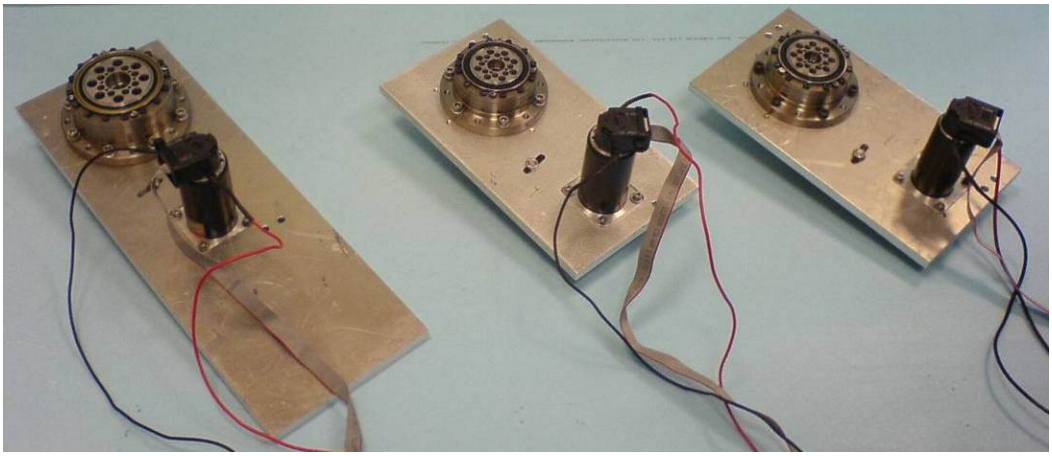

Figure 4.16 : Manufactured performance test setups (front sides with Harmonic Drive and motor detail)

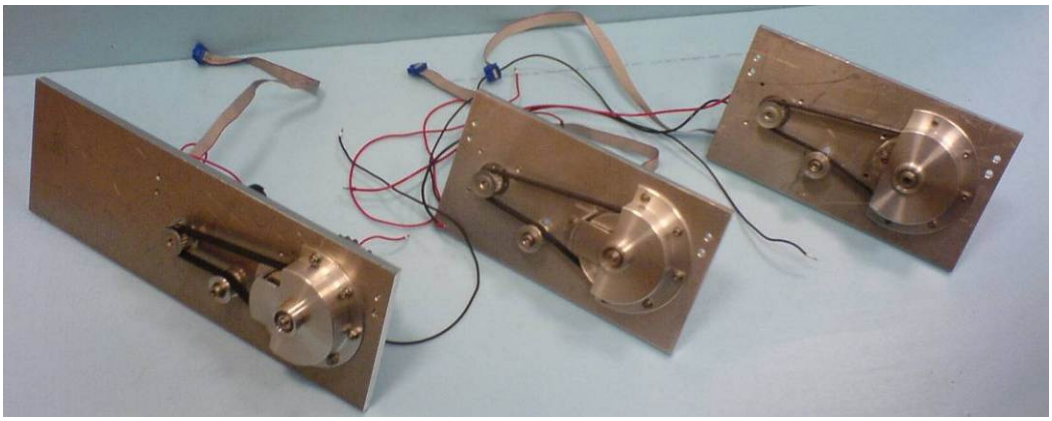

Figure 4.17 : Manufactured performance test setups (back sides with belt-pulley mechanism details)

Manufactured test setups with Harmonic Drive reduction units, Maxon DC motors and timing belt-pulley mechanisms are shown in Figures 4.16 and 4.17.

Investigating the advantages and disadvantages of designed test setups, the possible combinations that will be used in the humanoid robot are determined and modified according to related joint structures and prespecified torque and speed criteria. Using the actuation torque requirements obtained via simulation and the test results, the final actuation systems are selected. A combination of two motors is used at knee joints where the maximum torque is needed.

A secondary 3D design of a humanoid robot leg module with human proportions is developed with the integration of the selected actuation systems. CAD model is developed in SolidWorks environment. All components such as motors, reduction units, belt-pulley

mechanisms, fasteners, mechanical components and electrical components are modeled identical to originals. Ready-to-use 3D models are obtained via vendors and online CAD libraries when needed.

Typical walking motion angle requirements of a human are taken into consideration in the design. Joint and link designs are developed in such a manner to avoid component collisions. 6 Axis force/torque sensor integrations at the feet are implemented. Developed design is shown in Figures 4.18 and 4.19. Details of the waist design connecting the legs are shown in Figure 4.20.

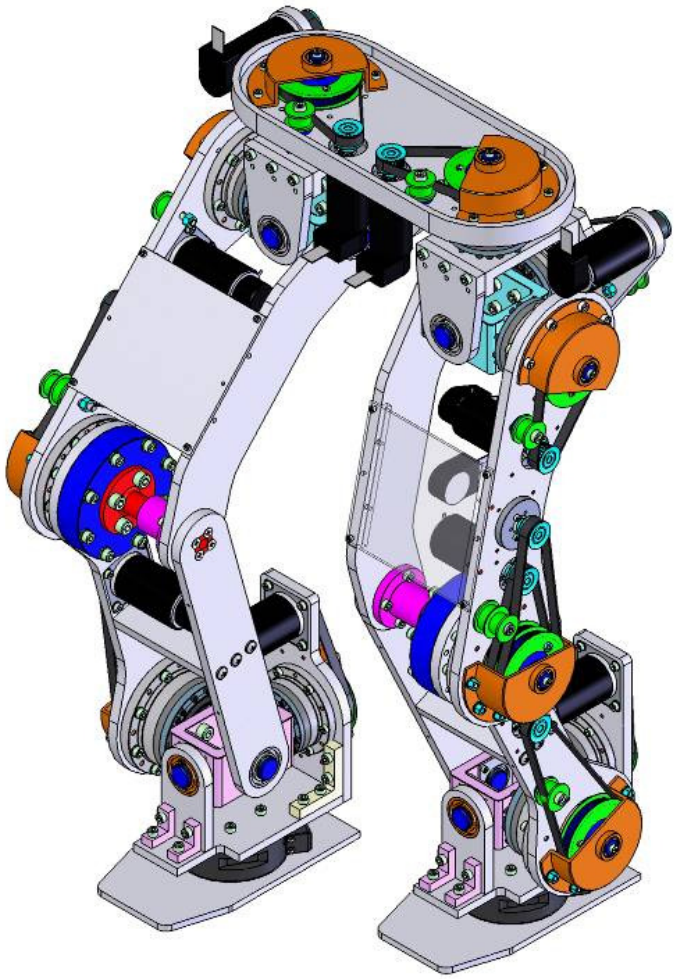

Figure 4.18 : Humanoid robot leg design

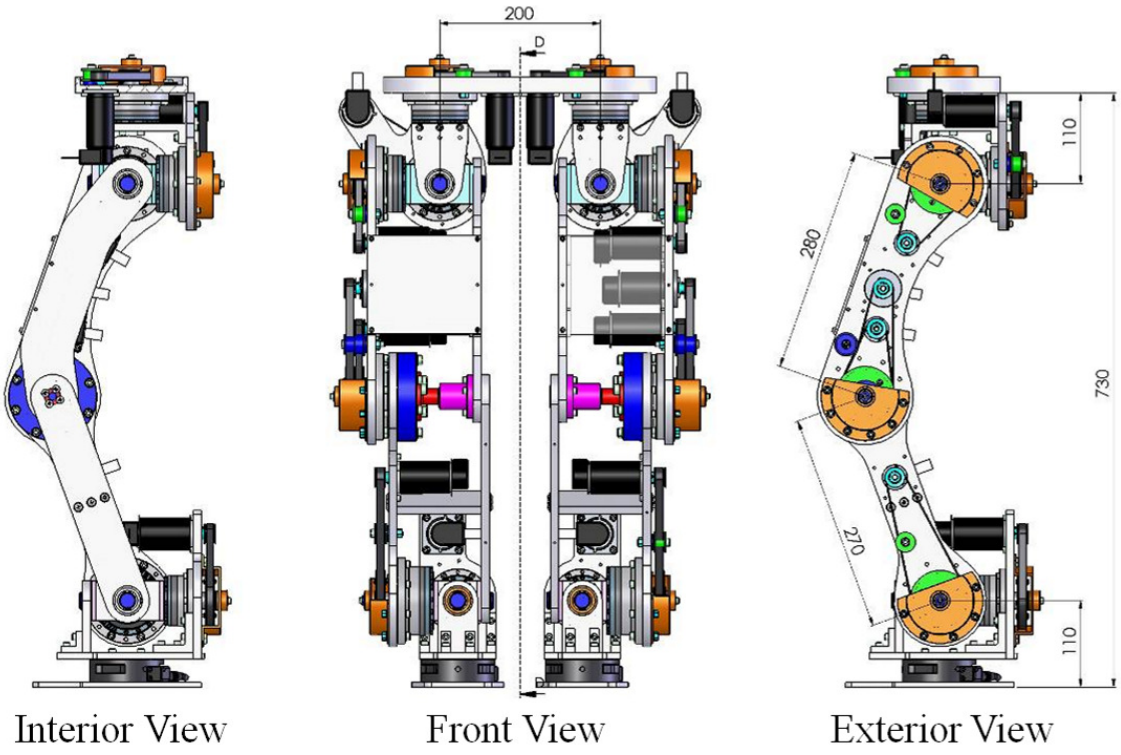

Figure 4.19 : Humanoid robot leg design interior, front and exterior views with dimensions

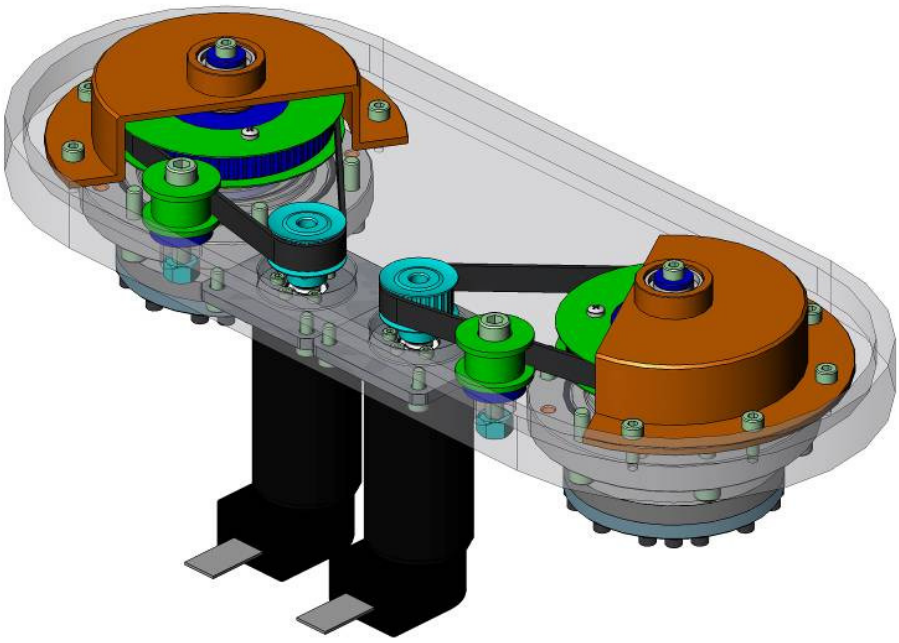

Figure 4.20 : Isometric view of waist design

The 3D models of six links' designs are given in Figures 4.21-4.26. The link designs in the figures belong to the left leg. Due to the symmetric relation between the legs, right leg link designs are not shown.

Figure 4.21 : Hip design isometric view

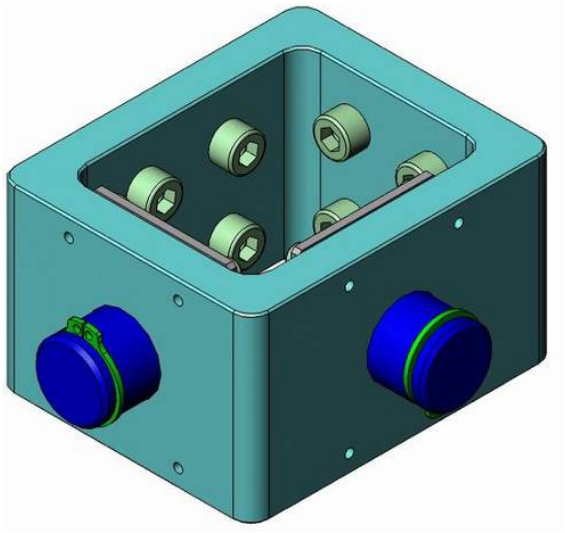

Figure 4.22 : Hip center design isometric view

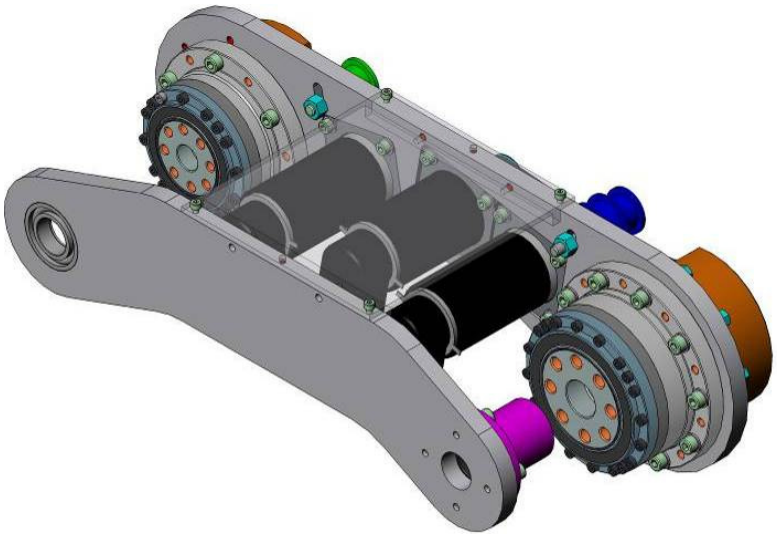

Figure 4.23 : Upper leg design isometric view

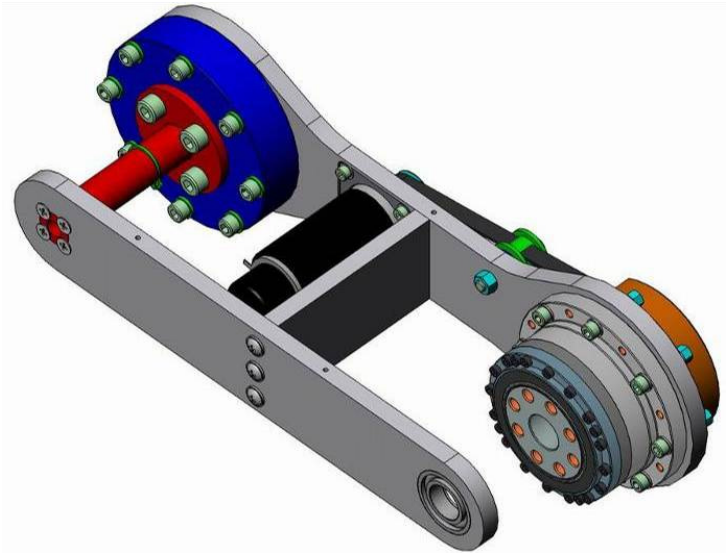

Figure 4.24 : Lower leg design isometric view

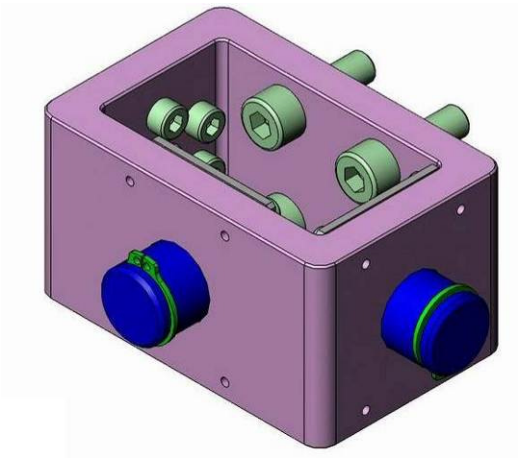

Figure 4.25 : Ankle center design isometric view

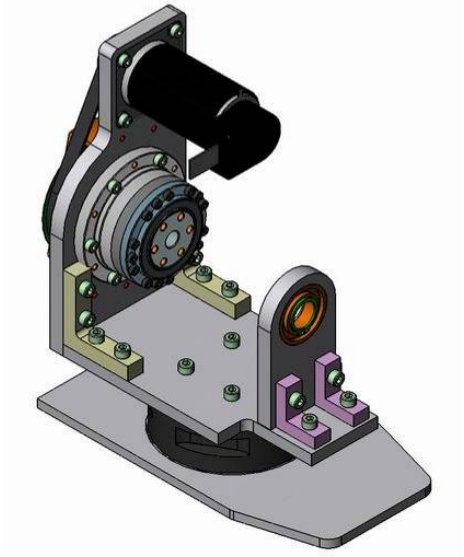

Figure 4.26 : Foot design isometric view

After this version of the leg design is completed, structural analysis is carried out to modify the components and acquire the final design. The contact force and torques between the links (applied at the joints) are obtained by running the Newton-Euler based full-dynamic simulation in inverse dynamics mode. These force and torque values are used as the inputs of structural analysis. Body position and orientation, joint angles, angular velocities, angular accelerations and ground contact forces are recorded during the walking simulation realized by the control strategy and reference generation methods in Bebek and Erbatur (2004). The obtained data are used as the inputs of inverse dynamics algorithm, and the forces and torques applied to a link by the previous and the next links are calculated. The forces and torques applied by the previous link are termed “lower” forces and torques. The forces and torques applied by the next link are termed “upper” forces and torques. For instance, lower forces applied at the lower leg link are applied by the upper leg and upper forces are applied by the ankle center. Upper and lower forces and torques on the links are expressed at Denavit-Hartenberg (DH) coordinate frames attached at the links. Structural analyses for all links are carried out through the stress, strain, displacement, deformation distribution results and factor of safety criterion is considered too. According to the analysis results, the most critical areas, by means of stress distribution, are in the upper and lower legs. Figures 4.27 and 4.28 shows the forces and torques applied at the upper leg link from its neighbors. Forces and torques applied at the lower leg are shown in Figure 4.29 and Figure 4.30.

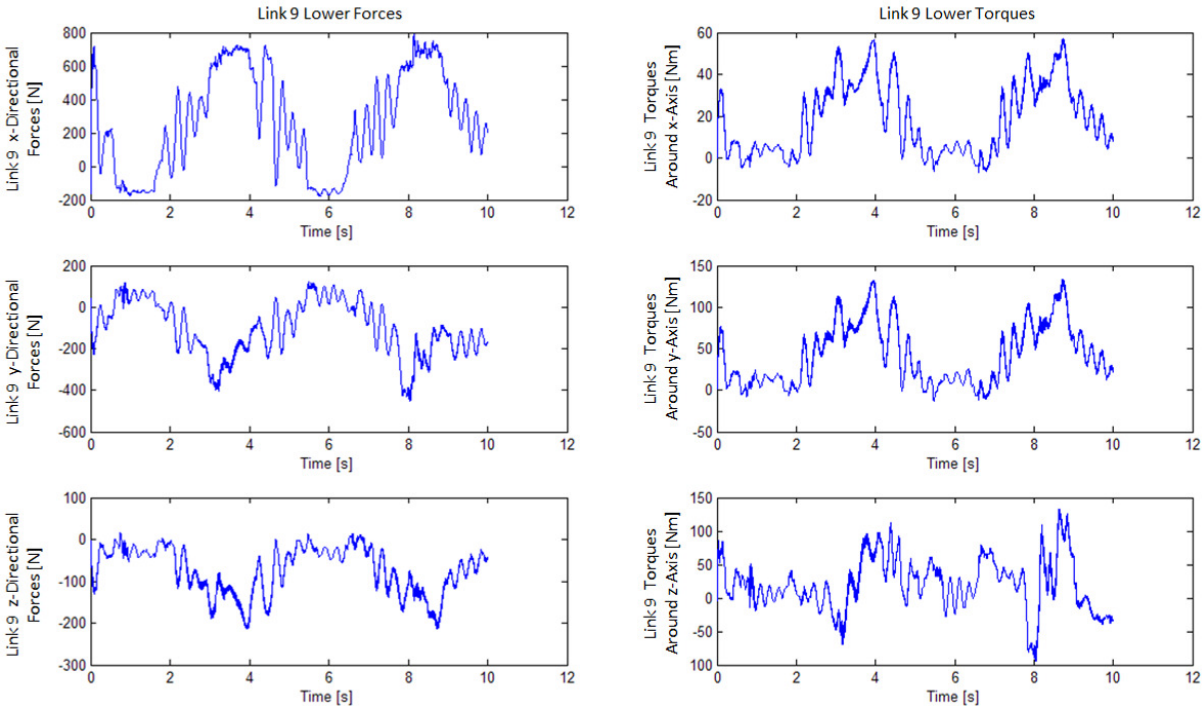

Figure 4.27 : Forces and torques applied at the upper leg from the hip center

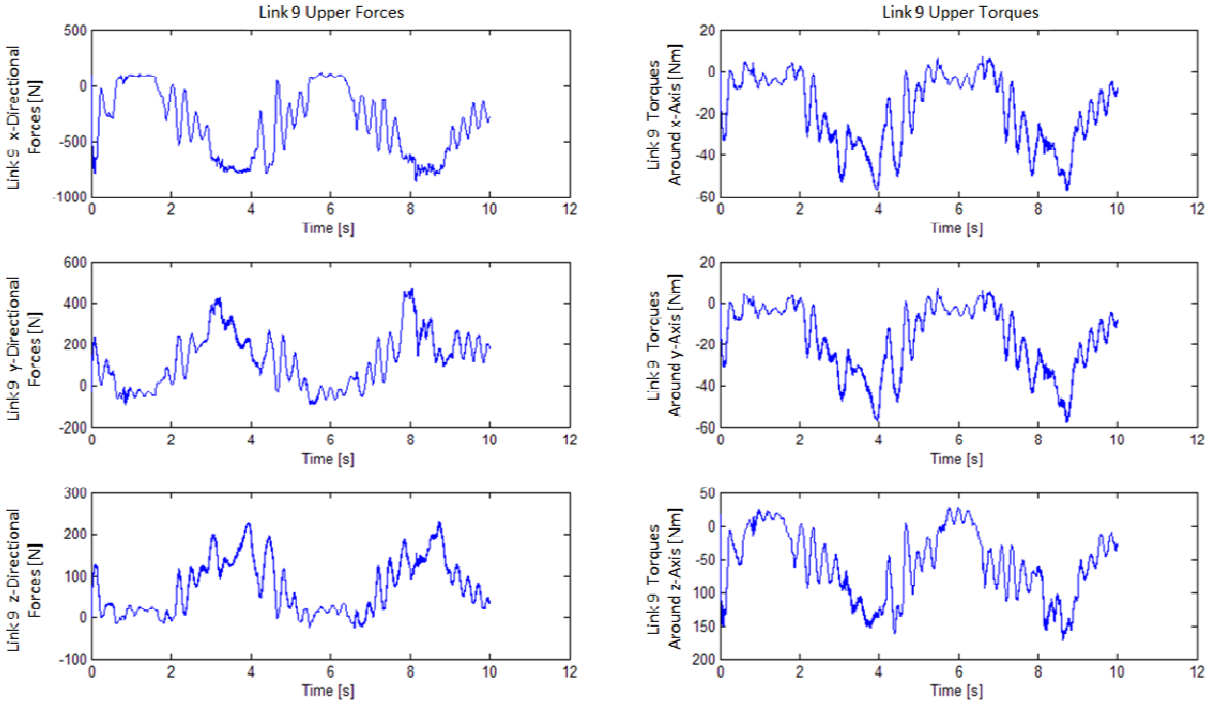

Figure 4.28 : Forces and torques applied at the upper leg from the lower leg

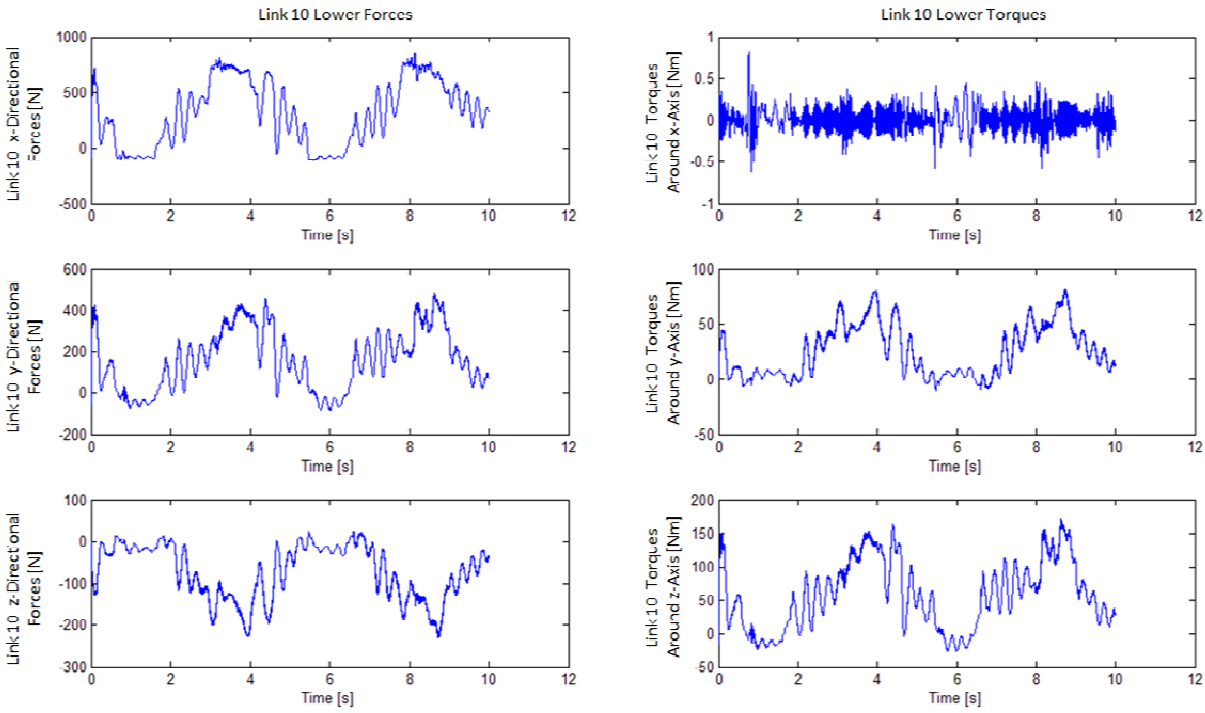

Figure 4.29 : Forces and torques applied at the lower leg from the upper leg

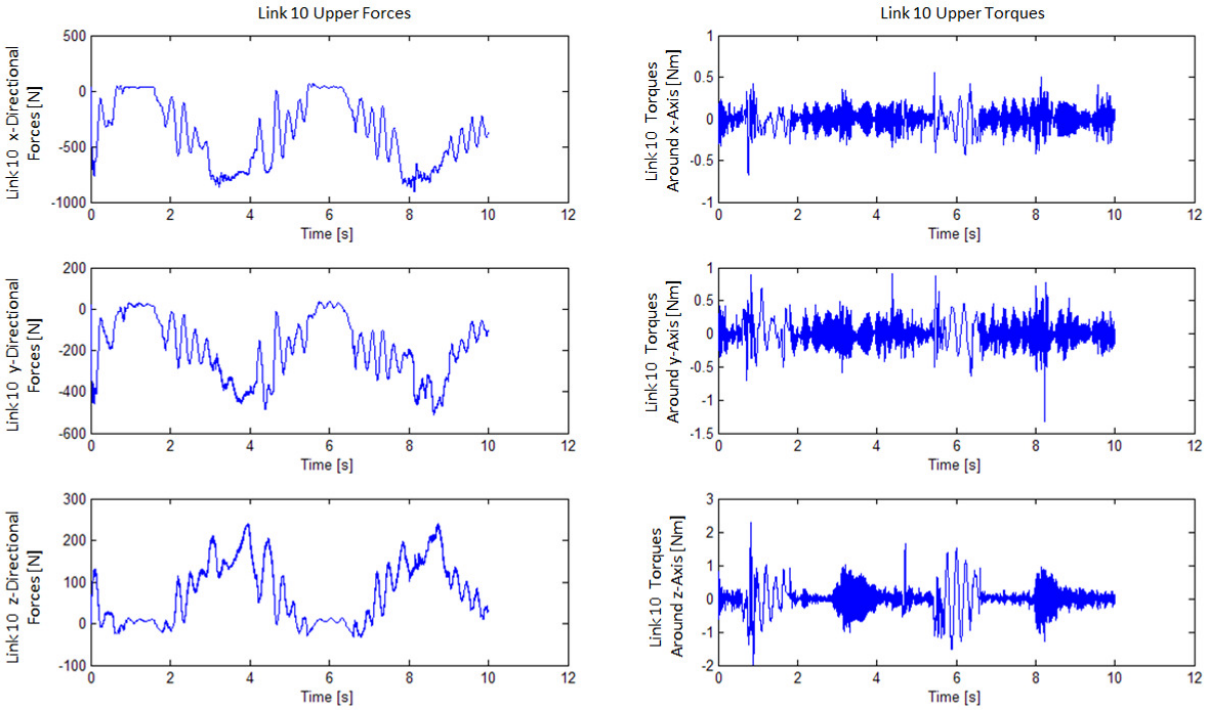

Figure 4.30 : Forces and torques applied at the lower leg from the ankle center

For the structural analysis of upper and lower leg constructions, the three part (side plates and a connecting plate) main frameworks shown in Figures 4.23 and 4.24 are taken into consideration.

The 3D modeling of these parts and assemblies are carried out with SolidWorks software. SolidWorks is chosen due to its user-friendly interface, wide help menu and capability of modeling each part separately, assembling them easily and drafting all models quickly. Structural analysis of constructions is realized via CosmosWorks 2007, the simulation module of SolidWorks.

In this study the reaction forces and torques from previous and next links applied at the joint points are taken as the maximum critical loads and static load analysis is carried out to check whether the factor of safety (FOS) criterion is above the threshold (A usually applied factor of safety is 1.5.) for required parts, or not. For two constraint options (from upper joint or lower joint), load definitions and mesh creation are defined as explained below.

1. "Study" Definition

After the creation of the models, an active study is defined according to analysis type (e.g. static, buckling, thermal, fatigue). In this study, static load analysis for required criteria is selected.

2. "Restraint" Definition

Restraint definitions are realized according to two scenarios, from the upper joint for the loads applied at the lower joint and from the lower joint for the loads applied at the upper joints. According to these scenarios upper leg receives loads from hip in the first analysis then receives loads from lower leg in the second analysis. Lower leg receives load from the upper leg in the first analysis then receives loads from the ankle in the second analysis. Structural analysis is carried out for both upper and lower leg in this manner.

3. "Force" Definition

The loads applied at the leg structures are defined with their application points, directions and amounts. The applied loads include not only the maximum forces in three axes, but also the resultant force and the torque it causes. The reason of this strategy is to optimize

the construction dimensions for all possible load combinations and design a structure durable enough to carry all loads.

4. "Material" Definition

7075 alloy aluminum (used in aerospace and aircraft industries) is selected as the construction material due to its high quality, lightweight and machining ease.

5. "Mesh" Definition

CosmosWorks is a finite elements method (FEM) based analysis software. In FEM method, the structure to be examined is separated into finite small particles. The loads are applied at the boundary intersection points of these particles, called "nodes". And the formed structure consisting of small finite particles is called "mesh". The loads applied to the structure are distributed to the related nodes and the final deformation at the desired location is calculated using the stress distribution. The quality and the precision of the analysis are directly proportional to the number of the nodes. However, increase in the number of nodes requires long calculation time because of the differential equations assigned for each node. For the construction of the mesh, various parameters are allowed to be adjusted in CosmosWorks software. In the analyses of upper and lower leg structures, the mesh quality is adjusted to the finest possible which creates nearly 270000 DOFs.

6. "Contacts/Gaps" Definition

The analyzed structures are connected via screws and nuts and therefore "Bonded" option is selected for the general contact between the components of the structures. The contact areas of screws and nuts are selected as the "contact pairs". These surfaces can lose their positions or orientations but not collide as connected with screws and nuts in real life. Moreover, the bearing connections placed in the side plates are fixed by "on cylindrical surface" option in order to maintain a realistic behavior. Thus the actuation torque is properly transmitted to the plate that it is connected.

7. Running the Defined Study

After all the parameters are defined properly, the analysis is executed. Analysis time depends on the number of input parameters and the complexity of the geometry and mesh.

8. Analysis Results

In this section the analysis results are explained for every static analysis scenario of upper and lower leg structures. The defined analysis parameters provide a situation that the actuation torque only effects the outer side plates and the actuation forces are distributed to both side plates homogeneously. By this way, the endurance and the stability of these structures are designed to match the demands of the walking experiments of the humanoid robot.

According to the quantitative results in the report, the maximum stress occurred in the structures is σ = 1.2452e+008 N/m^2. Since the yield strength of the chosen material is σ = 2.7572e+008 N/m^2, FOS is greater than 2. This means that the endurance of the designs is verified. As a result, it is justified that the designed leg structures are appropriate to carry a 50 kg upper body structure safely.

After the analysis is completed with CosmosWorks, a detailed report with parameters, inputs variables, graphical results and quantitative results is created by the program itself. Two analysis reports are generated for the scenario for the upper leg where it is fixed from the hip side and receives loads from the lower leg side and where it is fixed from the lower leg side and receives loads from the upper leg side. Similar analysis is also carried out for the lower leg and totally four analysis reports are generated which are used to confirm the endurance of the leg structure designs.

After the lower body (legs and waist) design is completed and confirmed, the next step in mechanical system design was the design and structural analyses of the arms (Figure 4.31). In the arm design, aluminum alloy molded parts are considered as an alternative to parallel plate structures used in the leg structure. The loads applied at the arms are considered as static loads like payloads carried in the hands for the structural analysis scenario. Structural analysis carried out in CosmosWorks 2007 environment indicated that the designed structure of the arms can front the determined requirements. Molded shoulder part is considered as the critical

part in the arm structure. The analysis structures of the arms are defined in a similar way to the leg analysis structures and successful results are obtained. With a static payload of 5 kg applied at the hands, FOS for the molded shoulder part is obtained as 1.97 (Figure 4.32).

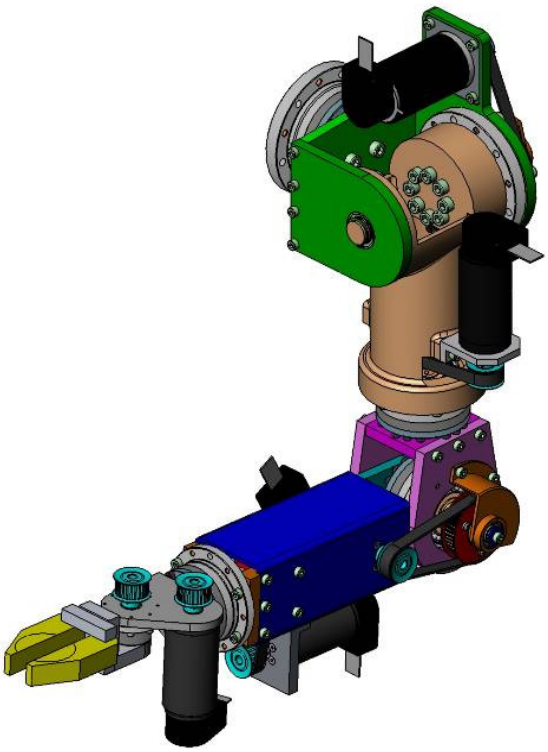

Figure 4.31 : Humanoid robot arm design

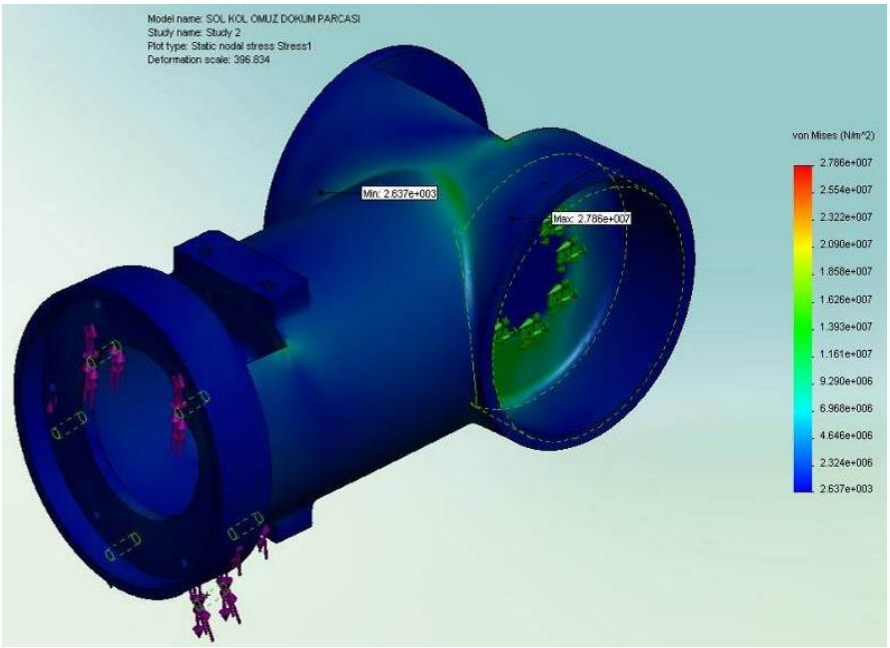

Figure 4.32 : Structural analysis for the left arm molded shoulder part indicated that the factor of safety is 1.97 for 7075 alloy aluminum material.

According to the planned guidelines of the humanoid robot project, the manufacturing process of the legs and waist of the robot are completed before the arms. Water-jet cutting and machining techniques are used to manufacture the designed parts. The assembly and integration of motors, reduction units and belt-pulley mechanisms followed. Figures 4.33 and 4.34 show this structure consisting of legs and waist with control electronics.

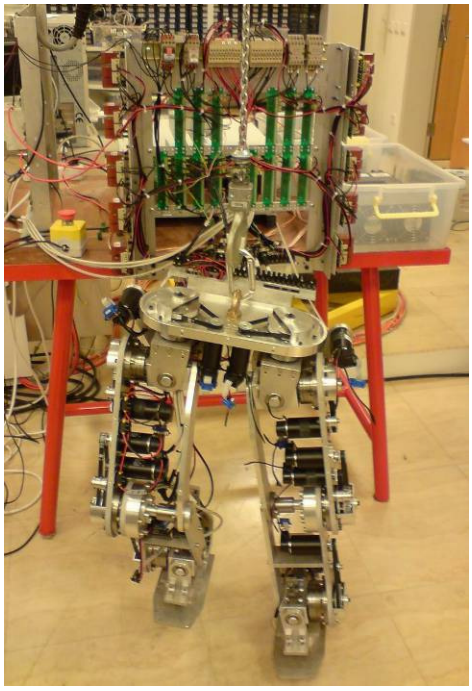

Figure 4.33 : Manufactured legs and waist assembly, front view

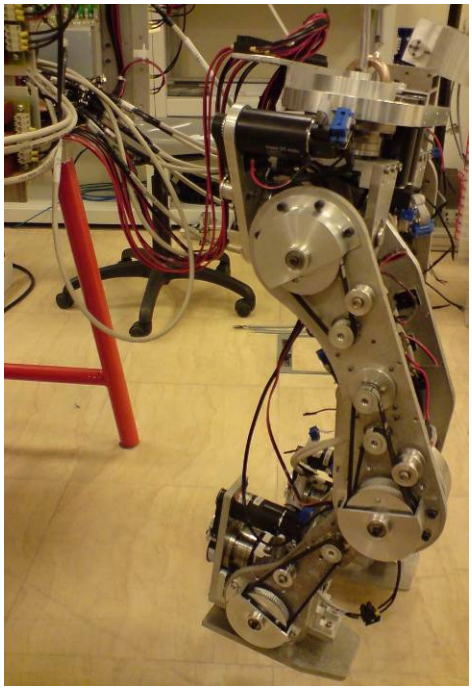

Figure 4.34 : Manufactured legs and waist assembly, side view

After the manufacturing of lower body, the neck and head structure is designed too. The neck is capable of rotating the cameras on board in a “pan-tilt” configuration. These joints are also driven by Maxon DC motors. Harmonic Drive gears and belt-pulley mechanisms are used as the reduction and transmission units. In addition, a skull structure is designed to obtain a human-like appearance and to cover the cameras. This system is shown in Figures 4.35, 4.36 and 4.37.

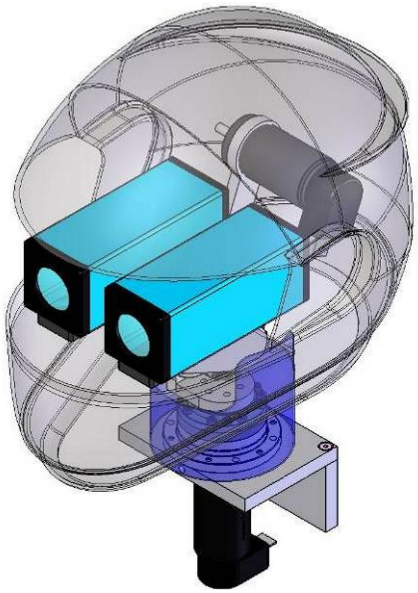

Figure 4.35 : Head and neck design CAD model – isometric view

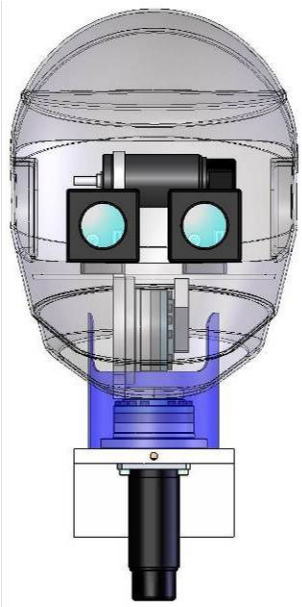

Figure 4.36 : Head and neck design CAD model – front view

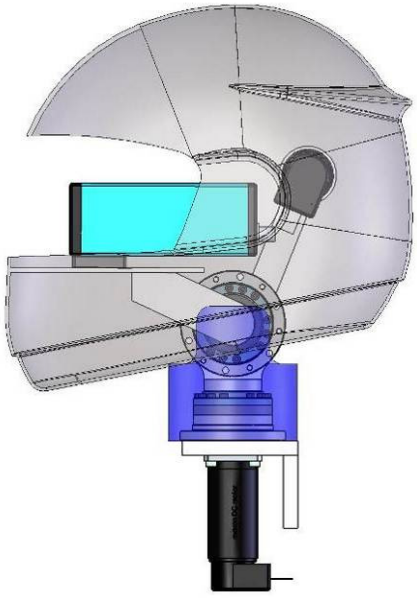

Figure 4.37 : Head and neck design CAD model – side view

After the completion of the leg design, the control system and lower body are combined with a preliminary upper body structure (Figures 4.38 and 4.39). Welded aluminum profile structure is used in the upper body. The humanoid robot is named SURALP as the abbreviation of **S**abancı **Ü**niversitesi **R**obot **A**raştırmaları **L**aboratuar **P**latformu (**S**abancı **U**niversity **R**obotics Rese**A**rch **L**aboratory **P**latform). The leg and upper body combination is called SURALP-L for the "leg module of SURALP". The parts of the arm structure are manufactured simultaneously.

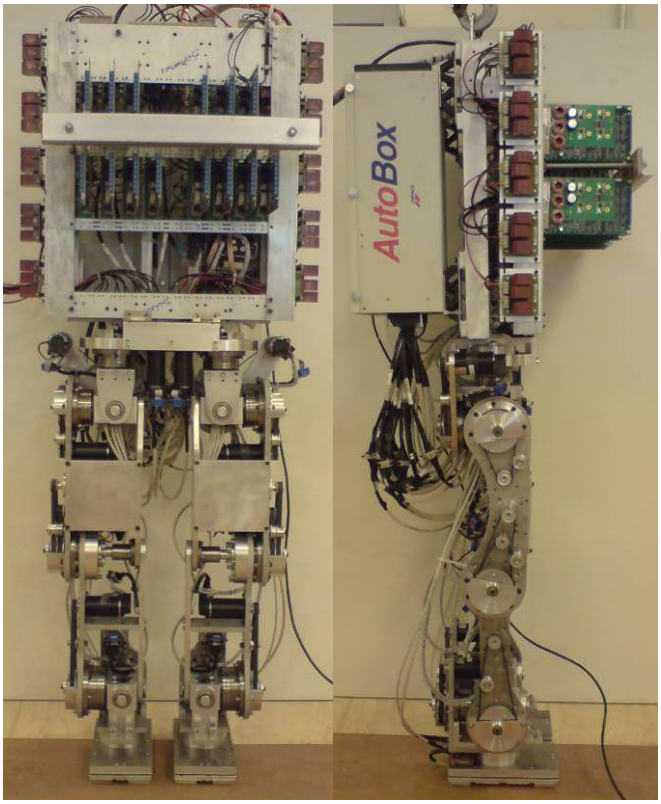

Figure 4.38 : Humanoid robot leg module SURALP-L with integrated control system, front and side views

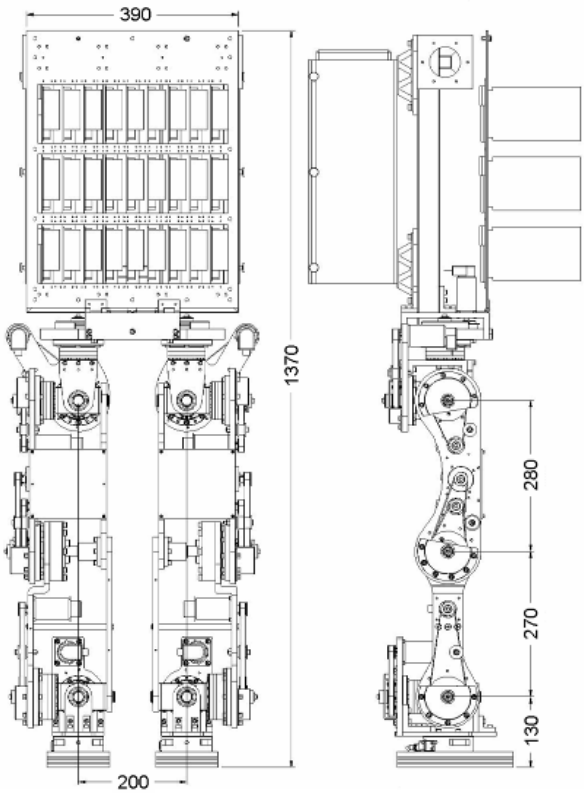

Figure 4.39 : Humanoid robot leg module and integrated control system – dimensions

The CAD model of the entire full-body robot is shown in Figure 4.40

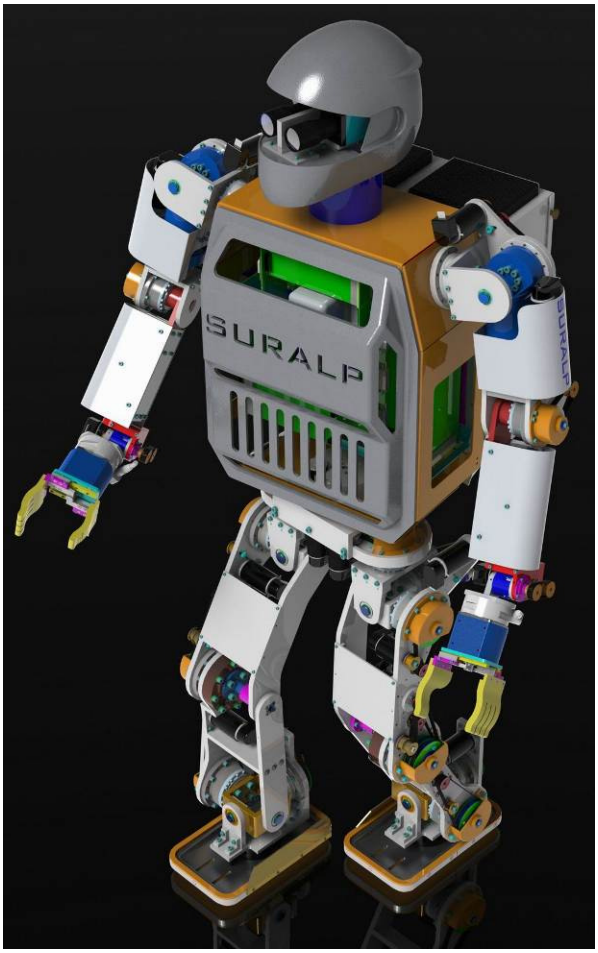

Figure 4.40 : SURALP design CAD model

The head and neck structure assembled to the upper body is shown in Figures 4.41-4.43.

Figure 4.41 : Pan-tilt joints of the manufactured neck mechanism

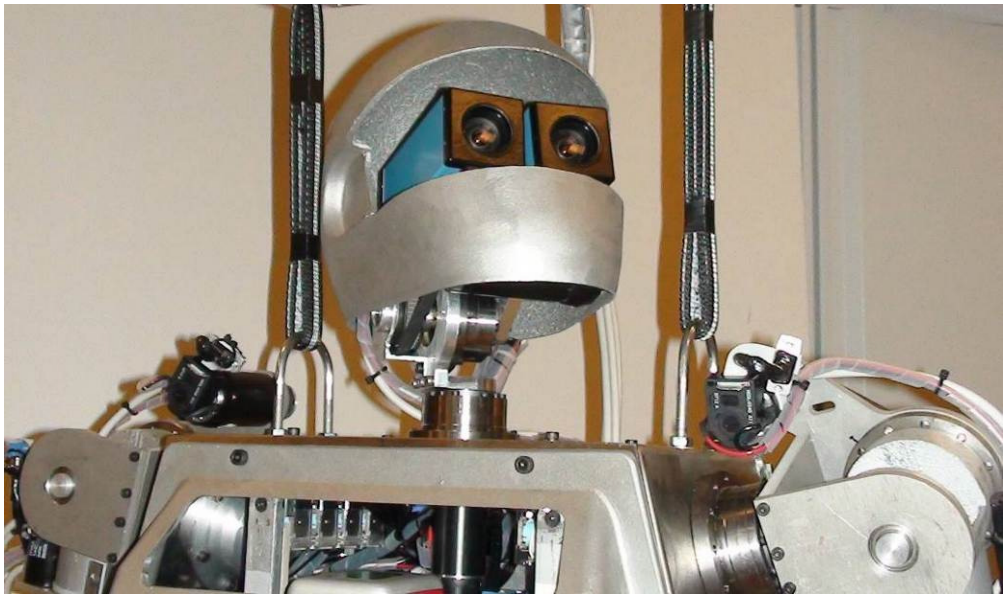

Figure 4.42 : Neck actuation system and head structure

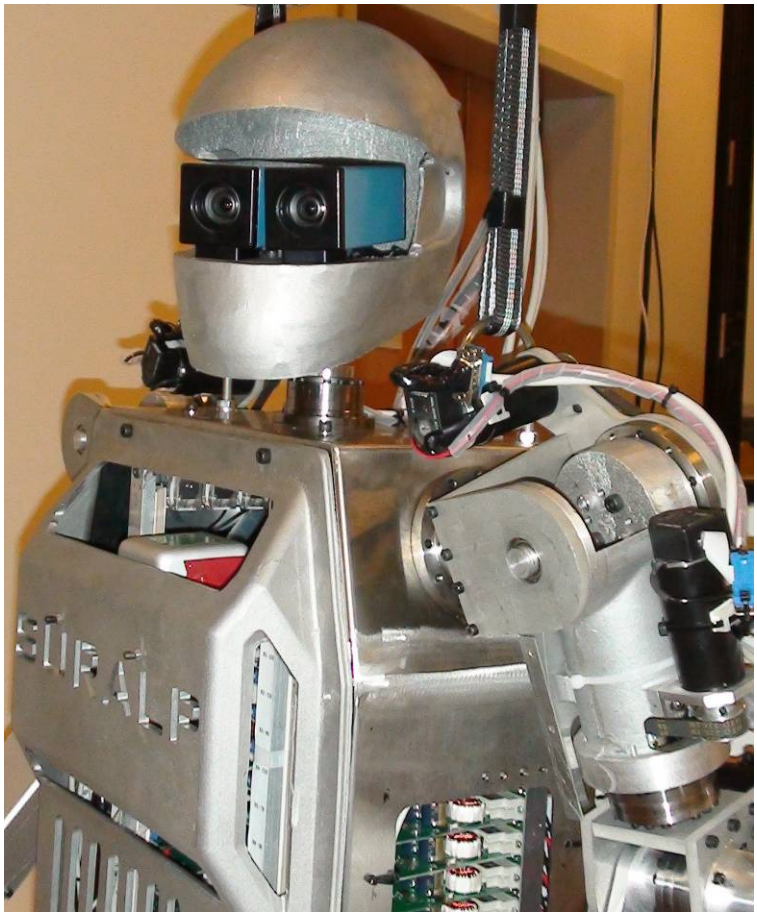

Figure 4.43 : Neck actuation system and head structure

The 6 DOF arms are manufactured via water-jet, milling, lathing, machining, sheet-metal bending and molding techniques. Figure 4.44 shows the assembled arm of the humanoid robot SURALP.

The robot hand shown in Figure 4.44 is designed and manufactured to allow the object manipulation and environmental interaction experiments. Figure 4.45 shows the rack-pinion based, linearly actuated hand's CAD model and a closed up view. The hands are designed in a manner like an industrial robot gripper to accommodate 1 DOF to hold and carry objects.

Figure 4.44 : 6 DOF arm and linear actuated hand structure

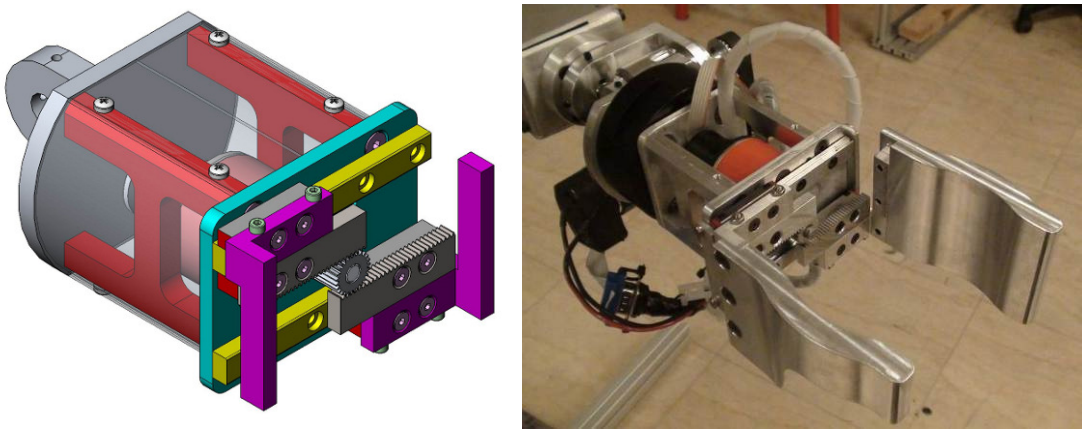

Figure 4.45 : Robot hand CAD model and closed up view

Figure 4.46 : Rubber foot sole

In order to absorb the ground reaction forces during walk, a multi-layered rubber structure and a molded rubber foot sole are designed, manufactured and integrated to the robot's feet. The molded rubber foot sole is shown in Figure 4.46.

In the final design, lower body, arms and the head are assembled on a stainless steel sheet metal bent and welded upper body construction. Figure 4.47 shows the sheet metal body construction. As seen in Figures 4.48 and 4.49, the upper body is connected to the lower body with a waist joint. The trunk is able to rotate. The final integration yielded the full-body robot SURALP. Figure 4.50 shows the research laboratory and the crane system which enables safe walking and environmental interaction experiments.

Figure 4.47 : Welded sheet metal upper body construction

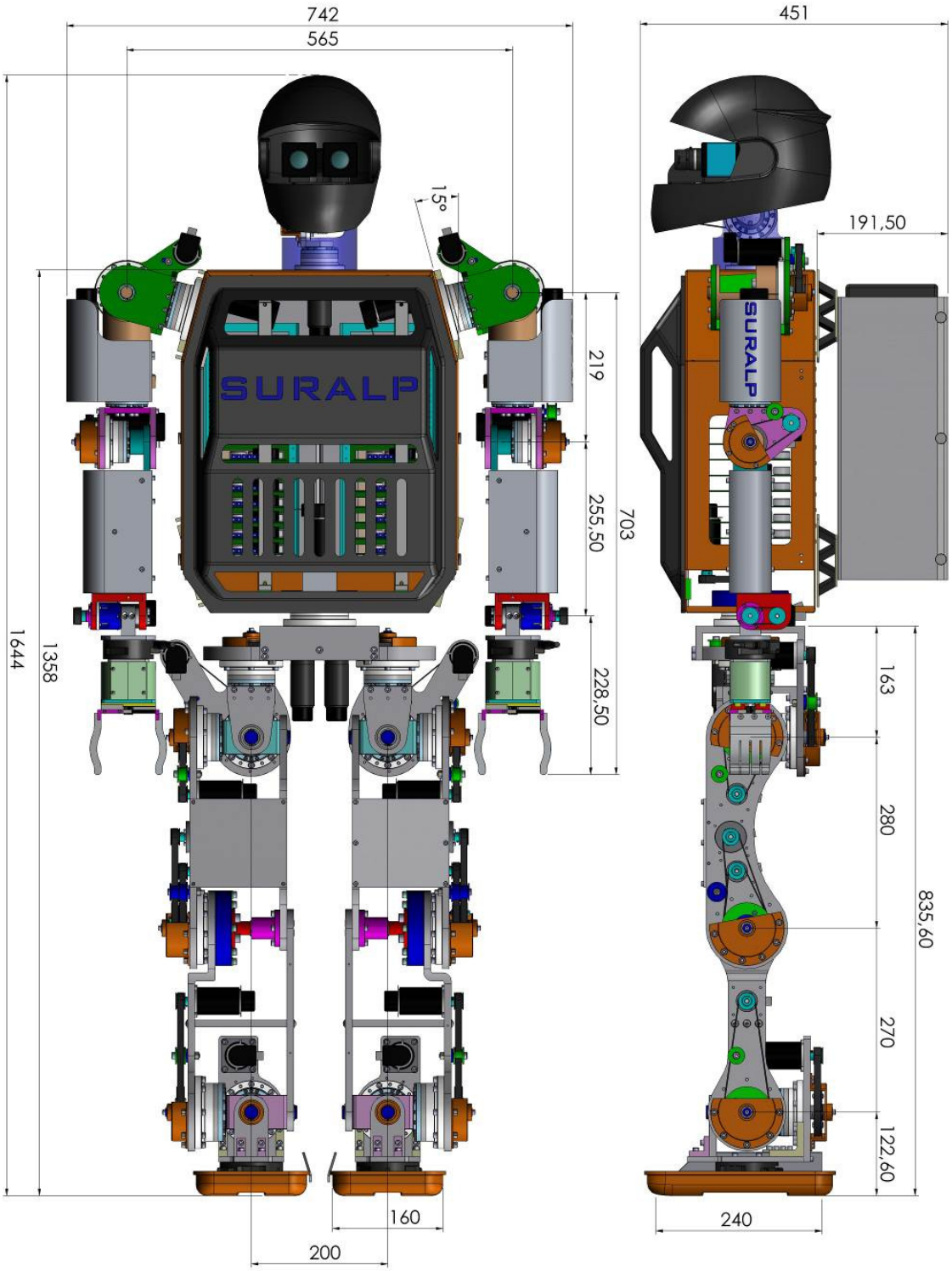

Figure 4.48 : SURALP Main assembly CAD model

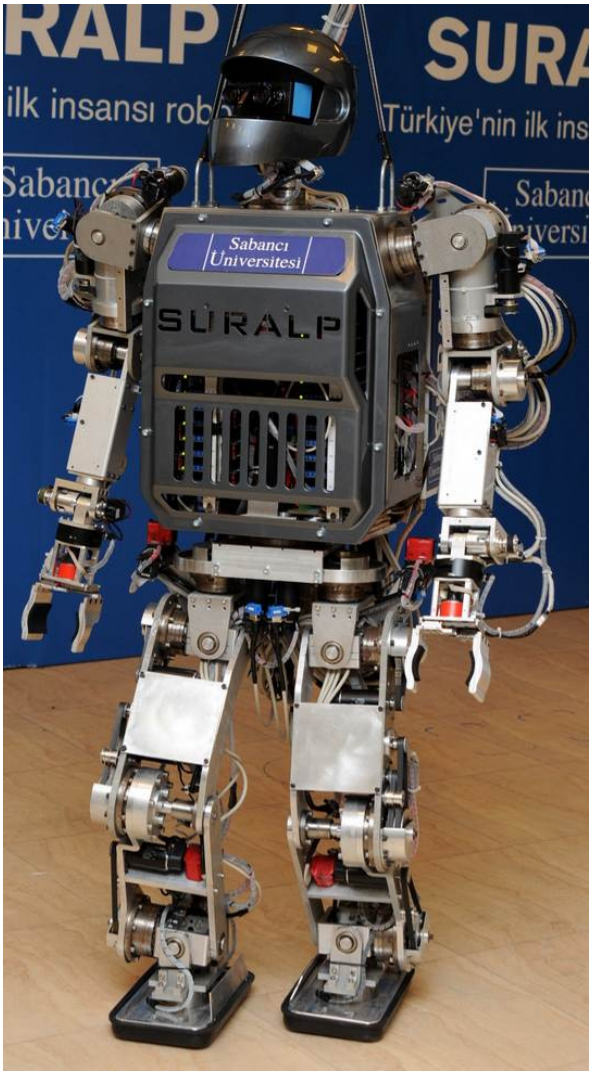

Figure 4.49 : The integrated SURALP

Figure 4.50 : SURALP, research laboratory and Cartesian crane system

Dimensions and weight data of SURALP are tabulated and shown in Table 4.1. Actuator, reduction and joint limit data are given in Table 4.2. The robot is designed in human proportions with 29 DOF, including 6-DOF legs, 6-DOF arms, 1 DOF hands, a 2-DOF neck and a 1-DOF waist. The weight is 114 kg. The kinematic arrangement of SURALP is shown in Figure 4.51.

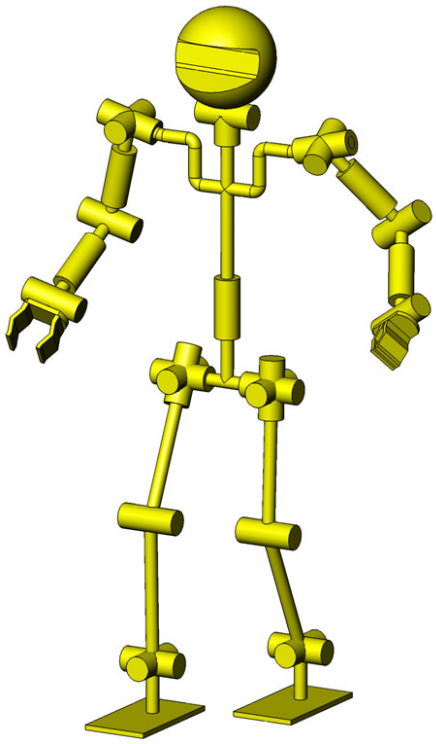

Figure 4.51 : The kinematic arrangement of the robot

Table 4.1 : Dimensions and weight data of SURALP

Upper leg length	280mm
Lower leg length	270mm
Ankle center to foot sole distance	124mm
Foot dimensions	240mm x 150mm
Upper arm length	219mm
Lower arm length	255mm
Robot weight	114 kg

Table 4.2 : Actuator, reduction and joint limits

Joint	**Motor Power**	**Pulley Ratio**	**Harmonic Drive Ratio**	**Joint Limits (°, mm)**
Hip-Yaw	90W	3	120	-50 to 90
Hip-Roll	150W	3	160	-31 to 23
Hip-Pitch	150W	3	120	-128 to 43
Knee 1	150W	3	160	-97 to 135
Knee 2	150W			
Ankle-Pitch	150W	3	100	-115 to 23
Ankle- Roll	150W	3	120	-19 to 31
Shoulder Roll 1	150W	2	160	-180 to 180
Shoulder Pitch	150W	2	160	-23 to 135
Shoulder Roll 2	90W	2	120	-180 to 180
Elbow	150W	2	120	-49 to 110
Wrist Roll	70W	1	74	-180 to 180
Wrist Pitch	90W	1	100	-16 to 90
Gripper	4W	1	689	0mm - 80mm
Neck Pan	90W	1	100	-180 to 180
Neck Tilt	70W	2	100	-24 to 30
Waist	150W	2	160	-40 to 40

4.2. Electronic Hardware

In this section, the electronic hardware of humanoid robot SURALP is presented in two main titles; sensory system and control hardware.

4.2.1. Sensor System

Sensor system of SURALP consists of four main components:

i) incremental motor encoders
ii) force/torque sensors
iii) inertial sensors
iv) CCD cameras

Motor positions are measured via 500 pulses per revolution (ppr) optical incremental encoders. Two types of force/torque sensors are used. First one of them is the 6 axis force/torque sensors placed at the ankles and wrists. Control strategies based on measurements of ground reaction force and tilting torques at the ankles (explained in the following sections), are realized via these sensors. The second force sensing system is obtained via a combination of Force Sensing Resistors (FSR) and signal processing boards. FSR sensors with dimensions of 40 mm x 40 mm x 0.5 mm are placed at four corners of feet to measure the forces. This system enables us to calculate the total ground reaction force and the torques at the ankles due to the ground reaction forces. Also it can be used as an indicator to understand which corner(s) of the feet are in contact with the ground. Force sensor platform placed at feet are shown in Figure 4.52. The shown sensor platform is similar to the system described in Erbatur et al. (2001) and Erbatur et al. (2002). The sensor platform described in this thesis includes rubber

components and multi-layer rubber structures instead of stiff kestamid layers presented in related references.

The robot is equipped with a gyroscope, an accelerometer and an inclinometer. The data obtained from these inertial sensors are directly transmitted to the controller and used in control algorithms as inputs. The sensor system of SURALP is tabulated in Table 4.3 with the ranges and locations of the sensors.

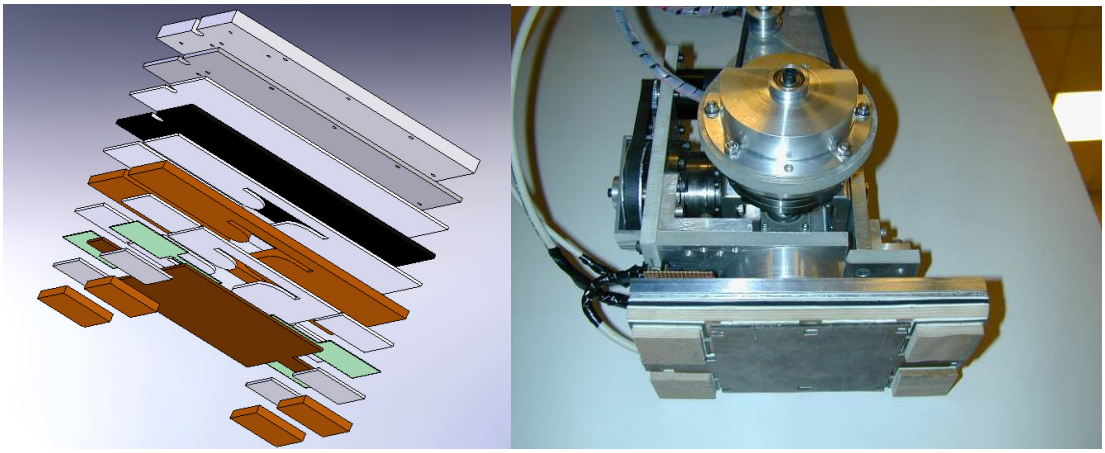

Figure 4.52 : Foot sensor platform layers. The uppermost plate of 10 mm thick aluminum is the main foot support plate. The details of the foot sensor platform are shown in the CAD model at the left.

Table 4.3 : Sensor System of SURALP

	Sensor	**Channels**	**Range**
Joints	Incremental optic encoders	1 channel per joint	500 pulse/rev.
Ankles	Force/Torque sensors	6 channel Per wrist	± 660 N (x, y) ± 1980 N (z) ± 60 Nm (x-y-z)
Torso	Accelerometer	3 channel	± 2 G
	Inclinometer	2 channel	± 30 deg
	Gyroscope	3 channel	± 150 deg/s
Wrists	Force/Torque sensors	6 channel per ankle	± 65 N (x, y) ± 130 N (z) ± 10 Nm (x-y-z)
Head	CCD Camera	2 channel	640x480 30 fps

4.2.2. Control Hardware

Main component of the control hardware is a dSpace modular digital signal processing system. Processor unit is the DS1005 board. All control algorithms run on this board. Seven DS3001 incremental encoder boards are able to communicate with 35 joint encoders. 31 channels of these encoder boards are used for SURALP's encoders. DS2002 and DS2103 boards are the analog input and analog output boards, respectively. DS4201-S serial interface board provides 4 serial communication channels with selective ports (RS232, RS422 or RS485). Gyroscope, accelerometer, inclinometer and 6 axis force/torque sensors are connected to the control hardware via analog input boards. Analog outputs provide torque references for the four-quadrant Maxon and Faulhaber motor drivers. Above described control hardware is housed in a dSpace Tandem Autobox case and placed at the back of SURALP. Control algorithms written in a personal computer via a user interface are uploaded to the DS1005 board by a data cable. CCD cameras are connected to the personal computer via FireWire interfaces. The control hardware is shown in Figure 4.53 schematically. Snapshots taken while cabling of power and signal connections are presented in Figure 4.54.

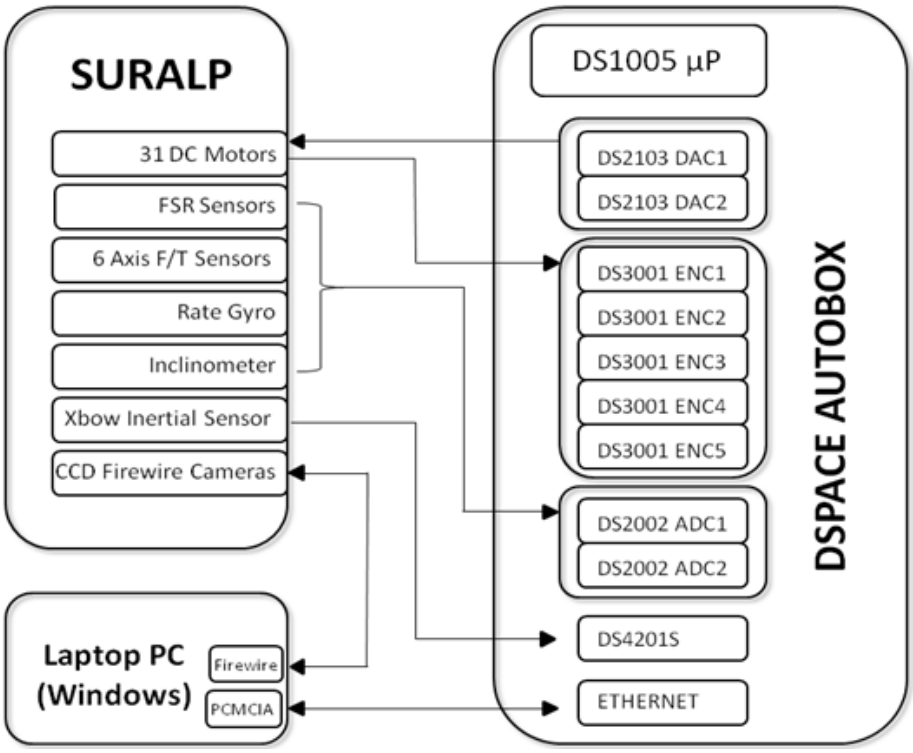

Figure 4.53 : Electronic hardware of SURALP

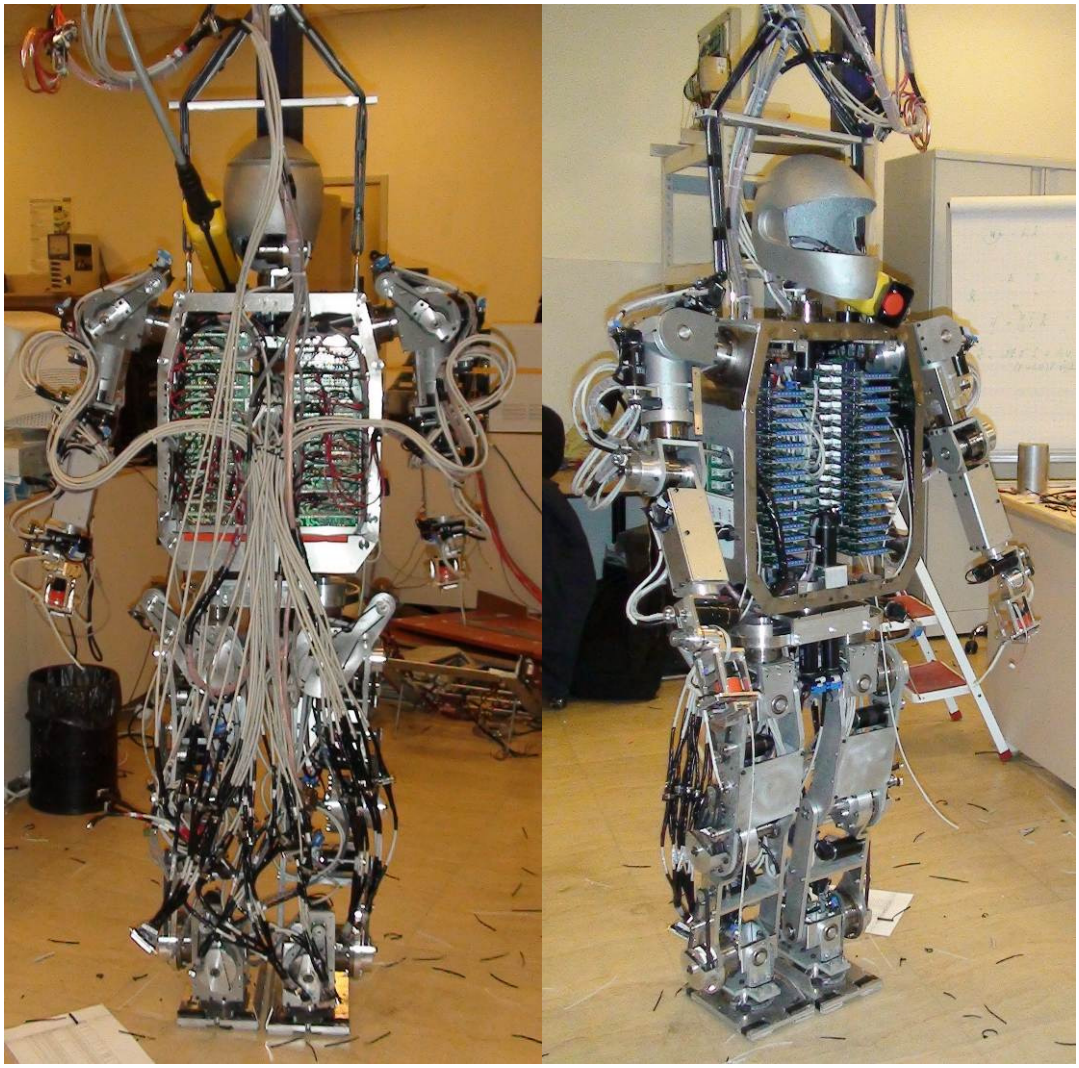

Figure 4.54 : Pictures taken while cabling

4.3. Walking Reference Generation for Even Floor

In place of using complex full dynamics models, the simple LIPM is more suitable for controller synthesis. In this model, a point mass is assigned to the COM of the robot and it represents the body (trunk) of the robot. The point mass is linked to a stable (not sliding) contact point on the ground via a massless rod, which is idealized model of a supporting leg. In the same manner, the swing leg is assumed to be massless too. With the assumption of a fixed height for the robot COM a linear system which is decoupled in the *x* and *y* directions is obtained. The system described above is shown in Figure 4.55. $c = (c_x \quad c_y \quad c_z)^T$ is position of the point mass in this figure. The ZMP is defined as the point on the *x*-*y* plane on which no horizontal torque components exist. For the structure shown in this figure, the expressions for the ZMP coordinates p_x and p_y are (Kajita et al. 2003):

$$p_x = c_x - (z_c / g)\ddot{c}_x \tag{4.1}$$

$$p_y = c_y - (z_c / g)\ddot{c}_y \tag{4.2}$$

z_c is the height of the plane where the motion of the point mass is constrained and g is the gravity constant. Suitable ZMP trajectories can be generated without difficulty for reference generation purpose (Choi, You and Oh 2004, Erbatur and Kurt 2009).

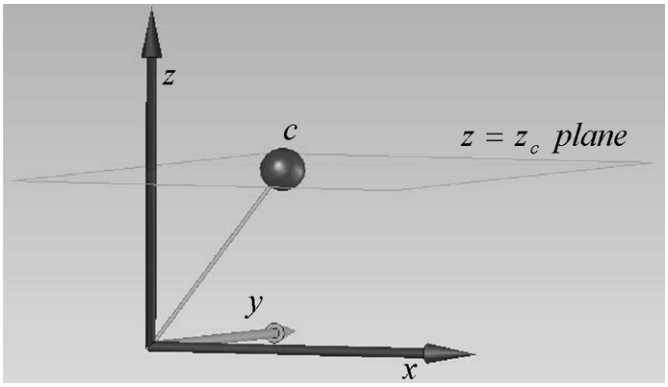

Figure 4.55 : The linear inverted pendulum model

As the only stability constraint, the ZMP should always lie in the supporting polygon defined by the foot or feet touching the ground. The ZMP location is generally chosen as the middle point of the supporting foot sole. Figure 4.56 shows a ZMP reference trajectory (Erbatur et al. 2009-1). Firstly, support foot locations are chosen. A in the figure is the distance between the foot centers in the y direction, B is the step size and T is the half of the walking period in this figure. Investigations in Dasgupta and Nakamura (1999), Erbatur et al. (2002), Zhu et al. (2004) show that the human ZMP moves forward under the foot sole. In the figure, b defines the range of the ZMP motion under the sole. The double support phase is introduced by using the parameter τ in Figure 4.56. Intervals equal to 2τ correspond to double support periods.

Having defined the curves, and hence the mathematical functions for $p_x^{ref}(t)$ and $p_y^{ref}(t)$, the next step is obtaining COM reference curves $c_x^{ref}(t)$ and $c_y^{ref}(t)$ from $p_x^{ref}(t)$ and $p_y^{ref}(t)$, respectively. Position control schemes for the robot joints with joint references obtained by inverse kinematics from the COM locations can be employed once the COM trajectory is computed.

The computation of COM trajectory from the given ZMP trajectory can be carried out in a number of ways (Kajita et al. 2003, Choi, You and Oh 2004). Choi, You and Oh (2004) proposes an approximate solution with the use of Fourier series representation to obtain COM references. In this process Fourier series approximations of the ZMP references $p_x^{ref}(t)$ and $p_y^{ref}(t)$ and of the COM references are obtained.

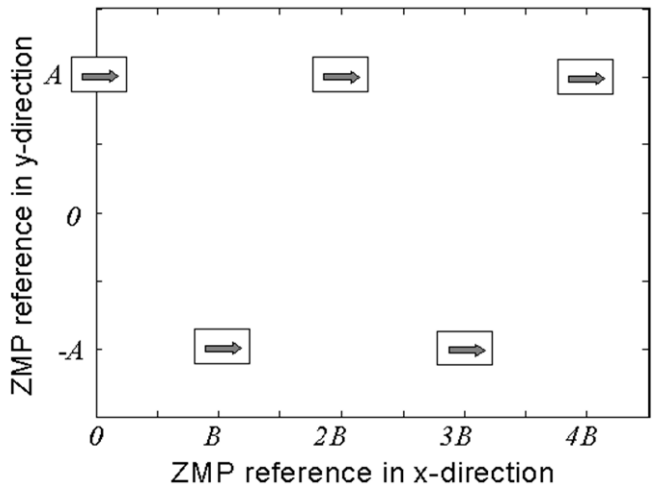

a)

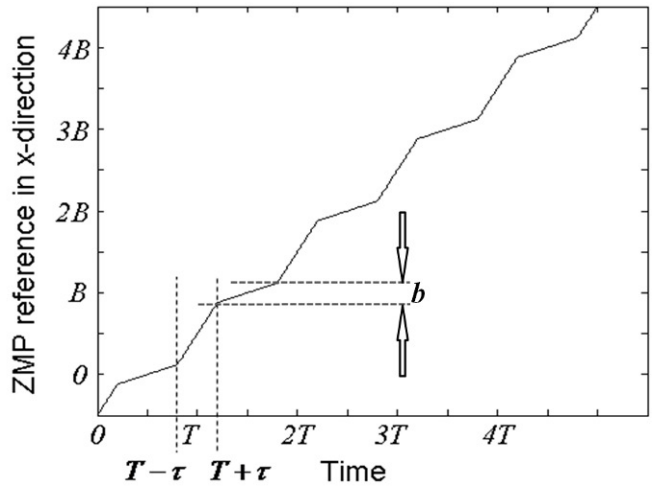

b)

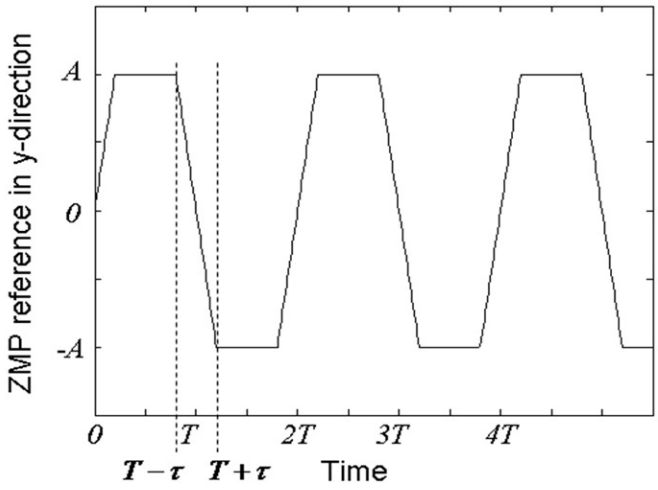

c)

Figure 4.56 : Forward moving ZMP references with pre-assigned double support phases. a) Foot locations and forward moving ZMP in single support phases. b) The x-directional ZMP reference. c) The y-directional ZMP reference.

The description of the $p_x^{ref}(t)$ in Figure 4.55 is given by

$$p_x^{ref} = (B/T)(t - T/2) + p_x'^{ref} \tag{4.3}$$

where $p_x'^{ref}$ is periodic with period T. $p_x'^{ref}$ is a combination of three line segments on $[0, T]$:

$$p_x'^{ref} = \begin{cases} \Omega_1 + \sigma_1 t & \text{if} \quad 0 \le t \le \tau \\ \Omega_2 + \sigma_2 t & \text{if} \quad \tau < t \le T - \tau \\ \Omega_3 + \sigma_3 t & \text{if} \quad T - \tau < t \le T \end{cases}. \tag{4.4}$$

$$\begin{aligned} &\Omega_1 = 0, \quad \sigma_1 = \delta/\tau, \quad \Omega_2 = \delta - \tau\sigma_2, \quad \sigma_2 = -2\delta/T - 2\tau, \\ &\Omega_3 = -\delta - (T - \tau)\sigma_3, \quad \sigma_3 = \sigma_1. \end{aligned} \tag{4.5}$$

with

$$\delta = (T - 2\tau/T)(B/2 - b). \tag{4.6}$$

Note that δ is the magnitude of peak difference between p_x^{ref} and the non-periodic component $(B/T)(t - T/2)$ of p_x^{ref}.

$p_y^{ref}(t)$ in Figure 4.56 is expressed as

$$\begin{aligned} p_y^{ref} = \sum_{k=1}^{\infty} \mathrm{A}(-1)^k \{ \; &(2/2\tau)(t - kT)[u(t - (kT - \tau)) - u(t - (kT + \tau))] \\ &+ [u(t - (kT + \tau)) - u(t - (kT + T - \tau))] \; \}, \end{aligned} \tag{4.7}$$

where $u(\cdot)$ represents the unit step function.

Defining $\omega_n \equiv \sqrt{g/z_c}$, we can rewrite (4.1) and (4.2) for the reference variables as follows.

$$\ddot{c}_x^{ref} = \omega_n^2 c_x^{ref} - \omega_n^2 p_x^{ref}, \tag{4.8}$$

$$\ddot{c}_y^{ref} = \omega_n^2 c_y^{ref} - \omega_n^2 p_y^{ref} . \tag{4.9}$$

Note that the y-direction ZMP reference $p_y^{ref}(t)$ is a periodic function with the period $2T$. It is reasonable to assume that $c_y^{ref}(t)$ is periodic too and that it has the same period. Hence, it can be approximated by a Fourier series

$$c_y^{ref}(t) = \frac{a_0}{2} + \sum_{k=1}^{\infty} a_k \cos(\frac{2\pi kt}{2T}) + b_k \sin(\frac{2\pi kt}{2T}) . \tag{4.10}$$

By (4.9) and (4.10), p_y^{ref} can be expressed as

$$\begin{aligned} p_y^{ref}(t) &= c_y^{ref} - \frac{1}{\omega_n^2}\ddot{c}_y^{ref} \\ &= \frac{a_0}{2} + \sum_{k=1}^{\infty} a_k (1 + \frac{\pi^2 k^2}{\omega_n^2 T^2}) \cos(\frac{2\pi kt}{2T}) + b_k (1 + \frac{\pi^2 k^2}{\omega_n^2 T^2}) \sin(\frac{2\pi kt}{2T}) \end{aligned} \tag{4.11}$$

Noting that this expression is in the form of a Fourier series for $p_y^{ref}(t)$, and since $p_y^{ref}(t)$ is an odd function, we conclude that $a_0/2$ and $a_k(1+(\pi^2 k^2)/(\omega_n^2 T^2))$ for $k = 1,2,3,\cdots$ are zero. The coefficients $b_k(1+(\pi^2 k^2)/(\omega_n^2 T^2))$ are computed by the Fourier integral:

$$b_k(1 + \frac{\pi^2 k^2}{\omega_n^2 T^2}) = \frac{2}{2T}\int_0^{2T} p_y^{ref} \sin(\frac{2\pi kt}{2T}) dt \tag{4.12}$$

As a result, after some arithmetical steps (omitted here), the coefficients b_k of $c_y^{ref}(t)$ in (4.10) can be obtained as

$$b_k = \begin{cases} \dfrac{\omega_n^2 T^2}{\omega_n^2 T^2 + \pi^2 k^2} \dfrac{2A}{\pi k} \left\{ \left[\dfrac{2}{\tau} \left\langle \dfrac{T}{\pi k} \sin(\dfrac{\pi k \tau}{T}) - \tau \cos(\dfrac{\pi k \tau}{T}) \right\rangle \right] \right. \\ \qquad \left. + \left[\cos(\dfrac{\pi k \tau}{T}) - \cos(\dfrac{\pi k (T-\tau)}{T}) \right] \right\} \text{ if } k \text{ is odd} \\ 0 \quad \text{if } k \text{ is even} \end{cases} \tag{4.13}$$

The second step is finding the Fourier series coefficients for c_x^{ref} . In Figure 4.56, p_x^{ref} is not a periodic function. It cannot be expressed as a Fourier series. However, as expressed above, this function is composed of the periodic function $p_x'^{ref}$ and the non-periodic function ($(B/T)(t-T/2)$). It is again a reasonable assumption that c_x^{ref} has a periodic part and a non-periodic part too. Further, if we suppose that the two non-periodic parts (of $p_x^{ref}(t)$ and c_x^{ref}) are non-equal, then the difference $p_x^{ref}(t) - c_x^{ref}$ will be non-periodic. This is not expected in a continuous walk as the one described in Figure 4.56. Therefore we conclude that the non-periodic parts of the two functions are equal. Note that, the period of the periodic part of $p_x^{ref}(t)$ is T and we can state the same for the period of the periodic part of c_x^{ref} . Finally, c_x^{ref} can be expressed as the sum of the non-periodic part of p_x^{ref} and a Fourier series:

$$c_x^{ref} = \frac{B}{T}(t - \frac{T}{2}) + \frac{\alpha_0}{2} + \sum_{n=1}^{\infty} \alpha_k \cos(\frac{2\pi n t}{T}) + \beta_k \sin(\frac{2\pi n t}{T}) \tag{4.14}$$

With (4.8) and (4.14) $p_x^{ref}(t)$ as a Fourier series is

$$\begin{aligned} p_x^{ref}(t) &= c_x^{ref} - (1/\omega_n^2)\ddot{c}_x^{ref} = (B/T)(t - T/2) + \alpha_0/2 \\ &+ \sum_{n=1}^{\infty} \alpha_k (1 + \frac{\pi^2 k^2}{\omega_n^2 T^2}) \cos(\frac{2\pi k t}{T}) + \beta_k (1 + \frac{\pi^2 k^2}{\omega_n^2 T^2}) \sin(\frac{2\pi k t}{T}) \end{aligned} \tag{4.15}$$

Therefore the Fourier coefficients of $p_x'^{ref}(t)$, the periodic part of $p_x^{ref}(t)$, are $\alpha_0/2$, $\alpha_k(1 + \pi^2 k^2/\omega_n^2 T^2)$ and $\beta_k(1 + \pi^2 k^2/\omega_n^2 T^2)$ for $k = 1, 2, 3, \cdots$

The Fourier coefficients $\alpha_0/2$, $\alpha_k(1+\pi^2k^2/\omega_n^2T^2$ of $p_x'^{ref}(t)$ are zero because this is an odd function.

The coefficients for $\beta_k(1+(\pi^2k^2)/(\omega_n^2T^2))$ can be found by

$$\beta_k(1+\pi^2k^2/\omega_n^2T^2)=\frac{2}{T}\int_0^T p_x'^{ref}(t)\sin(\frac{2\pi kt}{T})dt \tag{4.16}$$

This yields the result

$$\begin{aligned}\beta_k=&\frac{\omega_n^2T^2}{\pi^2k^2+\omega_n^2T^2}\frac{2}{\pi k}\left\{\ \sigma_1\left[-\tau\cos(\frac{2\pi k\tau}{T})+\frac{T}{2\pi k}\sin(\frac{2\pi k\tau}{T})\right]\right.\\&\left.+\sigma_2\left[\ \tau\cos(\frac{2\pi k\tau}{T})-\frac{T}{2}\left(\cos\left(\frac{2\pi k\tau}{T}\right)\right)-\frac{T}{2\pi k}\sin(\frac{2\pi k\tau}{T})\ \right]\ \right\}.\end{aligned} \tag{4.17}$$

The curves obtained for c_x^{ref} and c_y^{ref} are shown in Figure 4.57 together with the corresponding ZMP references defined in Figure 4.56. The infinite sums in (4.10) and (4.14) are approximated by finite sums of N terms. $N=24$ is used in the experiments. N is found by the inspection of the "Fourier-series-approximated" p_y^{ref} and p_x^{ref} curves obtained from (4.11) and (4.15), respectively. These approximated curves are computed, plotted and compared with the ZMP references in Figure 4.56 in order to validate the formulae derived for the Fourier series coefficients. The plots served a secondary purpose of determining a suitable value for N too. We observed that, with $N=24$, the approximated curves match with the original piecewise continuous ZMP reference curves in Figure 4.56. The matching quality we judged from the reproduction of the sharp corners of the original ZMP reference curves in their approximated versions. With lower values for N the matching quality is deteriorated. In Figure 4.56, the following parameter values are used: $A=0.1$ m, $B=0.1$ m, $b=0.04$ m, $T=1$ s and $\tau=0.2$ s.

In addition to the COM references, foot position reference trajectories have to be designed too. Firstly foot placement timing and world frame foot position and orientation references are defined for walking on even floor. Typical x and z-direction components of

the foot trajectories used in this thesis are shown in Figure 4.58. These curves are combinations of sinusoidal and constant function segments. T_d and T_s represent the double and single support periods, respectively. ($T_d = 2\tau$, $T_s = T - \tau$.) B is the step size from Figure 4.56. The y direction trajectories are constant at $-A$ and A for the right and left feet, respectively, where A is half of the foot to foot y direction distance also shown in Figure 4.56. h_s is the step height parameter and h_p is the ground push magnitude. The foot orientation references are generated in such a way that the feet are parallel to the even ground. The joint position references are obtained through inverse kinematics from COM and swing foot references defined in world frame coordinates. The process of reference generation is explained in detail in Taşkıran et al. (2010).

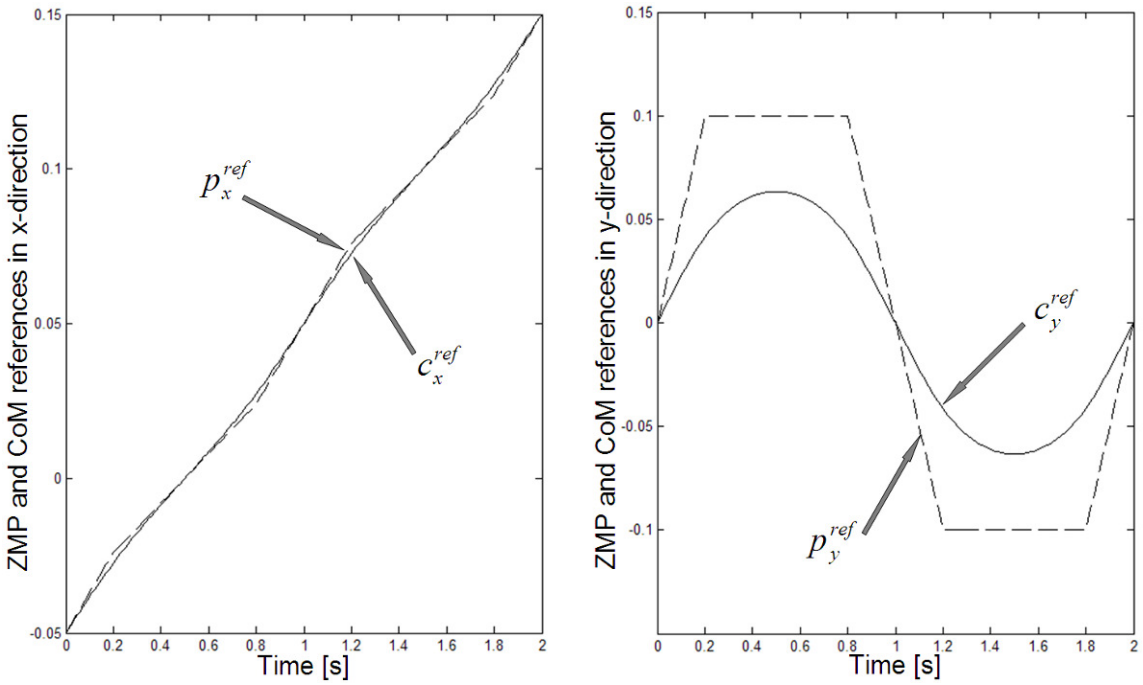

Figure 4.57 : x and y -direction COM and ZMP references

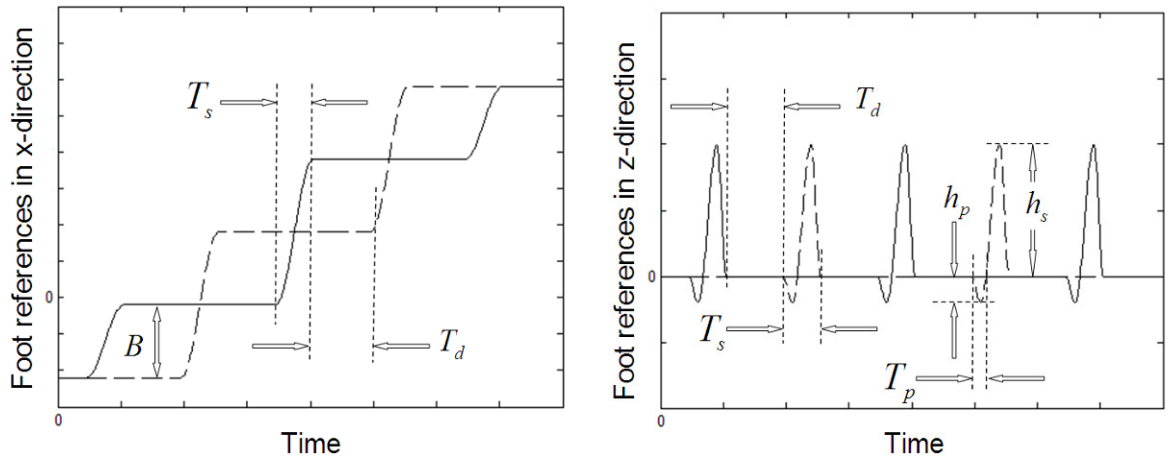

Figure 4.58 : x and z -direction foot frame references in as expressed in the world frame. Solid curves belong to the right foot, dashed curves indicate left foot trajectories. (The y -directional foot references are not shown are equal to $-A$ and A, respectively.)

4.4. Basic Control Actions

The basic control actions, also presented in Erbatur et al. (2009-2) are shortly described below.

4.4.1. Joint Level Control

The references for the leg joint positions are generated through inverse kinematics from Cartesian foot references and the ZMP based COM reference trajectory (Taşkıran et al. 2010). The arm, waist and neck joint position references are kept constant in the experiments presented in this thesis. These constant references can be observed from the walking snapshots in Figure 6.1. Mainly, the waist yaw reference angle was zero (pelvis and trunk links parallel to each other.) The head pan and tilt angles were zero too. Elbows were stretched and arms were in the lateral plane, each making an angle of 15 degrees with the body. The effect and contribution of the waist and arm motion on the walking performance on inclined planes is not considered in this thesis. Independent PID controllers are used for joint position control. The PID controller gains are obtained via trial and error.

In this work, joint actuators which are DC motors are controlled where couplings and other nonlinear dynamics are considered as disturbances applied at the input. Since very high gear ratios (e.g. 480 for the knee and hip roll joints, 360 for the hip pitch, hip yaw and ankle roll joints) are used, effects of couplings and nonlinear dynamics are reduced dramatically. Therefore, linear controllers are utilized to effectively control the system.

4.4.2. Foot Roll Control

In Kim, Park and Oh (2007), landing orientation controllers are proposed for the ankle joints. This approach assumes that there are roll joints present at the ankles (Figure 4.59). The

scheme computes ankle roll joint angle reference modifications in such a way that the feet are aligned parallel to the ground when they are in contact with the ground. The reference modification law in Kim, Park and Oh (2007) is the form of a first order filter applied on the foot to ground contact torques. This method is adopted for our control system too. The following reference modification law in the Laplace domain is employed for the two ankles separately.

$$\bar{\theta}_{roll}(s) = \theta_{roll}(s) + \left(K_{roll}/s + \lambda_{roll}\right)\tau_{roll}(s), \tag{4.18}$$

Here s is the Laplace variable. θ_{roll} is the ankle roll joint reference angle computed by inverse kinematics. $\bar{\theta}_{roll}$ is the reference ankle roll angle after the reference modification. τ_{toll} is the torque about the roll axis due to the interaction of the foot with the ground. This torque is measured by torque sensors positioned at the ankle in an experimental work. K_{roll} and λ_{roll} are low pass filter constants which are determined by trial and error in our approach. In the digital implementation, the Laplace domain transfer function in (4.18) is approximated by a difference equation. Tustin's approximation technique is used to obtain the difference equation. When the foot is in contact with the ground only with an outside or inside edge, a roll torque will be developed and with the application of (4.18), the joint angle references are modified in such a way to turn the ankles to achieve foot orientation parallel to the ground.

4.4.3. Ground Impact Compensation

Another important problem in achieving stable walking is the impact generated at the landing of the swing foot. A shock absorbing control law is employed as a solution. This control law is activated with every landing of the swing foot. In effect, a virtual mass-spring-damper system is positioned between the hip and ankle. The following second order relation modifies the distance between the hip and sole of the landing foot.

$$\bar{l}(s) = l(s) - \frac{1}{m_l s^2 + b_l s + k_l} F_z(s) \tag{4.19}$$

Here l represents the hip-to-sole distance reference (Figure 4.60) obtained from Cartesian foot reference trajectories. $\bar{l}$ is its shock absorber modified version. F_z is the z

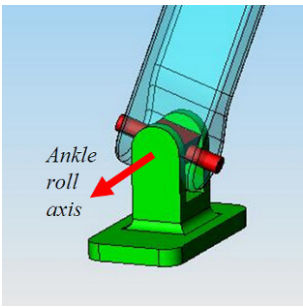

Figure 4.59 : The ankle roll axis

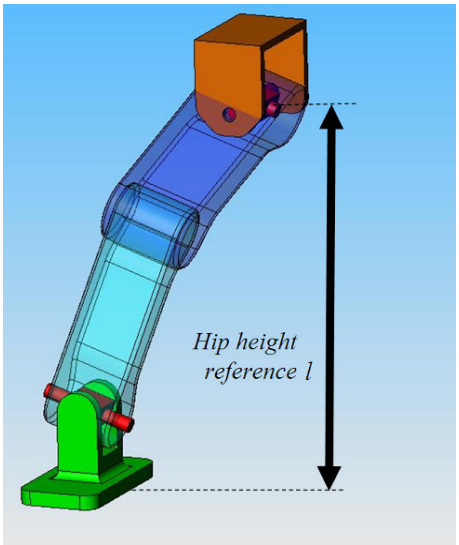

Figure 4.60 : The hip height reference

direction component of the ground interaction force acting on the foot. Again, an ankle-mount force sensor measures this force. m_l, b_l and k_l are the desired mass, damping and stiffness parameters of the mechanical impedance relation described in (4.19).

The impact compensator is deactivated after a certain time specified by the control designer. (In our case an activation time of 0.4 s is used.) However, at the end of this activation time the hip-to-sole distance is no more equal to its original value. In order to

resume the hip-to-sole distance which is originally planned in the reference generation process, at the end of the impact compensation phase the following relation is employed:

$$\bar{l}(t) = l(t) - 0.5(l(t_0) - \bar{l}(t_0))\left(1 + \cos((t_0 - t)\omega_{return}\right) \tag{4.20}$$

t_0 is the time at the end of the impact compensation phase. By (4.20), beginning with the final $\bar{l}$ value of the impact compensation phase, $\bar{l}$ returns to the original reference value l after a smooth transient behavior. ω_{return} is a parameter which determines the speed of return of $\bar{l}$ to l. As in the case of (4.18), Tustin's approximation of the continuous relation is obtained and applied for (4.19) and (4.20) too. These reference modification laws are applied for the two legs independently.

4.4.4. Early Landing Modification

One of the main problems of early landing of a swing foot is that when it is on the ground before the planned beginning of the double support phase, it will go on moving forward. When we inspect the x- direction foot references shown in Figure 4.58, we will see that the other foot (the planned support foot) will move at the same time backward in a trunk based coordinate system. In effect, the two feet on the ground will try to push the robot trunk in two different directions. The feet will slip; the robot will turn and possibly loose its balance. In order to avoid such a condition, the x- direction references in Figure 4.58 are modified in the case of an early landing. Specifically, this modification "stops" the x direction references of the feet at their values they had at the instant of early landing. These references are kept fixed until the next walking cycle and start from their fixed values, whenever the planned x direction references (as expressed in the body frame) reach them again.

Figure 4.61 shows a block diagram of the basic control scheme.

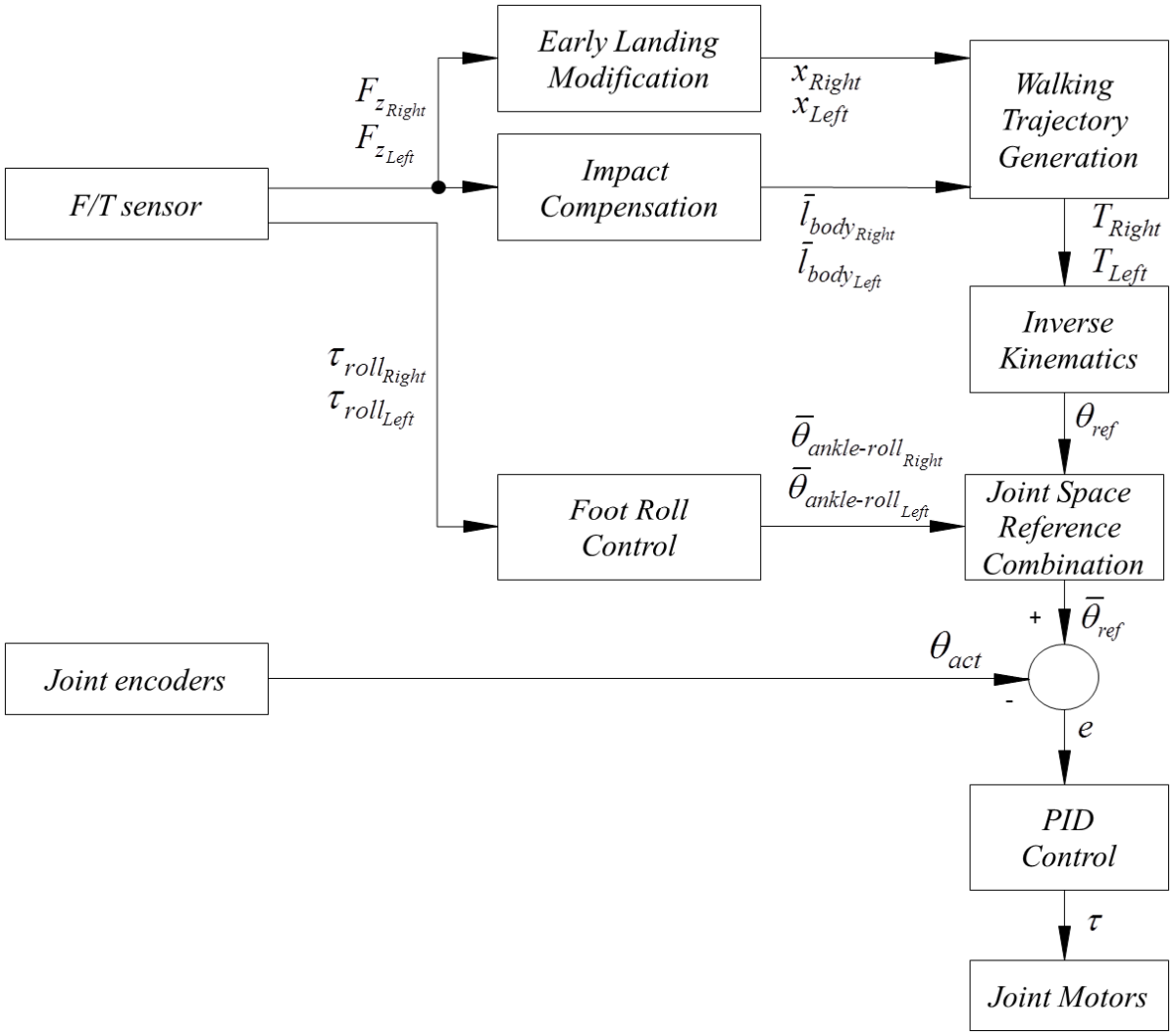

Figure 4.61 : The basic walking controller block diagram. z -directional force data obtained by 6 axis force/torque sensors are fed to *Early Landing Modification* and *Impact Compensation* blocks. Modified Cartesian reference trajectories are obtained for right and left feet separately. Using these reference trajectories, the position and orientation references of the feet with respect to body frame are generated. An inverse kinematics scheme converts the Cartesian space reference trajectories to joint space reference trajectories. The output of *Foot Roll Control* block (modified ankle roll angles obtained by 6 axis force/torque sensors) is directly combined (componentwise added) with the output (joint position reference vector) of *Inverse Kinematics* block. Combined joint space reference trajectories ($\bar{\theta}_{ref}$) are compared with the actual joint positions (θ_{act}) and independent joint PID controllers are employed. The output of PID controllers are fed to joint motor drivers running in torque (current) mode.

Chapter 5

5. FUZZY ADJUSTMENT OF THE REFERENCE WALKING PLANE FOR THE BIPEDAL WALK ON INCLINED PLANES

Figure 5.1 shows a typical humanoid robot walking on a surface topology consisting of flat floor and inclined planes with changing slopes. The motion of the robot is defined in a fixed coordinate frame called the world frame. The robot walking direction coincides with the x-direction of this fixed frame. Another frame is attached at the body of the robot. Coordinate frames are attached rigidly at the hips and foot soles, too, for the purpose of defining foot position and orientation references. These frames are shown in Figure 5.2. The body can be considered as a "central" link one since the legs are connected to it. Initially (before the start of the walk), the body frame axes are aligned parallel with the corresponding world frame axes. However, this parallel alignment changes during the walk due to various effects including gravitational forces, foot to ground interaction, changing slopes and coupling effects between the links. The body pitch angle, which is the angle the z-axis of the body frame makes with a vertical line is an indicator of the balance of the walk. This angle denoted by β is shown in Figure 5.3. Assuming that a gait with zero body pitch angle is planned in the reference generation, the online measurement of this angle can provide feedback indicating whether the robot is following this reference. It can also detect a falling forward or backward.

There are many control actions which can enhance the stability during the walk working on the body pitch angle. For robots with an independent pitch joint which divides the body into lower body and upper body sections (equivalently into pelvis and trunk links, respectively), the motion of this joint can directly be used for stability enhancement. Park (2003) uses this joint angle as a balance control variable for a 2D (sagittal plane) biped model. As mentioned above, Yılmaz, Seven and Erbatur (2010) and Yılmaz (2010) introduce the

"virtual pelvis pitch angle" and show that the body pitch motion can be applied as a control action for robots without an independent body pitch joint, too.

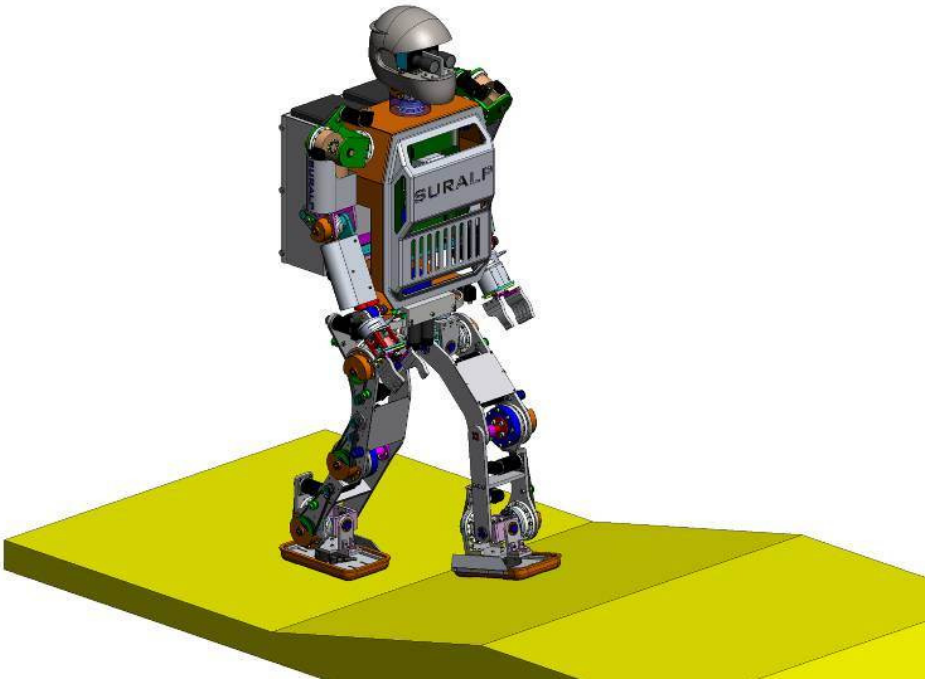

Figure 5.1 : Bipedal robot walk on changing slopes

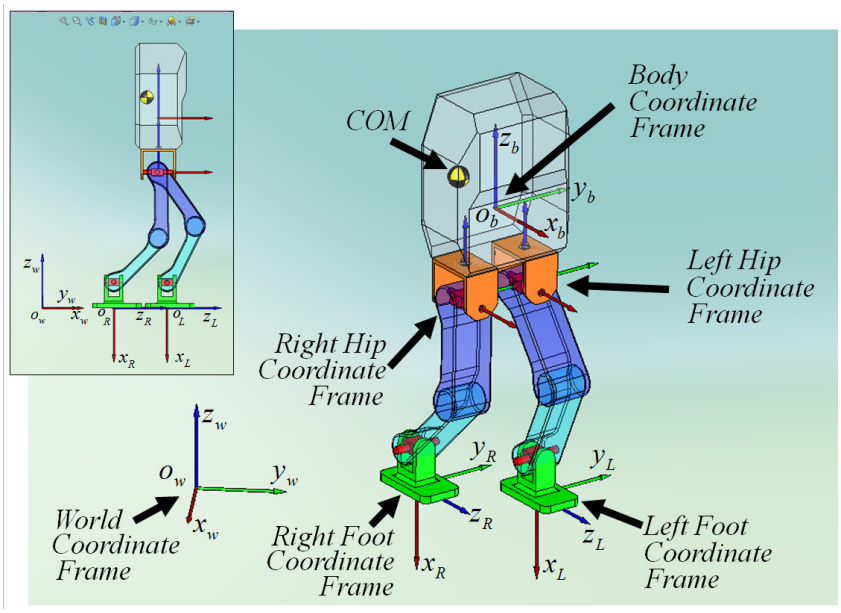

Figure 5.2 : Coordinate systems associated with walking reference generation. o_w and o_b stand for the origins of the world and body coordinate frames, respectively. The foot coordinate frames are fixed to the foot soles. The foot frame origin reference trajectories and reference orientations with respect to the body frame define the walk pattern.

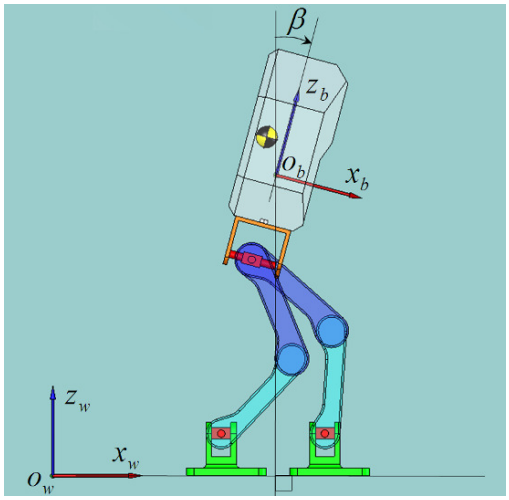

Figure 5.3 : The body pitch angle β

In some approaches the body pitch angle β of Figure 5.3 is actively modified with the benefit of increasing the robot moment of inertia about the world frame vertical axis. Yaw moment compensation techniques using this fact are studied in Fujimoto and Kawamura (1998).

Keeping the body pitch angle at a certain reference value is also a common practice in many applications, especially for object manipulation and human-robot cooperation.

In this thesis, the control objective is walking on changing slopes without losing balance. In contrast to Park (2003), Yılmaz, Seven and Erbatur (2010) and Yılmaz (2010), an upright body pitch orientation ($\beta = 0$) reference is employed. We believe that the upright posture has its own virtues on slopes. The minimal motion of the (presumably heavy) upper body induces only low amounts of interlink coupling torques and hence eases the walking control problem. However, this ease is at the expense of one degree-of-freedom in the control actions: The upper body rotary motion (via an independent joint between the pelvis and trunk, or via the "virtual pelvis pitch angle" in Yılmaz, Seven and Erbatur (2010) and Yılmaz (2010)) should be avoided.

The ZMP and LIPM based even-floor reference generation method in Erbatur and Kurt (2009) and Taşkıran et al. (2010) is employed in this thesis, too. However, the author proposes the modification of the walking plane by the rotation of the foot references about a pitch axis at the ground level. This axis is the y - axis of the frame F (with the origin o_F) in Figure 5.4, where the robot is shown in the standing posture. The purpose of introducing the frame F is

solely to define the place and sense of the rotation axis. The location of frame F, as expressed in the body coordinate frame, is fixed and defined by the parameters h_{body} and x_{offset} in this figure:

$$o_b^F = \begin{bmatrix} x_{offset} \\ 0 \\ -h_{body} \end{bmatrix}. \tag{5.1}$$

h_{body} is a constant body height reference parameter. x_{offset} is the mean of the right and left foot sole frame reference trajectory x-directional components, as expressed in the body coordinate frame. The role of this offset parameter is to place the center of the support polygon exactly below the center of mass of the robot. (The COM is shown as a circle in Figures 5.2-5.5.). Note that x_{offset} takes a negative value in the specific case of Figure 5.4. Figure 5.5.a depicts the robot while walking on even floor

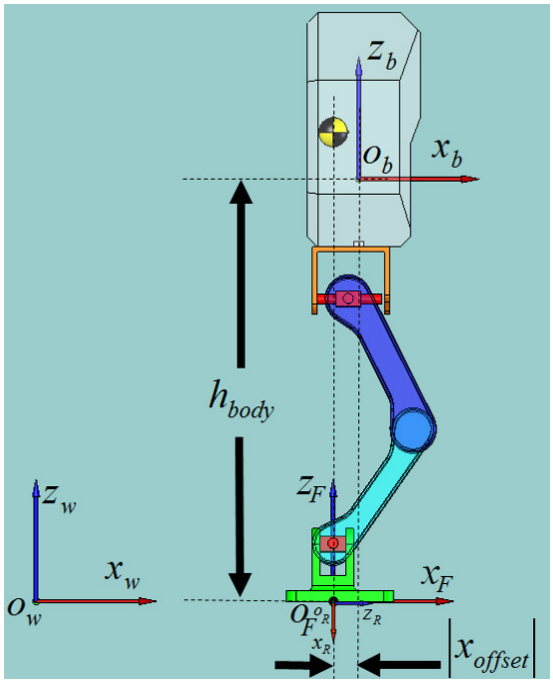

Figure 5.4 : The coordinate frame F is attached to the central point of the foot references on the ground level. This coordinate system serves in defining the axis of rotation of the foot references to change the walking plane. The origin of frame F and the origin of the right foot sole frame are shown at the same point in this side view. However, there is a y-directional offset as expressed in the body coordinate frame.

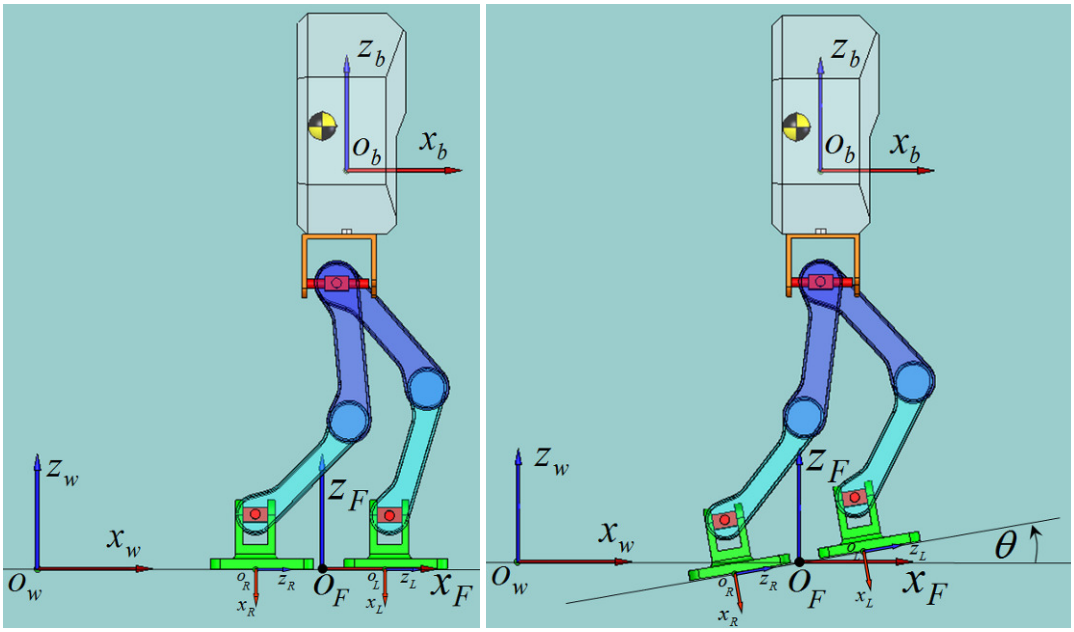

a) b)

Figure 5.5 : The pitch rotation by θ defines walk trajectories on a new plane. a) Robot walking with the foot reference trajectories generated for even floor. b) Robot configuration with the rotated foot reference trajectories. Snapshots belong to a double-support instance. The foot sole frames are indicated by smaller coordinate axes. Note that the foot sole frame origin locations and foot orientations are modified to move parallel to the new walking plane.

Placing the frame F at the foot trajectory central point, with a fixed orientation identical to the body coordinate frame, we define the angle θ in Figure 5.5.b as a rotation angle about the negative y-axis of this frame. We term this angle "foot pitch angle." The foot frame origin reference positions obtained by the method in Taşkıran et al. (2010), as expressed in frame F, are rotated into new references for any time. The result of this rotation is the change of the reference walking plane. Let the position of the right foot Denavit-Hartenberg frame origin position (as expressed in the body coordinate frame) be denoted by o_b^R. Also let the reference for this vector for a straight walk on an even surface denoted by $o_b^{R^{ref}}$. Since the reference orientations of the body and of frame F are the same, the expression of the right foot position reference in frame F is

$$o_F^{R^{ref}} = o_b^{R^{ref}} - o_b^F . \tag{5.2}$$

This reference vector is rotated about the negative y axis of the frame F by θ to obtain right foot position reference vector on an inclined plane. The new position reference vector is denoted by $o_{F_{new}}^{R^{ref}}$ and obtained as

$$o_{F_{new}}^{R^{ref}} = R_{y,-\theta} o_F^{R^{ref}}, \tag{5.3}$$

where $R_{y,-\theta}$ stands for the "basic rotation matrix about the y-axis, by $-\theta$". This matrix is the same as the rotation matrix about the negative y-axis, by θ. The explicit expression for this matrix is (Spong and Vidyasagar 1989)

$$R_{y,-\theta} = \begin{bmatrix} \cos\theta & 0 & -\sin\theta \\ 0 & 1 & 0 \\ \sin\theta & 0 & \cos\theta \end{bmatrix}. \tag{5.4}$$

The new reference is expressed in the body frame as

$$o_{b_{new}}^{R^{ref}} = o_{F_{new}}^{R^{ref}} + o_b^F. \tag{5.5}$$

This reference is further modified to be expressed in the right hip frame R_0 which is parallel to the body frame.

$$o_{R_{0_{new}}}^{R^{ref}} = o_{b_{new}}^{R^{ref}} - o_b^{R_0}, \tag{5.6}$$

where $o_b^{R_0}$ is the constant vector defining the position of the right hip Denavit-Hartenberg frame, as expressed in the body frame. $o_{R_{0_{new}}}^{R^{ref}}$ is ready to be used as an input for the inverse

kinematics routine of the 6-DOF right leg. Another input for the inverse kinematics is the frame orientation with respect to the hip frame.

In addition to the modification of the foot position references, foot orientation references are altered too. They are set parallel to the newly defined reference walking plane with slope angle θ.

Starting with the orientation reference $R_b^{R^{ref}}$ of the right foot frame with respect to the robot body, the right foot frame new orientation reference is computed. Since the body, frame F and right hip coordinate frames are all parallel to each other, we have

$$R_{R_{0_{new}}}^{R^{ref}} = R_{b_{new}}^{R^{ref}} = R_{F_{new}}^{R^{ref}} \tag{5.7}$$

and the matrix $R_{R_{0_{new}}}^{R^{ref}}$ is obtained as

$$R_{R_{0_{new}}}^{R^{ref}} = R_{y,-\theta} R_F^{R^{ref}} = R_{y,-\theta} R_{R_0}^{R^{ref}} = R_{y,-\theta} R_b^{R^{ref}} \tag{5.8}$$

The right foot inverse kinematics problem can then be solved for joint angles with the input position and orientation matrix references. The inverse kinematics computations (Seven 2007) are presented in Appendix A.

The computations for the new left foot references are performed similarly.

It should be reiterated that the rotational transformation of the foot references is more than a modification in foot orientations. This transformation also modifies the direction of foot reference motion. After the transformation, the foot motion originally defined parallel to the even floor becomes parallel to an inclined plane.

Section 5.1 presents a fuzzy logic system which adjusts the angle θ online by evaluating the body pitch angle β and ankle pitch torques measured by torque sensors. In the field of bipedal walking control, the online modification of walking references by utilizing sensor feedback is one of the most common control approaches. Therefore, in this thesis too, the online modification of the reference for θ is regarded as a control action. As mentioned

before, the fuzzy logic system, in combination with ground impact absorption, foot early landing and foot roll compliance compensators in Erbatur et al. (2009-2), is the backbone of the walking controller on changing slopes.

5.1. The Novel Fuzzy Parameter Adjustment System for the Adaptation to Sloped Surfaces

Previous simulation and experimental results with SURALP (Erbatur et al. 2008, Erbatur et al. 2009-2, Taşkıran et al. 2009, Taşkıran et al. 2010) suggest that the body pitch angle is oscillating during the walk. Even in a steady and stable walk the body pitch angle trajectory can be in the form of a periodic signal oscillating with peak values of a few degrees. Therefore, a single measurement of the angle can be misleading in deciding upon the balance condition of the robot. In order to infer whether the robot goes on with a steady walking pattern or is in the trend of falling, the average, rather than the instantaneous value of the body pitch angle is more suitable. Averaging can be done in many different ways. One question to be answered is related to the length of the averaging window. Another concern is the sampling period for the data to be averaged. Usually, joint space controller sampling times of one to ten milliseconds are employed in robotic applications. Using a long averaging window from the current sampling instant back with a low sampling period in the order of the joint control sampling period would require large storage space and consume online computational resources. There is a trade-off in the accuracy of the averaging computation and the efficient use of the computational power. Employing the number of samples N_p used in the average computation and the body pitch angle sampling period T_p as design parameters, the average value $\overline{\beta}$ of the body pitch angle β in Figure 5.3 is computed as

$$\overline{\beta}(kT_p) = \frac{1}{N_p} \sum_{l=0}^{N_p-1} \beta\big((k-l)T_p\big), \tag{5.9}$$

where k is the sampling index.

The following guidelines describe the role of $\overline{\beta}$ in the body pitch angle adjustment used in this thesis:

(i) When the average value of body pitch angle is positive we can infer that this is a posture inclined to a fall towards front, to the walking direction. In this case, the foot pitch angle should be decreased (and even made negative) to push the ground by the toes and compensate for the gravity effect of the forward leaned body.

(ii) In a similar way to the guideline (i) above, when the average value of body pitch angle is negative, the foot pitch angle should be increased to compensate for the gravity effect of the backward leaned body by pushing the ground with the heels.

The guidelines (i) and (ii) on their own can be used to devise a body pitch angle adjustment method as carried out in Seven et al. (2011). However, our experimental studies indicated that the "application intensity" of the two guidelines above needs to be modulated for "transient" and "steady state" cases. In other words, during a grade-to-grade transition, the foot pitch angle θ should be changed with a different rate (faster) than while the robot is walking on a constant slope.

Again observed in the experiments is that other sources of valuable information, as indicators of the above mentioned slope transition, are the pitch torques measured by torque sensors mounted at the ankles. In the proposed approach, they too, are employed as inputs of the control system which computes the foot pitch angle reference. In this thesis, a "slope transition indicator" denoted by $\tilde{\tau}$ is derived from the ankle pitch torque measurements as follows. Firstly, the right and left foot pitch torque average values ($\overline{\tau}_R$ and $\overline{\tau}_L$, respectively) are computed in a way similar to (5.9):

$$\overline{\tau}_R(kT_t) = \frac{1}{N_t}\sum_{l=0}^{N_t-1}\tau_R\big((k-l)T_t\big), \tag{5.10}$$

$$\overline{\tau}_L(kT_t) = \frac{1}{N_t}\sum_{l=0}^{N_t-1}\tau_L\big((k-l)T_t\big). \tag{5.11}$$

In (5.10), τ_R stands for the right ankle pitch torque. This is a low-pass-filtered version of the sensor measurement at the right ankle. τ_L in (5.11) is defined similarly for the left ankle. N_t is the number of samples used for the torque averaging, and T_t is the associated sampling time. As in (5.9), k is the time index. $\tilde{\tau}$ is computed as

$$\tilde{\tau}(kT_t) = \left|\tau_R(kT_t) - \bar{\tau}_R(kT_t)\right| + \left|\tau_L(kT_t) - \bar{\tau}_L(kT_t)\right| \tag{5.12}$$

Note that the expression in (5.12) assumes large values when quick changes are observed in the measured ankle torques. It is however close to zero when torque measurements vary slowly. Our experiments indicated that $\tilde{\tau}$ defined above is a good indicator of slope transitions.

The following guidelines describe the role of the slope transition indicator $\tilde{\tau}$ in generating the foot pitch angle reference in this thesis:

(iii) When high levels of slope transition indicator is observed, foot pitch angle should be changed (increased or decreased, according to the sign of the average body pitch angle) in a fast way to create a quick response to adapt to the new grade.

(iv) When low levels of slope transition indicator is observed, foot pitch angle should be changed slowly in order to allow the convergence of a steady state walking regime without causing undesired oscillations in the body pitch angle.

The four guidelines above can be used in various ways to construct an online computation scheme for the reference foot pitch angle θ. The method proposed in this thesis employs a fuzzy system for this purpose. Fuzzy systems are natural choices to exploit verbal descriptions (like the four guidelines above) of the plant or problem to obtain control or adaptation mechanisms (Lee 1990, Hsu and Fu 1995, Hsu and Fu 1996, Gerla 2005, Fanei and Farrokhi 2006).

Specifically, $\Delta\theta_k$, that is, the increment of the foot pitch angle at time index k, rather than the variable θ_k itself is computed by the fuzzy logic system. The increments are then periodically summed up to generate the foot pitch angle θ_k.

Table 5.1 and Figure 5.6 describe the nine fuzzy rules used in the control computation. In Table 5.1 the subscript "$P1$" of the rule strength $\Delta\theta_{P1}$ stands for positive small. "$\Delta\theta_{P2}$" is positive medium change in θ. $\Delta\theta_{P3}$ signifies a positive big change. ZZ symbolizes "zero" and $N1$ is negative small. Similarly defined are $N2$ and $N3$ for increasing magnitudes of rule strengths with a negative sign. The numerical values of the rule strengths and the corner positions of the membership functions in Figure 5.6 are tabulated in Table 6.2 in Chapter 6. The rules are summarized in Table 5.1. An example for a rule is: "*Rule 11: If* $\tilde{\tau}$ *is small and* $\overline{\beta}$ *is negative, then* $\Delta\theta_k$ *is positive of grade 1 (*$\Delta\theta_{P1}$*).*" The choice of the rule base and the membership functions satisfies the conditions (i) - (iv) above. The truth value of a rule is obtained by multiplying the membership values of $\tilde{\tau}$ and $\overline{\beta}$ fuzzy sets involved in the rule. For example, from Table 5.1, the truth value of *Rule 11*, denoted by w_{11}, is computed as

$$w_{11} = \mu_{Small\,\tilde{\tau}}(\tilde{\tau})\mu_{Negative\,\overline{\beta}}(\overline{\beta}) \tag{5.13}$$

In general, the truth value of Rule ij is denoted by w_{ij} and computed in a way similar to the computation of w_{11} in (5.13). Let the rule strength matrix $\Delta\Theta$ be defined from Table I as

$$\Delta\Theta = \begin{bmatrix} \Delta\theta_{P1} & \Delta\theta_{P2} & \Delta\theta_{P3} \\ \Delta\theta_{ZZ} & \Delta\theta_{ZZ} & \Delta\theta_{ZZ} \\ \Delta\theta_{N1} & \Delta\theta_{N2} & \Delta\theta_{N3} \end{bmatrix}. \tag{5.14}$$

Using this matrix, the defuzzification is carried out by the expression

$$\Delta\theta_k = \left(\sum_{i=1}^{3}\sum_{j=1}^{3} w_{ij}\Delta\Theta_{ij} \right) \Big/ \left(\sum_{i=1}^{3}\sum_{j=1}^{3} w_{ij} \right). \tag{5.15}$$

As mentioned before, the parameter θ is updated periodically by

$$\theta_{k+1} = \theta_k + K\Delta\theta_k \,, \tag{5.16}$$

where K is a tuning parameter. The update cycle time is denoted by T_θ. The computed θ_{k+1} value is applied as the reference for the foot pitch angle. This command value used as an input for the inverse kinematics computations. The "integrating nature" of (5.16) is very useful to adapt to inclined planes with unknown slopes. The rule strength $\Delta\theta_{ZZ}$ is chosen equal to zero and hence the central trapezoidal membership function in Figure 5.6 represents a dead zone about the vicinity of zero body pitch angle. This dead zone helps the convergence of the foot pitch angle without control activity (change in θ) in the steady state.

Table 5.1
The Fuzzy Rule Base

$\bar{\beta}$ \ $\tilde{\tau}$	**Small** $\tilde{\tau}$	**Medium** $\tilde{\tau}$	**Big** $\tilde{\tau}$
Negative $\bar{\beta}$	$\Delta\theta_{P1}$ *Rule 11*	$\Delta\theta_{P2}$ *Rule 12*	$\Delta\theta_{P3}$ *Rule 13*
Zero $\bar{\beta}$	$\Delta\theta_{ZZ}$ *Rule 21*	$\Delta\theta_{ZZ}$ *Rule 22*	$\Delta\theta_{ZZ}$ *Rule 23*
Positive $\bar{\beta}$	$\Delta\theta_{N1}$ *Rule 31*	$\Delta\theta_{N2}$ *Rule 32*	$\Delta\theta_{N3}$ *Rule 33*

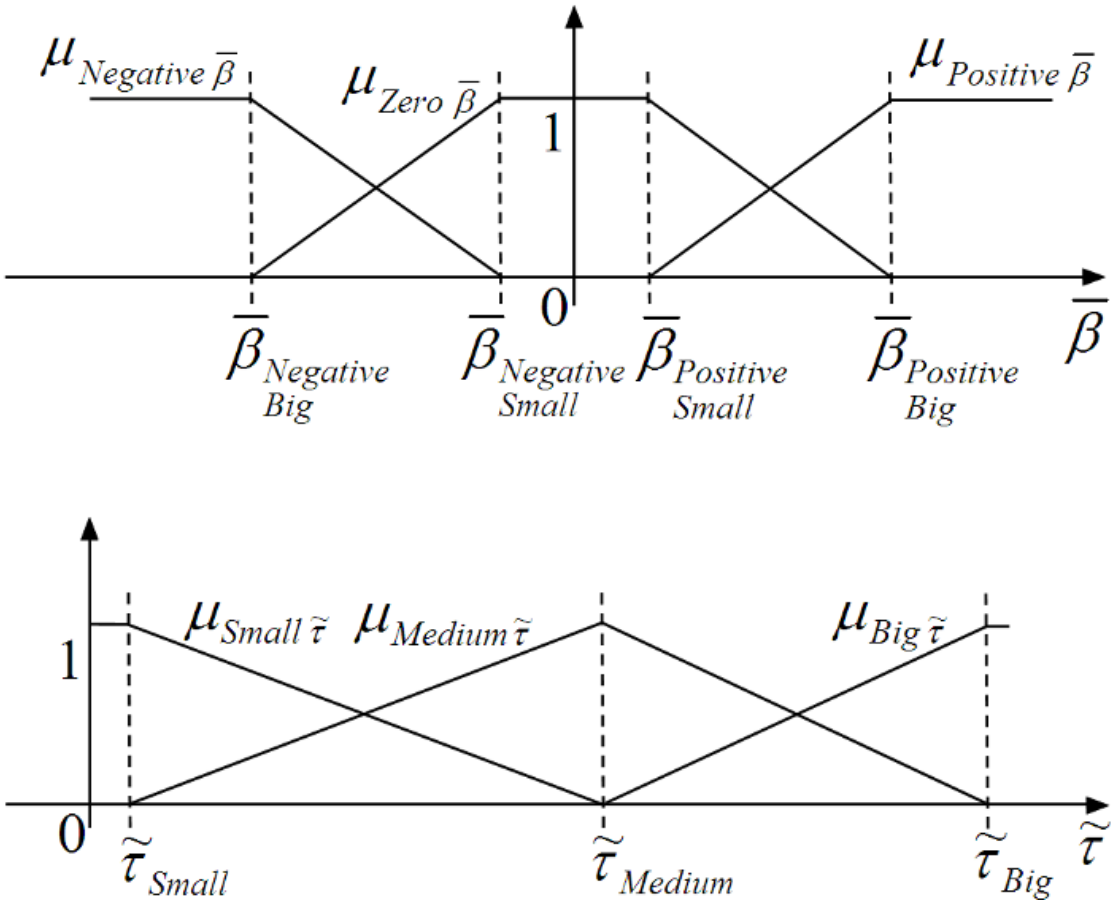

Figure 5.6 : The membership functions

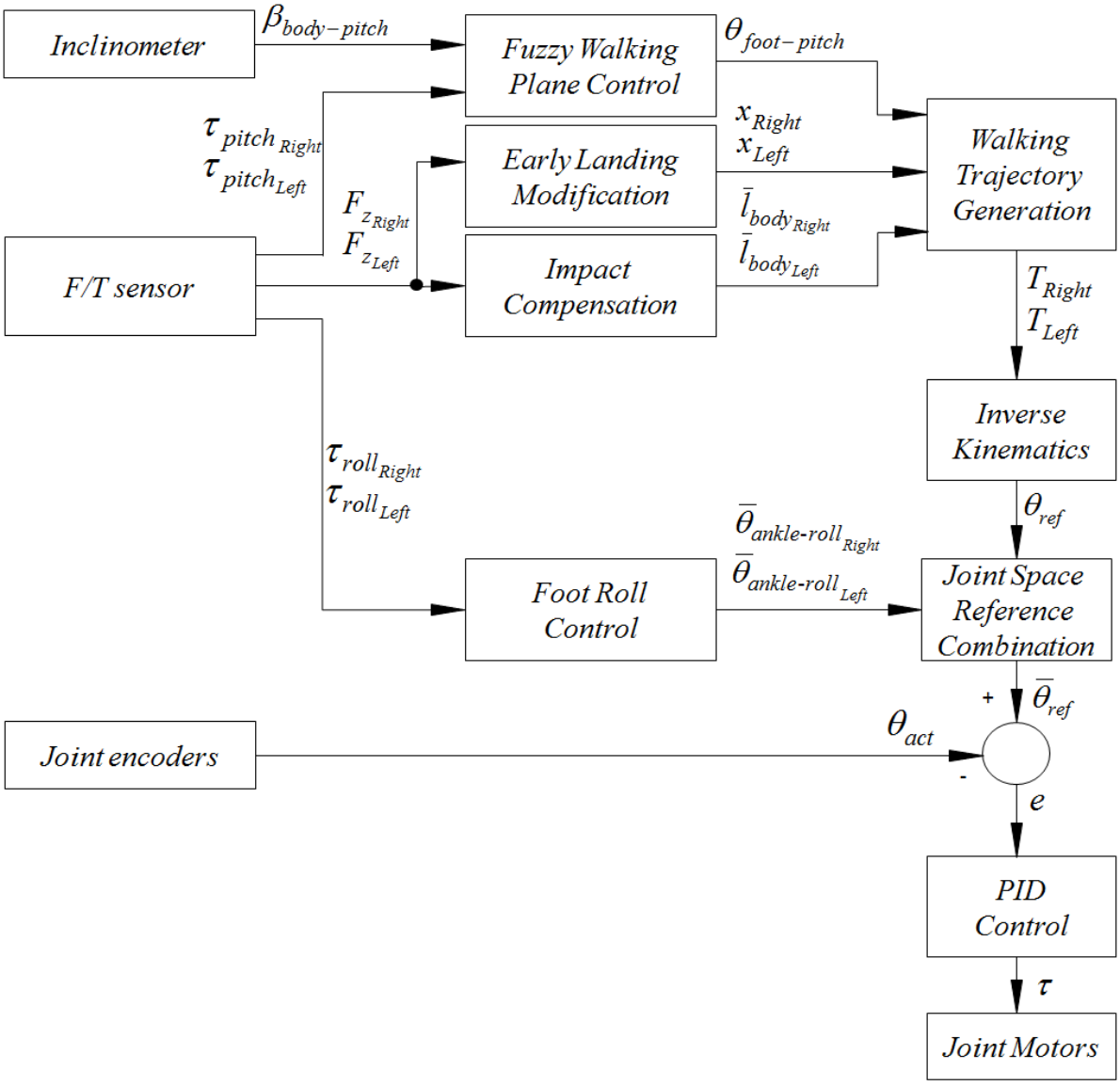

Figure 5.7 : The walking controller block diagram with fuzzy adjustment. *Fuzzy Walking Plane Control* block is added to the basic walking control scheme which uses inclinometer data ($\beta_{body-pitch}$) and ankle mounted 6 axis force/torque sensor data ($F_{z_{Right}}, F_{z_{Left}}$) in order to calculate the foot pitch angle reference trajectories ($\theta_{foot-pitch}$).

Chapter 6

6. EXPERIMENTAL RESULTS

In this chapter, experimental results with the humanoid robot SURALP are presented.

Parameters used for the even-floor walking reference generation are presented in Table 6.1. The reference generation and PID controller cycle time employed is 1 ms. The cycle time T_p for the computation of the average body pitch angle $\overline{\beta}$ is 200 ms and the number of samples N_p for this averaging is 10. The cycle time T_t for the update of $\tilde{\tau}$ is 100 ms. The number of samples N_t for the computation of ankle pitch torque averages $\overline{\tau}_R$ and $\overline{\tau}_L$ is 40. $\Delta\theta$ and θ are updated with a cycle time T_θ of 200 ms. Rule strengths and membership corner locations of the fuzzy parameter adjustment system in (5.9-5.16) are presented in Table 6.2. The gain K in (5.16) is equal to 1.5.

Table 6.1 :
Reference Generation Parameters

Symbol	Definition	Value
T_s	Single support period	1 s
T_d	Double support period	0.9 s
T_p	Push period	0.4 s
h_{body}	Hip height	61 cm
x_{offset}	x-directional foot reference offset	-3.5 cm
$2A$	y-directional distance between foot frame origins	28 cm
D	ZMP reference in y direction	7 cm
$2b$	ZMP motion under the sole	4 cm
B	Step size	4.5 cm
h_s	Step height	2 cm
h_p	Ground push magnitude	1 cm

Table 6.2 :

Rule Strengths and Membership Function Corner Locations

Rule Strength	**Numeric Value (Degrees)**	**Corner**	**Numeric Value (Degrees)**	**Corner**	**Numeric Value (Degrees)**
$\Delta\theta_{P1}$	1	$\overline{\beta}_{Negative\ Big}$	-5	$\tilde{\tau}_{Small}$	1
$\Delta\theta_{P2}$	2	$\overline{\beta}_{Negative\ Small}$	-0,25	$\tilde{\tau}_{Medium}$	3
$\Delta\theta_{P3}$	3	$\overline{\beta}_{Positive\ Small}$	0,25	$\tilde{\tau}_{Big}$	5
$\Delta\theta_{ZZ}$	0	$\overline{\beta}_{Positive\ Big}$	5		
$\Delta\theta_{N1}$	-1				
$\Delta\theta_{N2}$	-2				
$\Delta\theta_{N3}$	-3				

Experimental results obtained with this control system are shown in Figure 6.1 and Figure 6.2. The walking surface contains three parts: An even surface, a plane inclined with an 8.5 degrees grade (15% grade) and a flat top platform following the inclined plane. Snapshots of the experiment are shown in Figure 6.1.

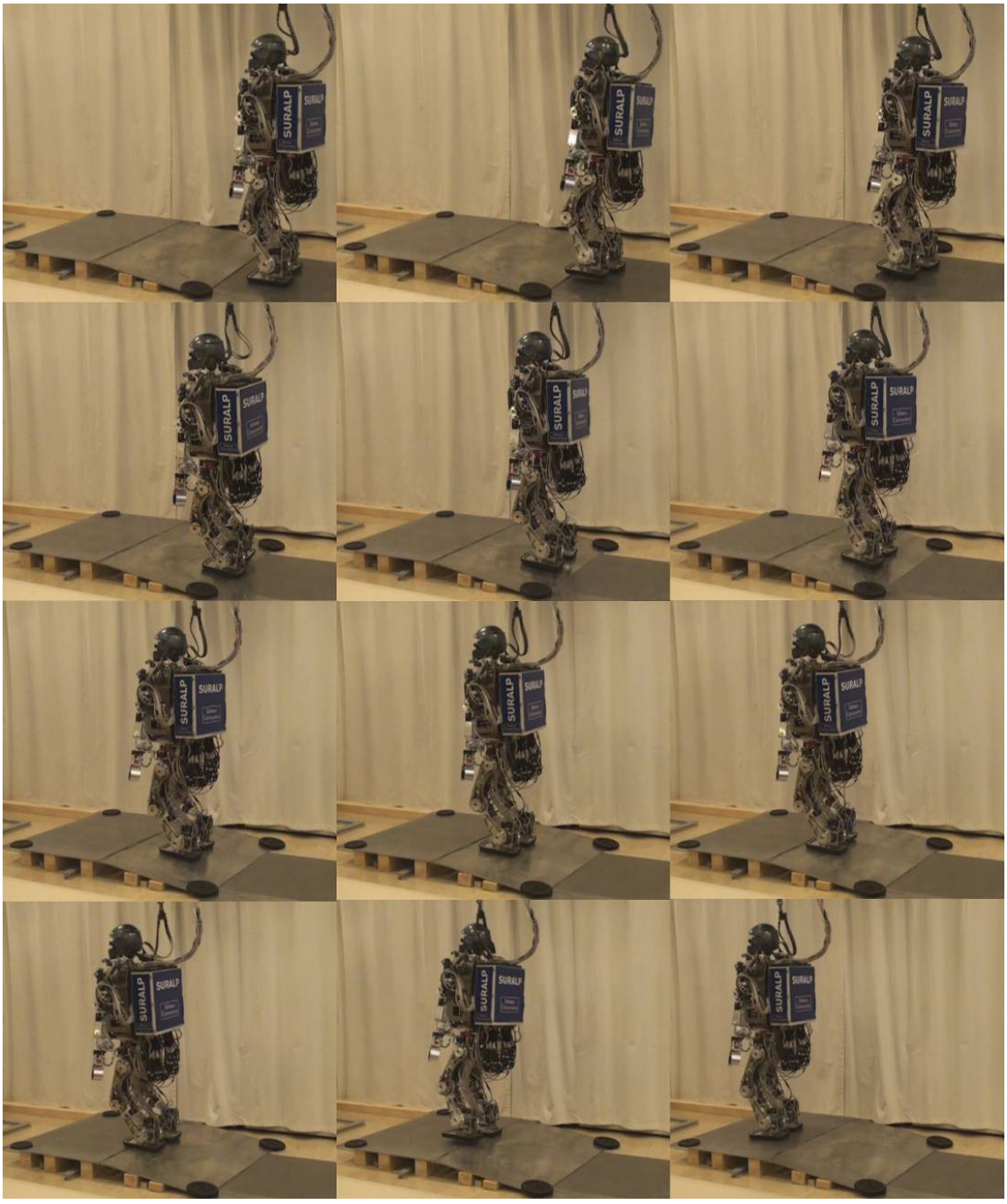

Figure 6.1 : The robot in the walk from even ground onto the inclined plane with 15% slope and the following flat top platform.

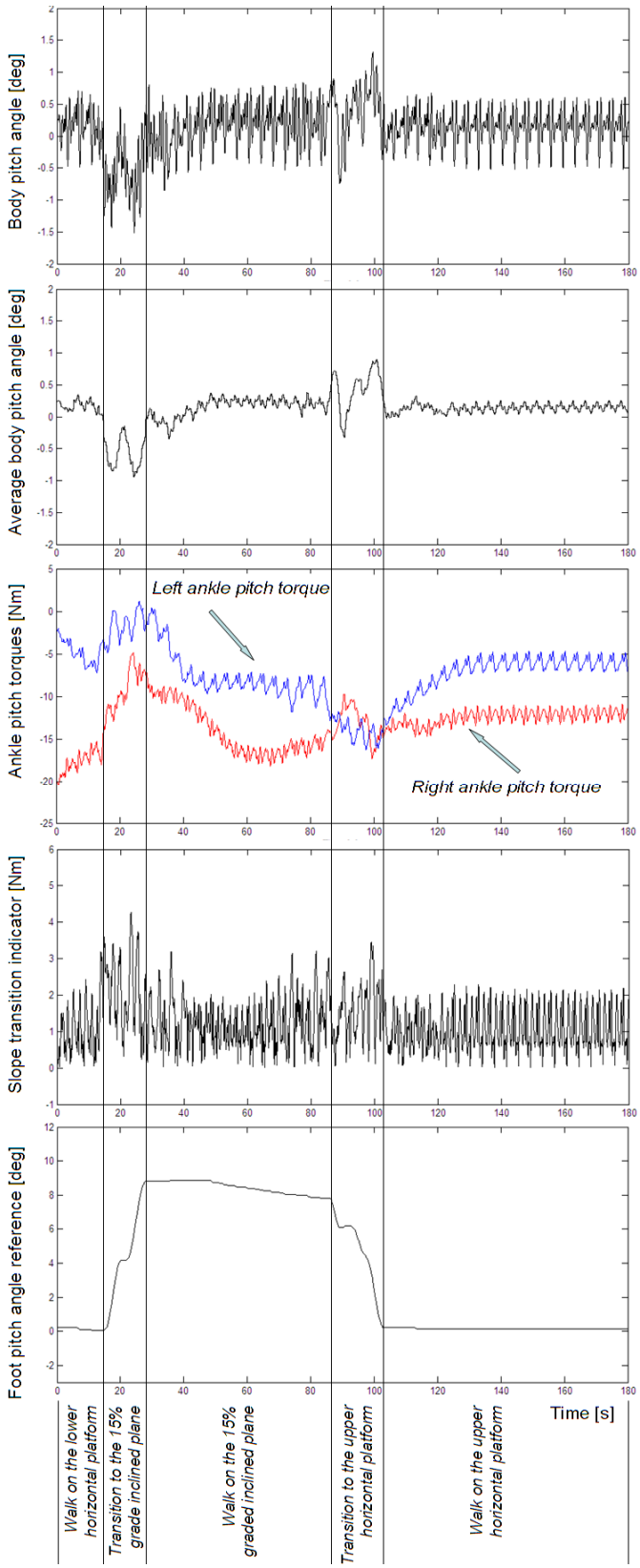

Figure 6.2 : Body pitch angle, ankle pitch torques, slope transition indicator and foot pitch angle reference during the 8.5 degrees (15%) slope experiment. The experiment is carried out on a walking surface of three segments: 1) Horizontal plane, 2) Uphill slope 3) Upper horizontal plane.

The walk starts with the robot in upright posture at a distance of 15 cm to the inclined plane. It can be observed from Figure 6.2 that the robot reaches to the inclined plane after approximately 15 seconds is elapsed from the start of the experiment. The $\overline{\beta}$ graph (second plot from the top) shows that the average oscillation of the upper body of the robot is small during this period. After the establishment of the contact with the inclined plane, $\overline{\beta}$ changes much faster. Also the slope transition indicator variable $\tilde{\tau}$ rises during the slope change. The fuzzy parameter adaptation system acts according to the fuzzy rule base and finds the appropriate foot pitch angle θ (plot at the bottom). Note that the walking reference plane is successfully established at a grade around 8.5 degrees, which is the actual inclined plane grade. After walking in a steady gait on the inclined plane, the robot enters the flat top region of our experimental setup about the 85^{th} second of the experiment. The slope transition indicator detects the slope change and the adaptation speed is increased by the rule base in Chapter 5. Since $\overline{\beta}$ assumes positive values, θ is decreased by the fuzzy system. After a steady walk period on the flat top, the robot stops walking.

To the best of the author's knowledge, the %15 graded slope is the steepest one, which could be entered and climbed successfully by a blind walking bipedal robot, reported to this date.

Experiments are carried out with grades less than 15% too. In all experiments, the integrating nature of the proposed fuzzy logic system forced the foot pitch angle to converge to the slope angle of the plane on which the robot walks, in a quick manner. Figure 6.3 shows the evolution of the foot pitch reference angle θ for four different slope experiments.

The stability of the walk in the experiments is investigated in Figure 6.4. As for Figure 6.3, four different grades are employed. The recorded pitch angles in the figure indicate that a steady body pitch oscillation regime is maintained in the horizontal and inclined plane walk phases. The stability of the walk during the prespecified walking period is justified via experimental work. The plane-to-plane transitions, however, display larger deviations from the upright orientation. These deviations increase with increasing grade difference between neighboring planes. They are most pronounced with the 15% slope. Steeper-than-15% slopes caused the robot to lose its balance and fall. The body roll angle plots in the same figure show that roll oscillation behavior is virtually independent of the slope grade.

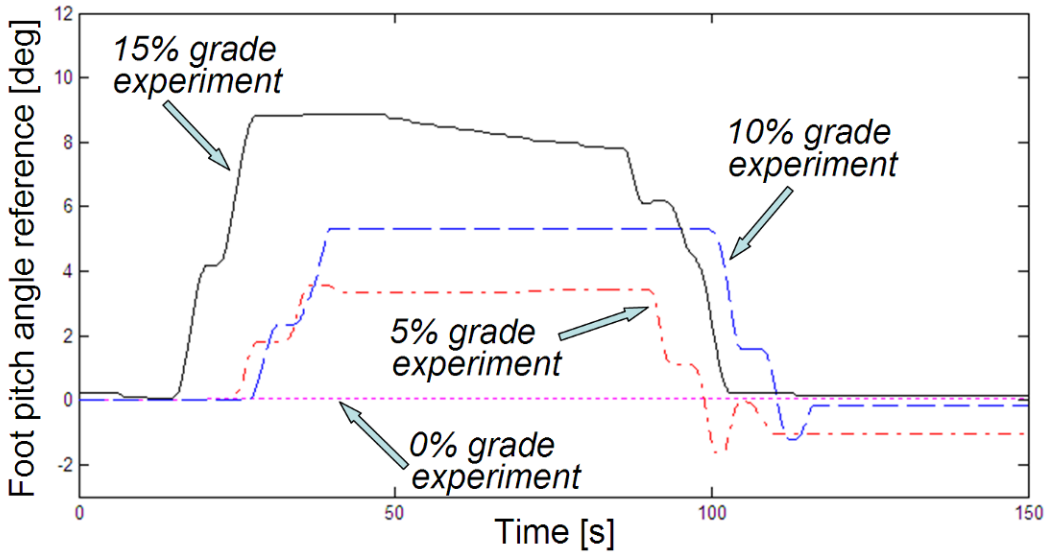

Figure 6.3 : The foot pitch angle reference in 0% (0 degrees), 5% (2.9 degrees), 10% (5.7 degrees) and 15% (8.5 degrees) grade plane walking experiments. Note that the pitch angle converges quickly to the slope angle once the robot enters the slope. When the robot reaches the upper platform, the foot pitch reference remains constant (possibly at a non-zero value due to the dead zone of $\overline{\beta}$ presented in Table 5.1 and Figure 5.6). The 5%, 10% and 15% grade experiments are carried out on a walking surface of three segments: 1) Horizontal plane, 2) Uphill slope 3) Upper horizontal plane.

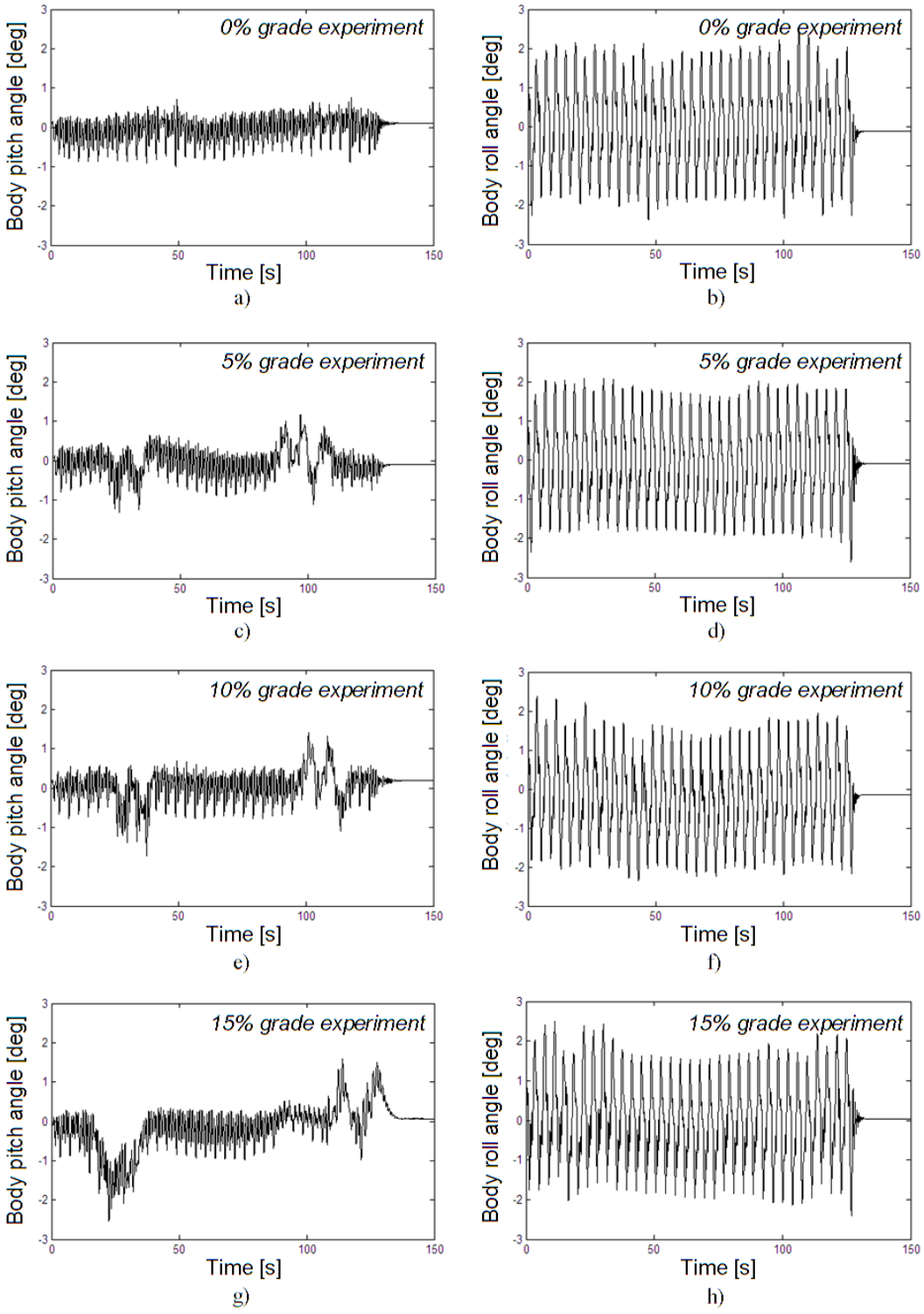

Figure 6.4 : Body pitch and roll angles: a) and b) for a horizontal surface (0% grade); c) and d) for a 5% grade inclined plane; e) and f) for a 10% grade inclined plane; and g) and h) for a 15% grade inclined plane. The 5, 10 and 15% grade experiments are carried out on a walking surface of three segments: 1) Horizontal plane, 2) Uphill slope 3) Upper horizontal plane.

The demands of the slope on the joint torques are explored, too. Figure 6.5 concentrates on leg joints in the pitch arrangement. These are the hip pitch joints, the knees and the ankle pitch joints (shown in Figure 4.51). The axes in the pitch arrangement are the ones which are most affected by the slope angle. Only the right leg pitch-configuration joint torques are shown in the figure. (Because of the symmetry of the walk, the left leg control torques are similar and omitted here for the simplicity of illustration.) The plots in Figure 6.5 display the similarities and contrasts of the 0% and 15% grade experiments. Figure 6.5. a shows the control torques of the pitch-configuration joints for the horizontal walk for an interval of two walking periods (50 s to 57.6 s). It can be observed that there is a repetitive torque pattern with a period of 3.8 s. (This value for the period can be obtained from Table 6.1 as well. The walking period equals to $2(T_s + T_d)$. The walk pattern, and hence the torques, repeat every two double support and two single support phases.) An interval of two walking periods is shown here in order to display the periodic behavior of the torque curves. Figure 6.5. b shows the joint torques for the 15% graded inclined plane case, for the same interval. In this interval, the robot is in the climbing phase. The same repetitive behavior with a 3.8 s period is observed. The shapes of the torque curves for respective joints are quite similar in the 0% and 15% cases. The averages of the torques in the interval are computed. The average values, denoted by $\tau_{average}$, are indicated on the torque plots in Figure 6.5. It is observed that the absolute values of the average torques increase with the increased slope. The absolute average torque increase is approximately 60% for the hip pitch joint, 9% for the knee and 48% for the ankle pitch joint. Still, the net increase in the absolute average torques are in the order of a few Nm's, much smaller than the peak torques displayed in Figure 6.5, and well below the torque capacities of the joints. (The torque capacity of the hip pitch joint with reduction is 96 Nm, that of the knee is 192 Nm and the ankle pitch joint can deliver a 96 Nm torque.)

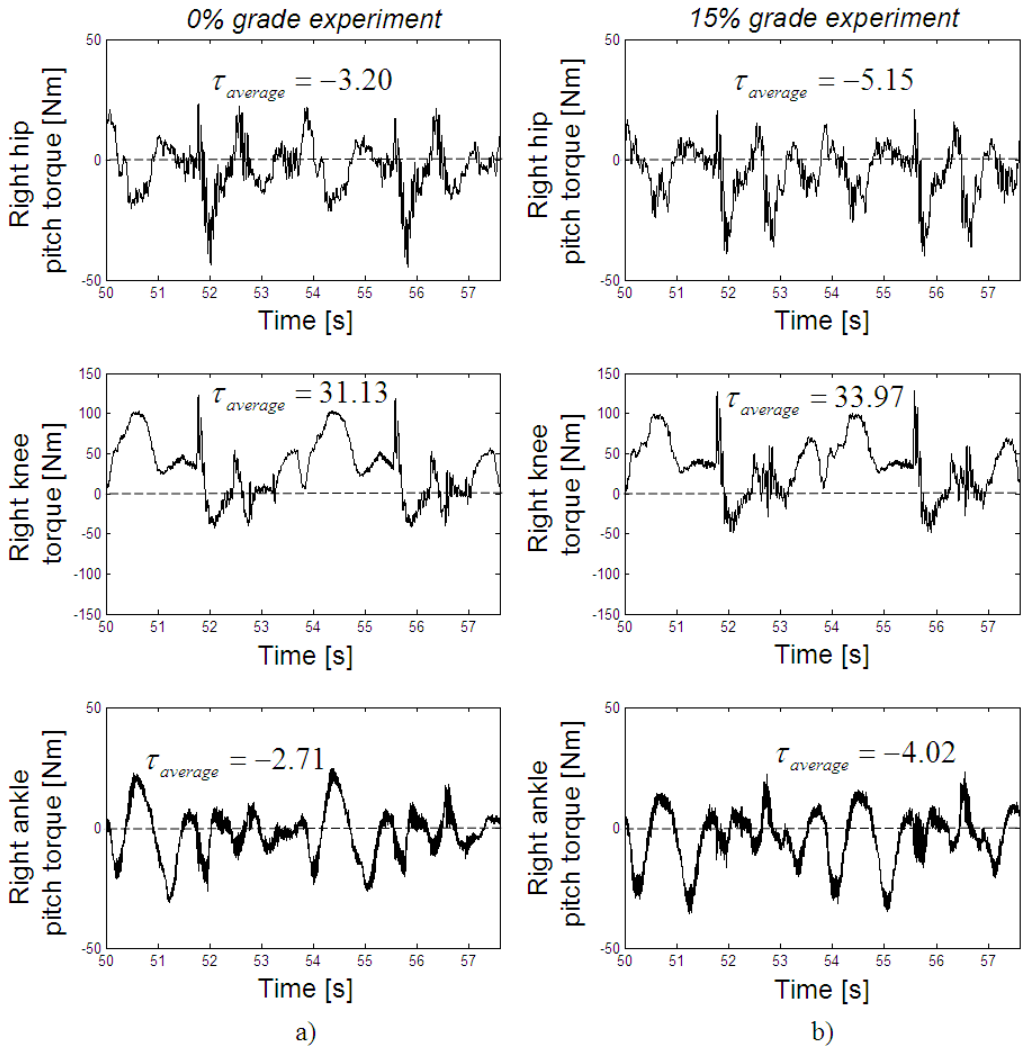

Figure 6.5 : Pitch joint (hip pitch, knee and ankle pitch) control torques on (a) 0% and (b) 15% graded planes for two periods of the walk. The 0% and 15% grade experiment pitch torque curves are quite similar. The absolute values of the averages ($\tau_{average}$) however increase with increased grade

Power requirements of the walk on inclined planes are studied as well. Again the 0%, 5%, 10% and 15% grade experiments are considered. Figure 6.6 shows the average power of the legs in these four experiments. The 5%, 10% and 15% experiment power data are obtained from the climbing phase. The leg section power computation is carried out as

$$P_{Legs} = \sum_{i=1}^{6} \left| \tau_{R_i} \omega_{R_i} \right| + \left| \tau_{L_i} \omega_{L_i} \right|, \tag{6.1}$$

where τ_{R_i} and τ_{L_i} are the control torques of the ith right and left leg joints, respectively. ω_{R_i} and ω_{L_i} stand for the joint angular velocities. As the joint reference position trajectories (and hence the reference velocities) are identical for all four slope cases (as obtained with parameters in Table 6.1), what accounts for power requirement changes are the joint torque differences on different slopes discussed in the paragraph above. Figure 6.6 indicates that, as expected intuitively, the power demand increases with increasing grade.

There are limitations of the proposed approach too: As mentioned above, in our experiments, the robot could not adapt to the inclined planes with slope angles larger than 8.5 degrees. It should also be mentioned that the walking step size has to be kept small (Table 6.1) to allow adaptation time in the plane-to-plane transition phases. Also, since the fuzzy control algorithm considers reference trajectory corrections on pitch angles only, the method is most effective when the walking direction is perpendicular to the boundary between the planes. In other cases, the adaptation to the inclination degrades because the slope creates roll disturbances in addition to the pitch disturbances as well.

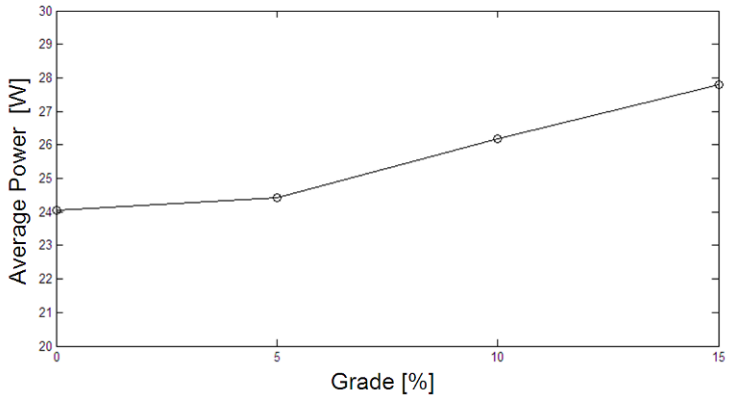

Figure 6.6 : Average output power of legs during walking on 0%, 5%, 10% and 15% graded planes. Averages for the inclined planes are computed only for the climbing phase. (The horizontal plane walking and plane-to-plane transition walking sections are not included in the average.)

Chapter 7

7. CONCLUSIONS

Bipedal walk on uneven surfaces is a crucial research area in humanoid robotics. In the future, our human shaped robotic co-workers are expected to walk on a variety of surface conditions. The balance of the walk has to be robust in the face of surface irregularities or deviations from flat and even floor. Inclined planes are typically encountered in our living environment. They represent structured uneven surfaces. Still, they can be regarded as valuable test beds for more general unevenness with continuous height profiles. The walk on inclined planes is studied in this thesis.

An online fuzzy logic parameter adjustment system is proposed and its use in combination with a set of other controller blocks is presented. Firstly, the balance condition of the robot is inferred by monitoring the body pitch angle. The "overall trend", rather than the instantaneous value of this angle is considered. Inclinometer sampling duration and intervals for the assessment of the "pitch" trend are obtained experimentally. The change of the reference walking plane is proposed as a means of adapting to planes with slopes. Fuzzy rules are devised to change the reference walking plane. While the average body pitch angle acts as the main input of the fuzzy system, the speed of adjustment is tuned by a secondary input. This input is a newly introduced "slope transition indicator" – a function of pitch torques measured by ankle mounted force/torque sensors, averaged in a manner similar to the average computation of the body pitch angle. What the fuzzy system computes as the output is the "increment" of the reference walking plane slope angle. This reference angle is computed by integrating the increment. The integrating nature of the computation provides the walking control system with a degree of robustness in that the robot can adapt to a quite large range of slope grades with the same set of fuzzy system parameters. The method is simple and effective.

The human-sized humanoid robot SURALP is used in the experiments which demonstrate the performance of the control algorithm under various slope conditions. The experimental results indicate that the control system is successful in obtaining a stable walk in the transition from a horizontal plane onto an inclined one with a 15% grade. To the author's knowledge this is the best performance of a blind walker reported to date. This said, it should be mentioned that a quite small step size is used in the experiments.

The transition from an inclined plane onto an even one is achieved in the experiments with the same success too.

Another contribution of this work is the mechanical design and construction of the humanoid robot SURALP.

An interesting future research direction is integrating visual control techniques with the proposed blind walking algorithm, in order to negotiate a larger class of obstacles in the human environment. Exploring the effects of waist and arm motion on the walking performance on inclined planes can also be considered as a future work.

REFERENCES

Ali F, Amran AC, Kawamura A (2010) Slope-Walking of a Biped Robot with Position and Orientation Based Inverse Kinematics Method. Proceedings of the International Conference of Control, Automation and Systems, pp 1724-1728

Ali F, Uğurlu B, Kawamura A (2010) Center of Mass based inverse kinematics algorithm for bipedal robot motion on inclined surfaces. Proceedings of the 11th IEEE International Workshop on Advanced Motion Control, pp 396-401

Bebek Ö, Erbatur K (2004) A Gait Adaptation Scheme for Biped Walking Robots. Proceedings of The 8th IEEE International Workshop on Advanced Motion Control, AMC 2004

Boone GN, Hodgins JK (1997) Slipping and Tripping Reflexes for Bipedal Robots. Autonomous Robots, vol 4, pp 259-271, Springer

Cheng G, Hyon S, Morimoto J, Ude A, Hale JG, Colvin G, Scroggin W, Jacobsen SC. (2007) CB: A Humanoid Research Platform for Exploring NeuroScience. Advanced Robotics, vol. 21, no. 10, pp 1097–1114

Choi Y, You BJ, and Oh SR (2004) On the stability of indirect ZMP controller for biped robot systems. Proceedings of International Conference on Intelligent Robots and Systems, vol.2, pp 1966-1971

Dasgupta A, and Nakamura Y (1999) Making feasible walking motion of humanoid robots from human motion capture data. Proceedings of IEEE International Conference on Robotics and Automation

Erbatur K, Takahashi T, Okazaki A and Kawamura A (2001) Design and Application of FSR Based ZMP Sensors for the Gait Generation of Biped Walking Robots. Proceedings of the International Conference on Information Technologies in Mechatronics, pp 185-190

Erbatur K, Okazaki A, Obiya K, Takahashi T and Kawamura A (2002) A study on the zero moment point measurement for biped walking robots. Proceedings of 7th International Workshop on Advanced Motion Control, pp 431 – 436

Erbatur K and Kawamura A (2003) A New Penalty Based Contact Modeling and Dynamics Simulation Method as Applied to Biped Walking Robots. CD Proceedings FIRA World Congress

Erbatur K, Seven U, Taşkıran E, Koca Ö, Kızıltaş G, Ünel M, Sabanovic A, Onat A (2008) SURALP-L, The Leg Module of a New Humanoid Platform. Proceedings of the IEEE/RAS International Conference on Humanoid Robots, pp 168-173

Erbatur K, Kurt O (2009) Natural ZMP Trajectories for Biped Robot Reference Generation. IEEE Transactions on Industrial Electronics, vol 56, no 3, pp 835-845

Erbatur K, Koca Ö, Taşkıran E, Yılmaz M and Seven U (2009-1) ZMP Based Reference Generation for Biped Walking Robots. ICICRA'09, International Conference Intelligent Control, Robotics and Automation

Erbatur K, Seven U, Taşkıran E, Koca Ö, Yılmaz M, Kızıltaş G, Ünel M, Sabanovic A, Onat A (2009-2) SURALP: A New Full-Body Humanoid Robot Platform. Proceedings of the IEEE/RSJ International Conference on Intelligent Robots and Systems, pp 4949-4954

Fanei A, Farrokhi M (2006) Robust adaptive neuro-fuzzy controller for hybrid position/force control of robot manipulators in contact with unknown environment. Journal of Intelligent & Fuzzy Systems: Volume 17 , Issue 2, Pages: 125-144

Fujimoto Y, Kawamura A (1998) Simulation of an autonomous biped walking robot including environmental force Interaction. IEEE Robotics and Automation Magazine, pp 33-42

FUJITSU http://www.fujitsu.com/my/news/pr/archives/month/2004/fms_20040902.html

Gerla G (2005) Fuzzy Logic Programming and fuzzy control. Studia Logica, 79 231-254.

Gienger M, Löffler K, Pfeiffer F (2001) Towards the design of a biped jogging robot. Proceedings of the IEEE International Conference on Robotics and Automation, vol. 4, pp 4140-4145

Harada K, Morisawa M, Nakaoka S, Kaneko K, Kajita S (2009) Kinodynamic Planning for Humanoid Robots Walking on Uneven Terrain. Journal of Robotics and Mechatronics, vol 21, no 3, pp 311-316, Fujipress

Hashimoto K, Sugahara Y, Ohta A, Sunazuka H, Tanaka C, Kawase M, Lim H, Takanishi A (2006) Realization of Stable Biped Walking on Public Road with New Biped Foot System Adaptable to Uneven Terrain. The First IEEE/RAS-EMBS International Conference on Biomedical Robotics and Biomechatronics, pp 226-231

Hirai K, Hirose M, Haikawa Y, Takenaka T (1998) The development of Honda humanoid robot. Proceedings of the IEEE International Conference on Robotics and Automation, vol 2, pp 1321 -1326

Hirose M, Ogawa K (2007-1) Honda humanoid robots development. Philosophical Transactions of the Royal Society, Series A, 365 (1850), pp 11-19

Hirose M, Ogawa K (2007-2) Walking biped humanoids that perform manual labour. Philosophical Transactions of the Royal Society, Series A, 365 (1850), pp 65-77

Hirukawa H, Hattori S, Kajita S, Harada K, Kaneko K, Kanehiro F, Morisawa M, Nakaoka S (2007) A Pattern Generator of Humanoid Robots Walking on a Rough Terrain. IEEE International Conference on Robotics and Automation, pp 2181-2187

HONDA (2009) http://world.honda.com/ASIMO/

Hsu FY, Fu LC (1995) A new design of adaptive fuzzy hybrid force/position controller for robot manipulators. in Proceedings of IEEE Conference on Robotics and Automation, pp 863–868

Hsu FY, Fu LC (1996) Intelligent robot deburring using adaptive fuzzy hybrid control. in Proceedings of 27th International Symposium on Industrial Robots, pp 847–852

Hu Y, Yan G, Lin Z (2010) Stable Walking for a Compass-like Biped Robot in Complex Environments. Proceedings of the American Control Conference (AACC), pp 6048-6053

Hyon S, Cheng G (2006) Gravity Compensation and Full-Body Balancing for Humanoid Robots. Proceedings of the IEEE International Conference on Humanoid Robots (Humanoids 2006), CD-ROM, pp 214-221

Iida F, Tedrake R (2010) Minimalistic Control of Biped Walking in Rough Terrain. Autonomous Robots, vol 28, pp 355-368

Ishida T, Kuroki Y, Yamaguchi J, Fujita M, Doi T (2001) Motion Entertainment by a Small Humanoid Robot Based on Open-R. Proceedings of the IEEE International Conference Intelligent Robots and Systems, vol.2, pp 1079-1086

Juang, JG (2002) Intelligent Locomotion Control on Sloping Surfaces. Transactions on Information Sciences, vol 147, pp 229-243, Elsevier

Kajita S, Kanehiro F, Kaneko K, Fujiwara K, Harada K, Yokoi K, Hirukawa H (2003) Biped Walking Pattern Generation Using Preview Control of The Zero-Moment-Point. Proceedings of The IEEE International Conference on Robotics and Automation, vol 2, pp 1620-1626

Kajita S, Tani K (1996-1) Experimental study of biped dynamic walking. IEEE Control Systems vol 16, pp 13-19

Kajita S, Tani K (1996-2) Adaptive gait control of a biped robot based on realtime sensing of the ground profile. Proceedings of the International Conference on Robotics and Automation, vol 1, pp 570-577

Kaneko K, Kanehiro F, Kajita S, Yokoyama K, Akachi K, Kawasaki T, Ota S, Isozumi T (2002) Design of prototype humanoid robotics platform for HRP. Proceedings of the IEEE International Conference on Intelligent Robots and Systems, vol 3, pp 2431-2436

Kaneko K, Harada K, Kanehiro F, Miyamori G, Akachi K (2008) Humanoid Robot HRP-3. Proceedings of IEEE/RSJ International Conference on Intelligent Robots and Systems, pp 2471-2478

Kang H, Hashimoto K, Kondo H, Hattori K, Nishikawa K, Hama Y, Lim H, Takanishi A, Suga K, Kato K (2010) Realization of biped walking on uneven terrain by new foot mechanism capable of detecting ground surface. IEEE International Conference on Robotics and Automation, pp 5167-5172

Kim JY, Park IW, Oh JH (2007-1) Walking Control Algorithm of Biped Humanoid Robot on Uneven and Inclined Floor. Journal of Intelligent and Robotic Systems, vol 48, pp 457-484, Springer

Kim JH, Kim JY, Oh JH (2007-2) Adjustment of home posture of a biped humanoid robot using an inertial sensor and force torque sensors. Proceedings of the International Conference on Intelligent Robots and Systems (IROS'07), pp 2223-2229

Kuroki Y, Fujita M, Ishida T, Nagasaka K, Yamaguchi J (2003) A Small Biped Entertainment Robot Exploring Attractive Applications. Proceedings of the IEEE International Conference on Robotics and Automation, vol.1, pp 471-476

Lee CC, (1990) Fuzzy Logic in Control Systems: Fuzzy Logic Controllers (part I and II). IEEE Transactions on Systems, Man and Cybernetics, vol 20, no 2, pp 405-435

Lohmeier S, Loffler K, Gienger M, Ulbrich H, Pfeiffer (2004) Computer system and control of biped "Johnnie". Proceedings of the IEEE International Conference on Robotics and Automation, vol 4, pp 4222- 4227

Lohmeier S, Buschmann T, Ulbrich H, Pfeiffer F (2006) Modular joint design for performance enhanced humanoid robot LOLA. Proceedings of the IEEE International Conference on Robotics and Automation, vol.4, pp 88-93

Manchester IR, Mettin U, Iida F, Tedrake R (2011) Stable Dynamic Walking Over Uneven Terrain. The International Journal of Robotics Research, vol 30, no 3, pp 265-279, Sage Publications

McGeer T (1990) Passive Dynamic Walking. Transactions on The International Journal of Robotics Research, vol 9, no 2, pp 62-82, Sage Publications

Nishiwaki V, Sugihara T, Kagami S, Kanehiro F, Inaba M, Inoue H (2000) Design and Development of Research Platform for Perception-Action Integration in Humanoid Robot: H6. Proceedings of the 2000 IEEE/RSJ International Conference on Intelligent Robots and Systems, vol.3, pp 1559-1564

Nishiwaki V, Kuffner J, Kagami S, Kanehiro F, Inaba M, Inoue H (2007) The experimental humanoid robot H7: a research platform for autonomous behavior. Philosophical Transactions of the Royal Society, Series A, 365 (1850), pp 79-107

Ogura Y, Aikawa H, Shimomura K, Kondo H, Morishima A, Lim H, Takanishi A (2006) Development of A New Humanoid Robot WABIAN-2. Proceedings of the IEEE International Conference on Robotics and Automation, pp 76-81

Oh JY, Kim JH (2004) Realization of dynamic walking for the humanoid robot platform KHR-1. Advanced Robotics, vol. 18, no. 7, pp 749-768

Ono T, Murakami T, Ohnishi K (1998) An approach to biped robot control according to surface condition of ground. 5th International Workshop on Advanced Motion Control, pp 129-134

PAL Robotics (2010) http://www.pal-robotics.com/robots

Park JH (2003) Fuzzy-Logic Zero-Moment-Point Trajectory Generation for Reduced Trunk Motions of Biped Robots. Fuzzy Sets and Systems, vol 134, no 1, pp 189-203, Elsevier

Park IW, Kim JY, Lee J, Oh JH (2006) Online Free Walking Trajectory Generation for Biped Humanoid Robot KHR-3 (KAIST Humanoid Robot-3: HUBO). 6th IEEE-RAS International Conference on Humanoid Robots, pp 398-403

Pratt J, Chew CM, Torres A, Dilworth P, Pratt G (2001) Virtual Model Control: An Intuitive Approach for Bipedal Locomotion. The International Journal of Robotics Research, vol 20, no 2, pp 129-143, Sage Publications

Sakagami Y, Watanabe R, Aoyama C, Shinichi M, Higaki N, Fujimura K (2002) The intelligent ASIMO: System overview and integration. Proceedings of the IEEE International Conference on Intelligent Robots and Systems, vol 3, pp 2478 - 2483

Salatian AW, Zheng YF (1992-1) Gait synthesis for a biped robot climbing sloping surfaces using neural networks. I. Static learning. Proceedings of the IEEE International Conference on Robotics and Automation, vol 3, pp 2601-2606

Salatian AW, Zheng YF (1992-2) Gait synthesis for a biped robot climbing sloping surfaces using neural networks. II. Dynamic learning. Proceedings of the IEEE International Conference on Robotics and Automation, vol 3, pp 2607-2611

Salatian AW, Yi KY, Zheng YF (1997) Reinforcement Learning for a Biped Robot to Climb Sloping Surfaces. Journal of Robotic Systems, vol 14-4, pp 283-296, Wiley-Blackwell

Seven U (2007) Linear Inverted Pendulum Model And Swing Leg Dynamics In Biped Robot Walking Trajectory Generation. Master Thesis, Sabanci University

Seven U, Akbaş T, Fidan KC, Yılmaz M, Erbatur K (2011) Humanoid Robot Walking Control on Inclined Planes. Proceedings of the IEEE International Conference on Mechatronics, pp 875-880

Seven U, Akbaş T, Fidan KC, Erbatur K (2012) Bipedal robot walking control on inclined planes by fuzzy reference trajectory modification. Soft Computing - A Fusion of Foundations, Methodologies and Applications, vol 500, Springer Berlin

Shih CL, Chiou CJ (1998) The motion control of a statically stable biped robot on an uneven floor. IEEE Transactions on Systems, Man, and Cybernetics, Part B: Cybernetics, vol 28, no 2, pp 244-249

Spong M, Vidyasagar M (1989) Robot Dynamics and Control. John Wiley and Sons

Sugahara Y, Hosobata T, Mikuriya Y, Hun-ok Lim, Takanishi A, (2003) Realization of stable dynamic walking by a parallel bipedal locomotor on uneven terrain using a virtual compliance control. Proceedings of the International Conference on Intelligent Robots and Systems, vol 1, pp 595- 600

Takanishi A, Ishida M, Yamazaki Y, Kato I (1985) The realization of dynamic walking by the biped walking robot WL-10RD. Proceedings of International Conference on Advanced Robotics, pp 459-466

Takanishi A, Lim H (2000) Waseda Biped Humanoid Robots Realizing Human-like Motion. Proceedings of the International Workshop on Advanced Motion Control, pp 525-530

Takanishi A, Lim H (2007) Biped walking robots created at Waseda University: WL and Wabian family. Philosophical Transactions of the Royal Society. Series A, 365 (1850), pp 49-64

Tan F, Fu C, Chen K (2010) Biped blind walking on changing slope with reflex control system. Proceedings of the IEEE International Conference on Robotics and Automation, pp 1709-1714

Taşkıran E (2009) Walking Trajectory Generation & Control of The Humanoid Robot SURALP. Master Thesis, Sabanci University

Taşkıran E, Seven U, Koca Ö, Yılmaz M, Erbatur K (2009) Walking Control of a Biped Robot on an Inclined Plane. Proceedings of the 2nd International Conference on Intelligent Systems and Control

Taşkıran E, Yılmaz M, Koca Ö, Seven U, Erbatur K (2010) Trajectory Generation with Natural ZMP References for the Biped Walking Robot SURALP. Proceedings of the IEEE International Conference on Robotics and Automation, pp 4237-4242

Vukobratovic M, Borovac B, Surla D and Stokic D (1990) Biped Locomotion: Dynamics, Stability and Application. Springer.

Vundavilli PR, Pratihar DK (2009) Soft computing-based gait planners for a dynamically balanced biped robot negotiating sloping surfaces. Transactions on Applied Soft Computing, vol 9, issue 1, pp 191-208, Elsevier

Whittle MW (2001) Gait Analysis: An Introduction. Butterworth-Heinemann

Xiang Y, Arora JS, and Abdel-Malek K (2010) Physics-based modeling and simulation of human walking: a review of optimization-based and other approaches, Structural and Multidisciplinary Optimization Volume 42, Number 1, pp 1-23

Yamaguchi J, Takanishi A, Kato I (1994) Development of a biped walking robot adapting to a horizontally uneven surface. In Proceedings of the Conference of Intelligent Robots and Systems, Advanced Robotic Systems and the Real World, vol 2, pp 1156-1163

Yi SJ, Zhang BT, Lee DD (2010) Online Learning of Uneven Terrain for Humanoid Bipedal Walking. Proceedings of the 24th AAAI Conference on Artificial Intelligence, pp 1639-1644

Yılmaz M, Seven U, Erbatur K (2010) Biped Robot Walking Control on Inclined Planes with Fuzzy Parameter Adaptation. Proceedings of the IFAC Workshop on Adaptation and Learning in Control Systems and Signal Processing, vol 10, part 1

Yılmaz M (2010) Humanoid Robot Omnidirectional Walking Trajectory Generation and Control. Master Thesis, Sabanci University

Yokoi K (2007) Humanoid Robotics. Proceedings of International Conference on Control, Automation and Systems

Zheng YF, Shen J, Sias FR Jr (1988) A motion control scheme for a biped robot to climb sloping surfaces. Proceedings of the IEEE International Conference on Robotics and Automation, vol 2, pp 814-816

Zheng YF, Shen J (1990) Gait synthesis for the SD-2 biped robot to climb sloping surface. IEEE Transactions on Robotics and Automation, vol 6, no 1, pp 86-96

Zhu C, Tomizawa Y, Luo X, and Kawamura A (2004) Biped walking with variable ZMP, frictional constraint, and inverted pendulum model. IEEE International Conference on Robotics and Biomimetics, pp 425 - 430

LIST OF AUTHOR'S RELATED PUBLICATIONS

Erbatur K, Seven U, Taşkıran E, Koca Ö, Kızıltaş G, Ünel M, Sabanovic A, Onat A (2008) SURALP-L, The Leg Module of a New Humanoid Platform. Proceedings of the IEEE/RAS International Conference on Humanoid Robots, pp 168-173

Erbatur K, Koca Ö, Taşkıran E, Yılmaz M and Seven U (2009-1) ZMP Based Reference Generation for Biped Walking Robots. ICICRA'09, International Conference Intelligent Control, Robotics and Automation

Erbatur K, Seven U, Taşkıran E, Koca Ö, Yılmaz M, Kızıltaş G, Ünel M, Sabanovic A, Onat A (2009-2) SURALP: A New Full-Body Humanoid Robot Platform. Proceedings of the IEEE/RSJ International Conference on Intelligent Robots and Systems, pp 4949-4954

Seven U (2007) Linear Inverted Pendulum Model And Swing Leg Dynamics In Biped Robot Walking Trajectory Generation. Master Thesis, Sabanci University

Seven U, Akbaş T, Fidan KC, Yılmaz M, Erbatur K (2011) Humanoid Robot Walking Control on Inclined Planes. Proceedings of the IEEE International Conference on Mechatronics, pp 875-880

Seven U, Akbaş T, Fidan KC, Erbatur K (2012) Bipedal robot walking control on inclined planes by fuzzy reference trajectory modification. Soft Computing - A Fusion of Foundations, Methodologies and Applications, vol 500, Springer Berlin

Taşkıran E, Seven U, Koca Ö, Yılmaz M, Erbatur K (2009) Walking Control of a Biped Robot on an Inclined Plane. Proceedings of the 2nd International Conference on Intelligent Systems and Control

Taşkıran E, Yılmaz M, Koca Ö, Seven U, Erbatur K (2010) Trajectory Generation with Natural ZMP References for the Biped Walking Robot SURALP. Proceedings of the IEEE International Conference on Robotics and Automation, pp 4237-4242

Yılmaz M, Seven U, Erbatur K (2010) Biped Robot Walking Control on Inclined Planes with Fuzzy Parameter Adaptation. Proceedings of the IFAC Workshop on Adaptation and Learning in Control Systems and Signal Processing, vol 10, part 1

APPENDIX A

In this appendix the inverse kinematics equations for the leg design presented in the previous sections are obtained. This solution is used in the reference generation algorithms presented in the Section 4.3 and in the proposed reference walking plane fuzzy adjustment method in Chapter 5. The inverse kinematics problem is solved for the 6-DOF manipulator (leg) between the hip and foot coordinate frames. Without restriction of generality, the solution is obtained for the left leg. The expressions for the right leg are identical since the Denavit-Hartenberg parameter tables (Table A.1) of the right and left legs are identical too.

Table A.1 :
Denavit-Hartenberg Parameters of the biped leg

Link	$\mathbf{a_i}$	$\boldsymbol{\alpha_i}$	$\mathbf{d_i}$	$\boldsymbol{\theta_i}$
1	0	$-\pi/2$	0	θ_1^*
2	0	$\pi/2$	0	θ_2^*
3	L_3	0	0	θ_3^*
4	L_4	0	0	θ_4^*
5	0	$-\pi/2$	0	θ_5^*
6	L_6	0	0	θ_6^*

A quite often used way applied for the inverse kinematics of biped walking robots is to employ the Newton-Raphson method. However a closed form solution is more favorable for computational efficiency, both in simulations and implementations.

It is well-known that, a closed form solution can be found for industrial type manipulators with a spherical wrist by decoupling the problem into the position inverse kinematics and orientation inverse kinematics problems. A spherical wrist is defined as the combination of three revolute joints which are positioned as the last three degrees of freedom

in the kinematic arrangement, with their joint axes intersecting at a common point. Since the ankle of the robot accommodates only two revolute joints, the spherical wrist based decoupling idea can not be implemented as it is done for industrial manipulators. However, the hip structure consists of three revolute joints, and the decoupling of inverse kinematics problems is possible by considering it as a "spherical hip".

The formal statement of the problem is that the homogeneous transformation matrix $T_{L_0}^{L_6}$ is given and q_L, the joint variable vector for the left leg is wanted. In order to use the spherical hip idea, in the solution procedure, the leg is considered firstly as an upside down manipulator with its base at the robot foot and its tool tip at the hip center shown in Figure A.1. The given $T_{L_0}^{L_6}$ is inverted to obtain the desired homogeneous transformation matrix for the foot based manipulator:

$$T_{desired} = \left(T_{L_0}^{L_6}\right)^{-1} \tag{A.1}$$

$T_{desired}$ can be written as

$$T_{desired} = \begin{bmatrix} A_{desired} & d_{desired} \\ 0\,0\,0 & 1 \end{bmatrix} \tag{A.2}$$

If we shift the foot frame in Figure A.1 up to the ankle without rotating it and add the "ankle length" a_6 to the x_6 direction component we obtain a simpler problem.

This new frame is denoted as (o'_6, x'_6, y'_6, z'_6) and the new desired homogeneous transformation matrix relating the ankle and hip frames is written as

$$T_{desired,ankle} = \begin{bmatrix} A_{desired} & d_{desired} + a_6 \\ 0\,0\,0 & 1 \end{bmatrix} \tag{A.3}$$

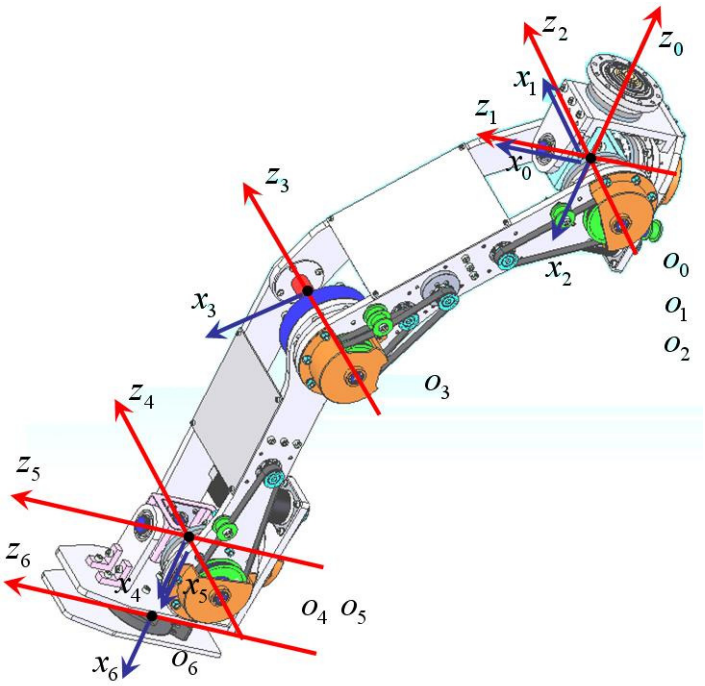

Figure A.1 : Denavit-Hartenberg joint axis representations for one leg

Defining $d_{desired,ankle}$ as $d_{desired,ankle} = d_{desired} + a_6$ we can state that the distance between hip and ankle centers is $d_{desired,ankle}$. The basic robot leg model in Figure A.2 is used in the discussions which follow.

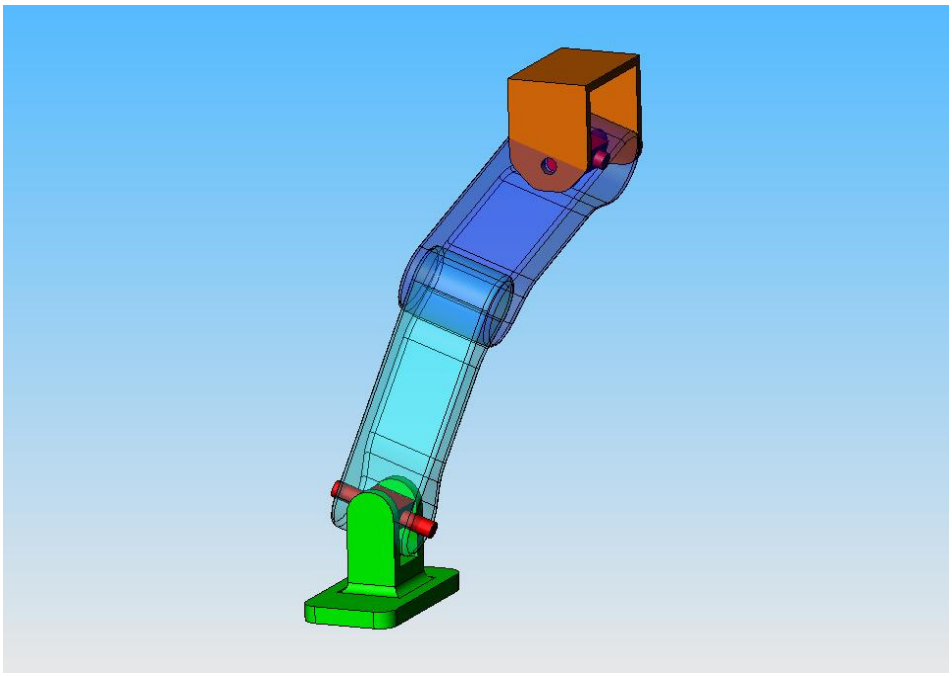

Figure A.2 : A simple leg structure with the kinematic arrangement described in Table A.1

The shank, the thigh and the vector $d_{desired,ankle}$ form a triangle as shown is Figure A.3. Applying the cosine law on this triangle q_{L4} can be obtained. As

$$\cos(q_{L4}) = \frac{a_3^2 + a_4^2 - \left|d_{desired,ankle}\right|}{2a_3^2 a_4^2} \tag{A.4}$$

Where $\left|\cdot\right|$ stands for vector norm. This yields two solutions for q_{L4}:

$$q_{L4} = a\tan 2(\pm\sqrt{1-\cos(q_{L4})}, \cos(q_{L4})) \tag{A.5}$$

The negative solution corresponds to the "knee front" configuration and it is the one preferred because it is the natural human knee.

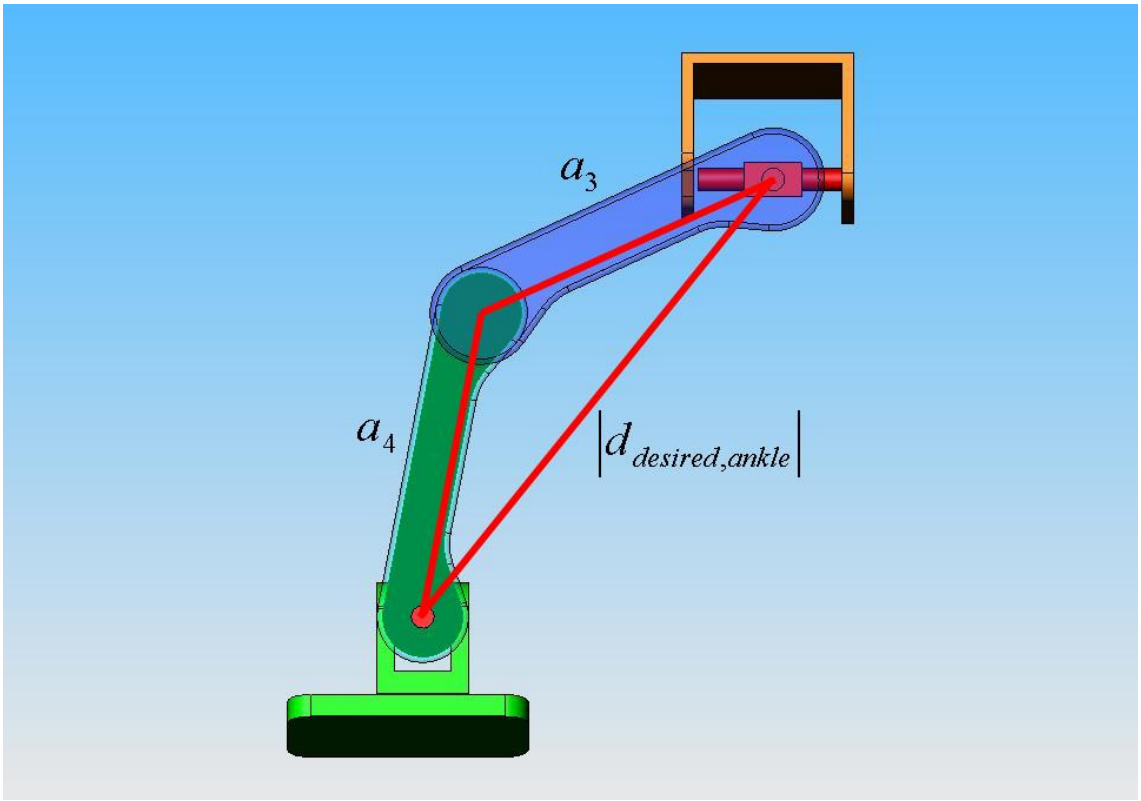

Figure A.3 : The view normal to the shank and thigh

Figures A.4 and A.5 show the joint variable q_{L_5}. q_{L_5} is defined as the angle between the coronal plane and the shank in Figure A.4. However, this angle does not change if we see it from a direction normal to the ankle-knee-hip triangle as seen in Figure A.5. With the indicated lengths and defined of angles in Figure A.6, q_{L_5} is computed as

$$q_{L5} = \frac{\pi}{2} - \alpha - \beta \tag{A.6}$$

where

$$\alpha = \text{acos}(-d_{desired,ankle_z} / \left| d_{desired,ankle} \right|) \tag{A.7}$$

and

$$\beta = \text{asin}(a_3 \sin(-q_{L_4}) / \left| d_{desired,ankle} \right|) \tag{A.8}$$

Finally, q_{L_6} is obtained from Figure A.7 as

$$q_{L6} = -\text{atan2}(d_{desired,ankle_y}, d_{desired,ankle_x}) \tag{A.9}$$

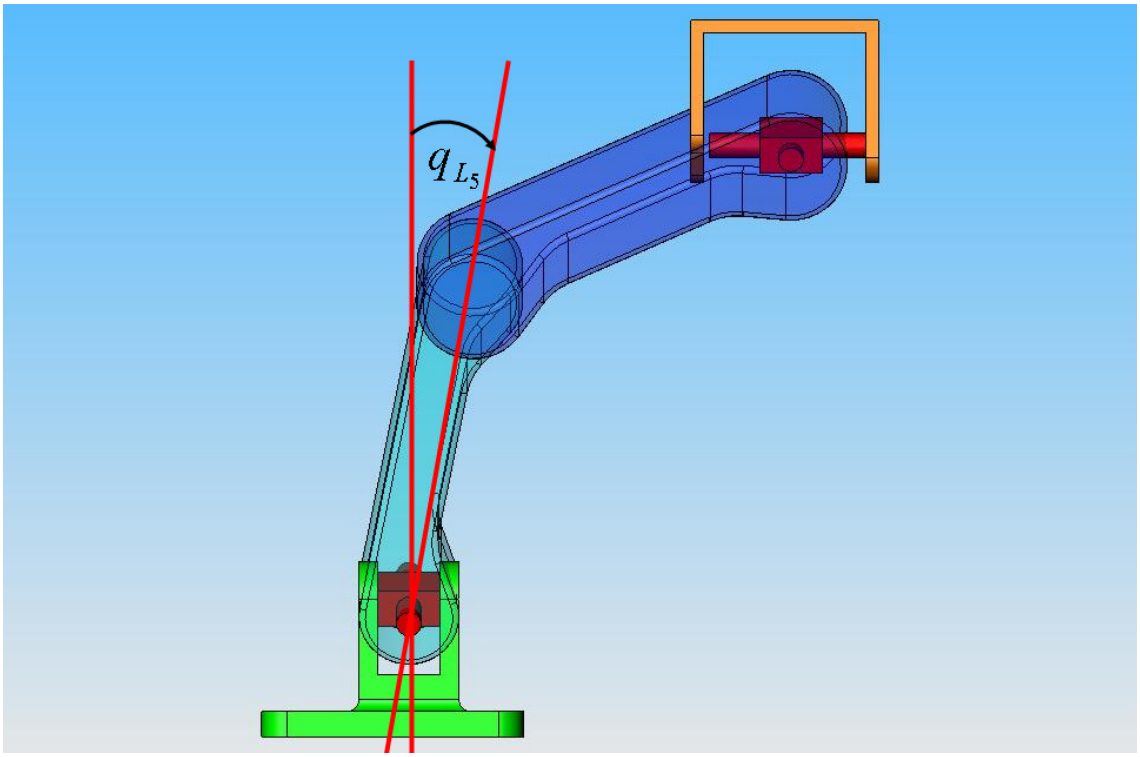

Figure A.4 : The view normal to the side of the foot

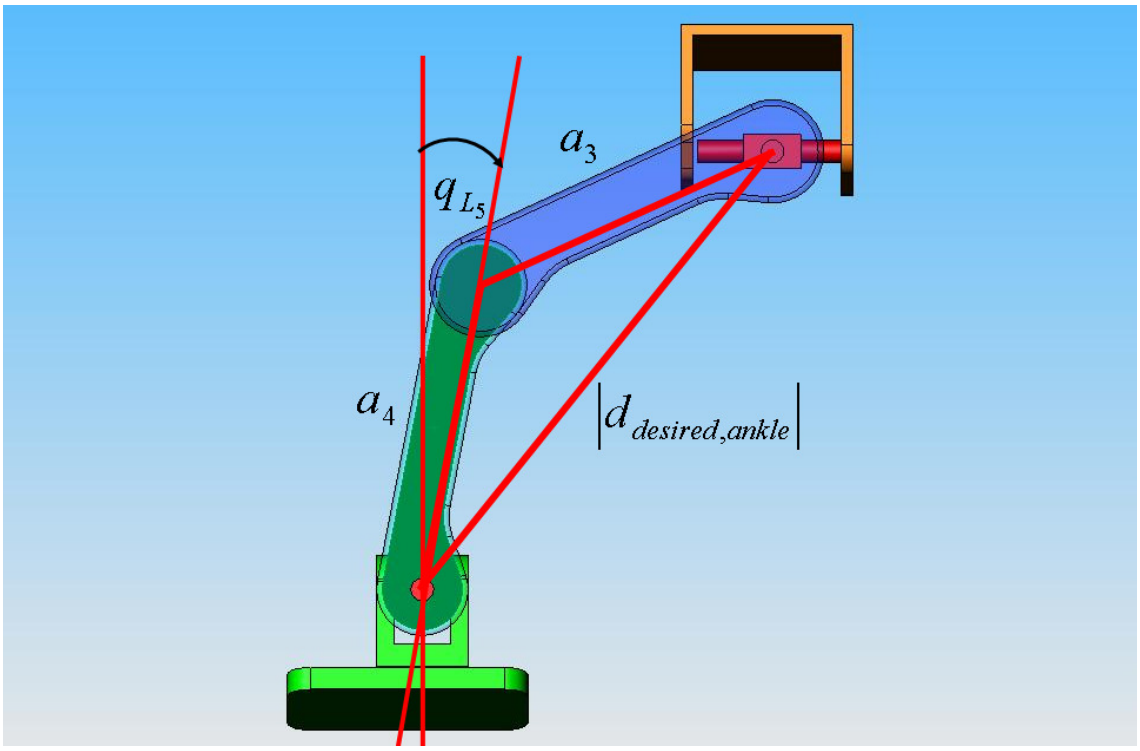

Figure A.5 : The view normal to the shank and thigh. q_{L_5} is defined in this plane too.

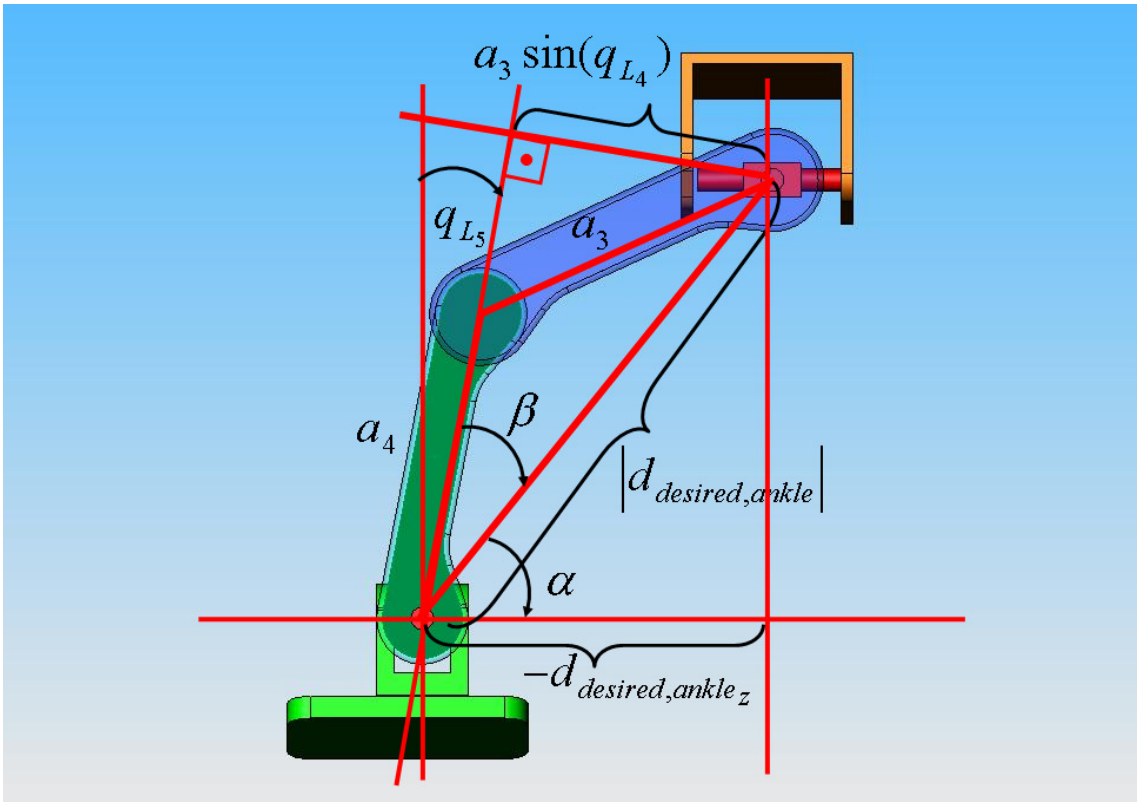

Figure A.6 : The view normal to the shank and thigh. Computation of q_{L_5}.

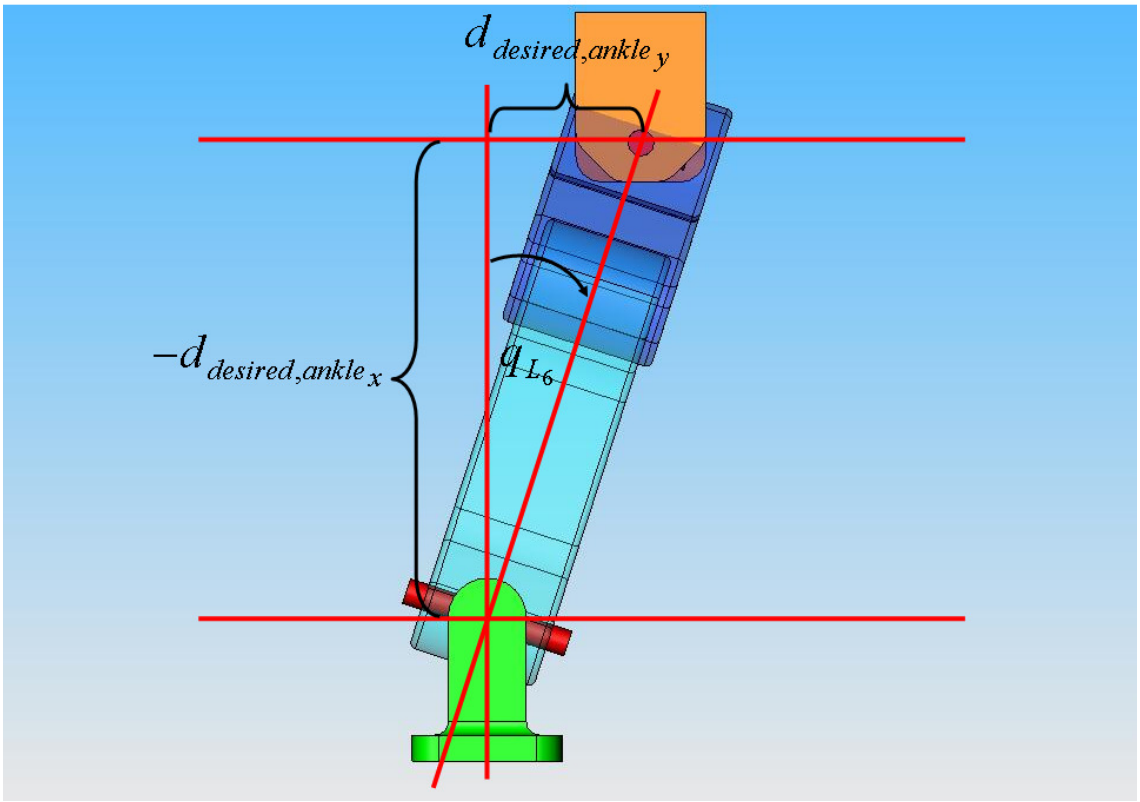

Figure A.7 : The view normal to the foot front side

In order to obtain the remaining of the joint variables an inverse orientation problem is solved. For this problem, the original given homogeneous transformation matrix $T_{L_0}^{L_6}$ can be employed.

$$T_{L_0}^{L_6} = \begin{bmatrix} A_{L_0}^{L_6} & d_{L_0}^{L_6} \\ 0\,0\,0 & 1 \end{bmatrix} \tag{A.10}$$

where $A_{L_0}^{L_6}$ and $d_{L_0}^{L_6}$ are the wanted orientation matrix and position vector, respectively. For

$A_{L_0}^{L_6}$, the following equation holds:

$$A_{L_0}^{L_6} = A(q_{L_1})A(q_{L_2})A(q_{L_3})A(q_{L_4})A(q_{L_5})A(q_{L_6}) \tag{A.11}$$

Because q_{L_4}, q_{L_5} and q_{L_6} are computed, the last three rotation matrices in the product above can be computed too. Hence, the product $A(q_{L_4})A(q_{L_5})A(q_{L_6})$ is known at this stage of the inverse kinematics solution. For $A(q_{L_1})A(q_{L_2})A(q_{L_3})$ the following equation holds

$$A(q_{L_1})A(q_{L_2})A(q_{L_3}) = A_{L_0}^{L_6}(A(q_{L_4})A(q_{L_5})A(q_{L_6}))^T \equiv A \tag{A.12}$$

and this defines the inverse orientation problem. The joint variables q_{L_1}, q_{L_2} and q_{L_3} are obtained by solving this equation.

The expression $A(q_{L_1})A(q_{L_2})A(q_{L_3})$ can be written in a more detailed way as

$$A(q_{L_1})A(q_{L_2})A(q_{L_3}) = \begin{bmatrix} c_1c_2c_3 - s_1s_3 & -c_1c_2s_3 - s_1c_3 & c_1s_2 \\ s_1c_2c_3 + c_1s_3 & -s_1c_2s_3 + c_1c_3 & s_1s_2 \\ -s_2c_3 & -s_2s_3 & c_2 \end{bmatrix} \tag{A.13}$$

where c_i stands for $\cos(q_{L_i})$ and s_i is $\sin(q_{L_i})$.

From (A.13), the joint variables q_{L_1}, q_{L_2} and q_{L_3} are obtained as

$$q_{L_1} = \text{atan2}(A_{23}, A_{13}) \tag{A.14}$$

$$q_{L_2} = \text{atan2}(\sqrt{1 - A_{33}^2}, A_{33}) \tag{A.15}$$

and

$$q_{L_3} = \text{atan2}(A_{32}, -A_{31}) \tag{A.16}$$

where the matrix A is as defined in (A.12).

This completes the solution of the inverse kinematics problem.